

Assessing Neurophysiological States Through the BioVRsea Paradigm

Federica Pescaglia

Dissertation submitted to the Department of Engineering at Reykjavík University in partial fulfillment of the requirements for the degree of Doctor of Philosophy

September 4th, 2026

Thesis Committee:

Paolo Gargiulo, Supervisor
Professor, Reykjavík University, Iceland

Luigi Bianchi, Examiner
Associate Professor, University Tor Vergata, Rome, Italy

Valgerður Guðrún Halldórsdóttir, Examiner
Assistant Professor, University of Iceland, Iceland

Giorgio Di Lorenzo, Committee
Professor, University Tor Vergata, Rome, Italy

Magnús Kjartan Gíslason, Committee
Associated Professor, Reykjavík University, Iceland

Halldor Jr Jónsson, Committee
Emeritus Professor, Reykjavík University, Iceland

Hannes Petersen, Committee
Professor, University of Iceland, Iceland

ISBN 978-9935-577-16-0 Electronic version
ISBN 978-9935-577-15-3 Print version
ORCID Federica Pescaglia 0009-0008-6006-6219
https://orcid.org/0009-0008-6006-6219
Copyright © 2026 Federica Pescaglia

This document is licensed under a Creative Commons Attribution 4.0 (CC BY-NC-SA) (http://creativecommons.org/licenses/by-nc-nd/4.0/) license. However, this license does not cover the Reykjavik University logo (word- and figurative mark). The Reykjavik University logo is a registered trademark and remains the intellectual property of Reykjavik University. Any reuse, redistribution, or modification of the Reykjavik University logo is strictly prohibited without explicit written permission from Reykjavik University.

You may copy and redistribute the material in any medium or format, provide appropriate credit, link to the license and indicate what changes you made. You may do so in any reasonable manner, but not in any way that suggests the licensor endorses you or your use. You may not use the material for commercial purposes. If you remix, transform or build upon the material, you may not distribute the modified material.

The images or other third party material in this thesis are included in the book's Creative Commons license, unless indicated otherwise in a credit line to the material. If material is not included in the book's Creative Commons license and your intended use is not permitted by statutory regulation or exceeds the permitted use, you will need to obtain permission directly from the copyright holder. The use of general descriptive names, registered names, trademarks, service marks, etc. in this publication does not imply, even in the absence of a specific statement that such names are exempt from the relevant protective laws and regulations and therefore free for general use.

The undersigned hereby certify that they recommend to the Department of Engineering at Reykjavík University for acceptance this Dissertation entitled



Assessing Neurophysiological States Through the BioVRsea Paradigm

submitted by **Federica Pescaglia** in partial fulfillment of the requirements for the degree of **Doctor of Philosophy (Ph.D.) in Engineering**

.....

date

Student:

.....

Federica Pescaglia

Thesis Committee:

.....

Paolo Gargiulo

.....

Luigi Bianchi

.....

Valgerður Guðrún Halldórsdóttir

.....

Giorgio Di Lorenzo

.....

Magnús Kjartan Gíslason

.....

Hálldor Jr Jónsson

.....

Hannes Petersen

Abstract

Introduction: Postural control is a complex sensorimotor function that depends on the integration of visual, vestibular, somatosensory, muscular, and cortical mechanisms. Impairments in this system are particularly relevant in Parkinson's disease, where postural instability may emerge even in the early stages and contribute to reduced mobility, impaired adaptation, and increased fall risk. This doctoral thesis investigates postural control through the BioVRSea paradigm, an immersive virtual-reality and moving-platform protocol designed to elicit controlled sensory conflict while simultaneously recording neurophysiological and biomechanical responses.

Results: The BioVRSea paradigm revealed distinct postural-control profiles across populations and experimental phases. In Parkinson's disease, CoP results indicated a more constrained sway pattern, particularly after perturbation, suggesting reduced postural flexibility rather than improved stability. EMG findings showed muscle-specific alterations, with the gastrocnemius lateralis, tibialis anterior, and soleus contributing differently to postural regulation. EEG analyses revealed frequency-specific reorganization of brain dynamics, with alterations in alpha-band connectivity and distinct delta, theta, and beta Brain Network State patterns. These changes suggest that Parkinson's disease affects both peripheral neuromuscular strategies and large-scale cortical network organization during postural control. In seafarers, BioVRSea further highlighted habituation and adaptation mechanisms related to repeated exposure to unstable environments.

Conclusion: This thesis demonstrates that BioVRSea is a sensitive multimodal framework for investigating postural control under controlled sensory-conflict conditions. By integrating EEG, EMG, and CoP, the paradigm captures complementary aspects of balance regulation, from cortical network dynamics to muscular activation and sway behavior. The findings support the potential of BioVRSea as an advanced assessment tool for detecting altered postural strategies in Parkinson's disease and for studying adaptive mechanisms in healthy and occupationally exposed populations.

Keywords: Parkinson's disease; postural control; BioVRSea; virtual reality; electroencephalography; electromyography; center of pressure; dynamic functional connectivity; Brain Network States; balance adaptation.

Ágrip

Inngangur: Stöðustjórnun er flókið skynhreyfiferli sem byggist á samspili sjónar, jafnvægiskerfis, líkamsstöðu- og hreyfiskyns, vöðvavirkni og heilaberkarstarfsemi. Truflanir á þessu kerfi eru sérstaklega mikilvægar í Parkinsonsveiki, þar sem óstöðugleiki í líkamsstöðu getur komið fram jafnvel á fyrstu stigum sjúkdómsins og stuðlað að skertri hreyfigetu, minni aðlögunarhæfni og aukinni fallhættu. Í þessari doktorsritgerð er stöðustjórnun rannsökuð með BioVRSea-aðferðinni, sem er sýndarveruleika- og hreyfipallakerfi hannað til að framkalla stýrðan skynárekstur á sama tíma og taugalífeðlisfræðileg og lífaflfræðileg svör eru mæld.

Niðurstaða: BioVRSea-aðferðin sýndi fram á ólík mynstur stöðustjórnunar milli hópa og tilraunafasa. Hjá einstaklingum með Parkinsonsveiki bentu niðurstöður úr þrýstingsmiðjumælingum til takmarkaðra líkamsveiflna, sérstaklega eftir truflunina, sem bendir frekar til minnkaðs sveigjanleika í stöðustjórnun en aukins stöðugleika. Niðurstöður vöðvarits sýndu vöðvasértækar breytingar, þar sem ytri kálfavöðvi, fremri sköflungsvöðvi og ilvöðvi höfðu ólíkt framlag til stöðustjórnunar. Heilaritsgreiningar sýndu tíðnisértæka endurskipulagningu á heilavirkni, með breytingum í alfa-tengingu og aðgreindum heilanetsástandsmynstrum í delta-, þeta- og beta-tíðnisviðum. Þessar breytingar benda til þess að Parkinsonsveiki hafi áhrif bæði á útlægar tauga- og vöðvaaðferðir og á skipulag stórra heilabarkarneta við stöðustjórnun. Hjá sjómönnum sýndi BioVRSea einnig fram á aðlögunar- og vönunarmynstur sem tengjast endurtekinni útsetningu fyrir óstöðugu umhverfi.

Samantekt: Þessi ritgerð sýnir að BioVRSea er næmt fjölþátta rannsóknarkerfi til að meta stöðustjórnun við stýrðar aðstæður skynáreksturs. Með samþættingu heilarits, vöðvarits og þrýstingsmiðjumælinga fangar aðferðin ólíka en samverkandi þætti jafnvægisstjórnunar, allt frá kvikum heilavirkni- og tengslamynstrum til vöðvavirkni og líkamsveiflna. Niðurstöðurnar styðja möguleika BioVRSea sem háþróaðs matskerfis til að greina breyttar stöðustjórnunaraðferðir í Parkinsonsveiki og til að rannsaka aðlögunarferli hjá heilbrigðum einstaklingum og hópum sem verða reglulega fyrir óstöðugu umhverfi.

Leitarorð: Parkinsonsveiki; stöðustjórnun; BioVRSea; sýndarveruleiki; heilaritun; vöðvaritun; þrýstingsmiðja; kvik starfræn tenging; heilanetsástand; jafnvægisaðlögun.

Contents

Abstract **i**

Ágrip **iii**

Contents **iv**

Acknowledgments **ix**

1 Introduction **1**
1.1 Physiological Postural Control Mechanisms 1
1.2 Postural Control Under Sensory Conflict 3
1.2.1 Sensory Mismatch, Postural Instability, and Motion Sickness 4
1.2.2 Postural Instability in Neurological and Neurodegenerative Disorders 5
1.3 Quantitative Assessment of Postural Control 6
1.3.1 Force-Platform Stabilometry 7
1.3.2 Quantitative Parameters Derived from the Stabilogram 8
1.3.3 Complementary Quantitative Measurements 9
1.4 Aim and Thesis Structure 10

2 Parkinson's Disease **13**
2.1 Risk Factors and Disease Etiology 14
2.2 Clinical Manifestations 14
2.3 Diagnosis, Staging, and Clinical Assessment 15
2.3.1 Clinical Diagnosis and Disease Staging 15
2.3.2 Clinical and Functional Assessment 16
2.3.3 Biomarkersand and Instrumental Assessment 16
2.3.4 Assessment Across Disease Progression 17
2.3.5 Therapeutic Approaches 20
2.4 Postural Control Impairment in Early-Stage Parkinson's Disease 20

3 BioVRSea: A Multimodal Paradigm for Quantitative Postural-Control Assessment **23**
3.1 The BioVRSea Paradigm 23
3.1.1 Motion Sickness and Sensory-Conflict Framework 25

3.1.2 Initial Application in Seafarers 28
3.1.3 Data Acquisition 31
3.1.3.1 Virtual Reality System 31
3.1.3.2 Electroencephalography 31
3.1.3.3 Electromyographic Data Acquisition and Pre-Processing 33
3.1.3.4 Center of Pressure Data Acquisition and Pre-Processing 36
3.1.4 Statistical Analysis 38
3.2 Ethical Approval and Consent 39

4 BioVRSea Adaptation Strategies in Early-Stage PD 41
4.1 Introduction 41
4.2 Materials and Methods 43
4.2.1 Participants 43
4.2.2 Statistical Analysis 43
4.3 Results 43

5 Alpha Connectivity in Parkinson's Disease 47
5.1 Introduction 47
5.2 Materials and methods 49
5.2.1 Participants 49
5.2.2 Data processing: Connectivity analysis to dynamic network computation 50
5.2.3 Data processing: Association of BNSs with RSNs 54
5.3 Results 54
5.3.1 BNSs presence 54
5.3.2 Correlations between questionnaire scores and brain state metrics 55
5.3.3 Statistical analysis of BNSs 55
5.3.4 Association between BNSs and RSNs 56

6 Frequency-Specific Connectivity in Parkinson's Disease 59
6.1 Introduction 59
6.2 Materials and Methods 60
6.2.1 Participants 60
6.2.2 Data processing: Connectivity analysis and dynamic network computation 61
6.2.3 Data processing: Association of BNSs with RSNs 63
6.3 Results 63
6.3.1 Delta 63
6.3.1.1 Association between BNSs and RSNs 63
6.3.1.2 Statistical analysis of BNSs 64
6.3.2 Theta 64
6.3.2.1 Association between BNSs and RSNs 64
6.3.2.2 Statistical analysis of BNSs 64

6.3.3 Beta 64
6.3.3.1 Association between BNSs and RSNs 64
6.3.3.2 Statistical analysis of BNSs 65

7 CoP and Muscle Activation in Parkinson's Disease 69
7.1 Introduction 69
7.2 Material and Methods 70
7.2.1 Participants 70
7.3 Results 71
7.3.1 Center of Pressure 71
7.3.2 Electromyography 74
7.3.2.1 Soleus 74
7.3.2.2 Gastrocnemius Lateralis 74
7.3.2.3 Tibialis Anterior 75

8 Discussion 81
8.1 BioVRSea as a Multisystem Framework for Postural-Control Assessment 81
8.1.1 Center of Pressure as a Marker of Postural Strategy . . 82
8.1.2 Electromyography as a Marker of Neuromuscular Adaptation 86
8.1.3 Electroencephalography as a Marker of Cortical Involvement 90

9 Conclusions 99

10 Limitations and Future Perspectives 103
10.1 Limitations Across Studies 103
10.2 Future Perspectives 104

11 Appendices 107
11.1 Shared Supplementary Methods for Brain Connectivity Analyses 107
11.1.1 ROI–Node–RSN Mapping 107
11.1.2 Phase-Locking Value (PLV) Calculation 108
11.1.3 Computational Methods for BNSs metrics 109
11.2 Paper 2: Exploring dynamic alpha band connectivity in Parkinson's disease: A novel approach to postural control assessment using the BioVRSea paradigm 110
11.2.1 Linear Mixed Model: Statistical Results in Alpha Band 110
11.2.1.1 Statistical Result of Coverage. 110
11.2.1.2 Statistical Result of Occurrence. 110
11.2.1.3 Statistical Result of Duration. 110
11.3 Paper 3: Dynamic connectivity patterns in Parkinson's disease: A new framework for postural control assessment with BioVRSea 111
11.3.1 Time-resolved BNS occupancy: descriptive visualization 111
11.3.2 Phase-wise BNS presence across frequency bands 113
11.3.3 Detailed discussion of individual BNSs 116

11.3.3.1 Delta band 116
11.3.3.2 Theta band 120
11.3.3.3 Beta band 121
11.3.4 Linear Mixed Model: Statistical Result in Bands 125

List of Figures **127**

List of Tables **134**

Bibliography **137**

Acknowledgments

First and foremost, I would like to express my deepest gratitude to my supervisor, Paolo, for giving me the opportunity, four years ago, to embark on this journey. What began as an exchange thesis project gradually grew into something much greater, allowing me to continue what I had started, explore new directions, and grow both as a researcher and as a person.
My heartfelt gratitude goes to Halldór for his endless kindness, generosity, and willingness to help throughout these years. Thank you for always being there for us, not only when we needed guidance or support, but also with comforting words, a warm smile, and a reassuring hug whenever things became difficult.
One of my greatest thanks goes to Michelangelo, my partner in life, my strength, and my safe place during the most difficult moments. Without you, Iceland would have been an even colder place. You and your love turned it into somewhere special, a place that felt like home for such an important chapter of my life. Now, as this chapter comes to an end, I feel that our journey deserves to continue somewhere new. Whatever challenges lie ahead, I hope we will always face them as we have until now: together, happy, deeply connected, and by each other's side.
To my family, especially Michela and Vittorio, thank you from the bottom of my heart. Without you, I would never have had the opportunity to come here in the first place, and I would have missed out on so many wonderful experiences, people, and memories that have shaped who I am today.
I am also truly grateful to my lab colleagues, especially Lorena, my right hand through every challenge and every happy moment. Thank you for sharing this journey with me and for making even the difficult days a little easier. My gratitude also goes to all the students I had the privilege of supervising over the years.
A heartfelt thank you also goes to all the friends who became our family here in Reykjavík. Together, we shared countless adventures, weathered Icelandic storms, played endless games, and gathered around tables full of good food and laughter. You filled these years with warmth, friendship, and unforgettable memories, making a place so far from home feel like home.
And finally, thank you, Iceland. Thank you for helping me grow, mature, freeze more times than I can count, find the love of my life, and experience my first real steps into adulthood. You have been the setting of some of the most meaningful years of my life, a place where I discovered not only who I am, but also who I want to become.
For all of this, I will always be grateful.

Chapter 1

Introduction

1.1 Physiological Postural Control Mechanisms

Postural control (PC) is a multisystem physiological process that enables the body to maintain, achieve, or restore balance during quiet standing, voluntary movement, and external perturbations. It depends on the continuous interaction between sensory inputs, central neural integration, and musculoskeletal responses. Information about the position and movement of the body is primarily provided by the visual, vestibular, and somatosensory systems. These sensory signals are integrated by different structures of the central nervous system, which generate and continuously adapt the motor commands required to maintain the body's centre of mass within the base of support [1–3]. The physiological organisation of this sensorimotor process is summarised in Fig. 1.1. Visual input supplies information about body orientation and movement relative to the surrounding environment. The vestibular system detects linear and angular acceleration of the head and contributes to the estimation of head orientation relative to gravity. Somatosensory information, including proprioceptive, cutaneous, and joint-related inputs, provides information about body-segment position, muscle length and tension, pressure distribution, and contact with the support surface [3, 5, 6].

These sensory signals are integrated at multiple levels of the central nervous system. The spinal cord mediates rapid postural reflexes and coordinates basic sensorimotor responses, while the brainstem, particularly the vestibular nuclei and reticular formation, contributes to the regulation of muscle tone, head and trunk orientation, and automatic postural reactions. The cerebellum integrates sensory feedback with internal predictions of movement, contributing to timing, coordination, error correction, and adaptation to repeated perturbations. Higher-order structures, including the basal ganglia and cortical regions involved in motor planning, sensory processing, and spatial orientation, contribute to the selection and modulation of postural strategies, particularly during voluntary, complex, or attention-demanding tasks. Through descending motor pathways, these structures regulate the activation of axial and limb muscles, producing the

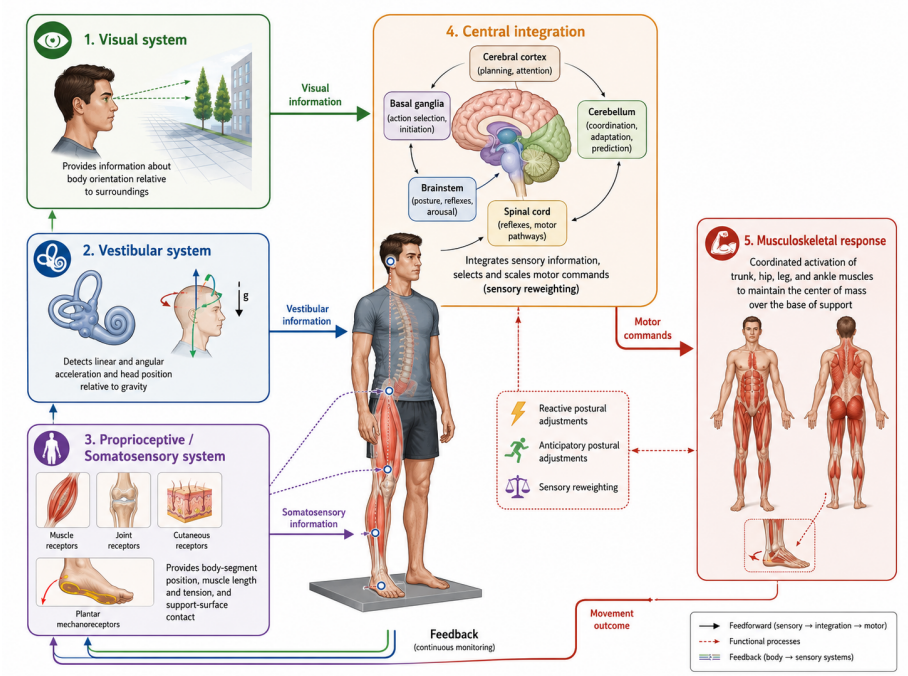


Figure 1.1: **Physiological mechanisms underlying postural control.** Visual, vestibular, and proprioceptive/somatosensory information is integrated at multiple levels of the central nervous system, including the cerebral cortex, basal ganglia, cerebellum, brainstem, and spinal cord. The resulting motor commands generate coordinated musculoskeletal responses that maintain the centre of mass within the base of support. Continuous sensory feedback, sensory reweighting, and reactive and anticipatory postural adjustments enable postural responses to adapt to environmental and task-related demands [1, 3, 4].

coordinated musculoskeletal responses required to stabilise the body's centre of mass relative to the base of support [2, 4, 7].

Postural control is therefore not a purely reflexive process but includes both reactive and anticipatory mechanisms. Reactive postural adjustments are generated in response to unexpected disturbances, whereas anticipatory postural adjustments occur before a voluntary movement or an expected perturbation and reduce the destabilising effects of the upcoming event. Predictive mechanisms are particularly important during repeated or foreseeable perturbations, as previous sensory experience can be used to adapt postural responses to changing environmental and task-related conditions [8, 9].

From a biomechanical perspective, postural stability is maintained through coordinated motor strategies that control the position of the body's centre of mass relative to the base of support. Among these, ankle and hip strategies are two of the principal mechanisms used to recover stability following perturbations.

The ankle strategy is primarily involved in correcting small and relatively slow perturbations, particularly in the anteroposterior direction, and relies on coordinated activation of muscles around the ankle joint. The hip strategy is generally recruited during larger or faster perturbations, when the support surface is narrow or unstable, or when ankle-based corrections are insufficient. These strategies are not mutually exclusive and may be combined with stepping or grasping responses when the centre of mass approaches or exceeds the limits of stability. Their selection and magnitude are continuously modulated by the central nervous system according to the intensity, direction, velocity, and predictability of the postural challenge [1, 2, 10].
The contribution of each sensory system is not fixed but is dynamically adjusted according to the reliability of the available information through a process commonly referred to as sensory reweighting. Under normal conditions, the central nervous system combines visual, vestibular, and somatosensory information to generate an accurate estimate of body orientation. When one source becomes absent, inaccurate, or conflicting, greater weight may be assigned to the remaining sensory inputs [3, 11, 12]. Vision generally plays an important role in postural regulation by providing continuous information about body orientation relative to the surrounding environment. Accordingly, congenital and acquired visual impairment have been associated with poorer postural control and increased anteroposterior and mediolateral sway [13]. Nevertheless, partial compensation may occur through increased reliance on proprioceptive and vestibular information [3, 13].

1.2 Postural Control Under Sensory Conflict

Effective postural control depends on the construction of a coherent internal estimate of body orientation and movement. The central nervous system continuously combines visual, vestibular, and somatosensory information with prior experience and predictions about the sensory consequences of movement. When these signals are mutually consistent, appropriate postural responses can be selected and scaled to maintain the centre of mass within the base of support. However, environmental or task-related changes may alter the availability or reliability of individual sensory inputs, producing a discrepancy between the actual movement of the body, the movement perceived through the different sensory systems, and the movement predicted by the central nervous system.
This discrepancy is commonly described as a sensory mismatch or sensory conflict. It may arise when different sensory systems provide incompatible information about body orientation or self-motion. For example, movement of the visual environment may indicate self-motion while vestibular and somatosensory inputs indicate that the body remains stationary. Conversely, during passive movement inside a vehicle, vestibular and somatosensory receptors may detect acceleration while the visual environment appears relatively stable. Mismatch may also occur when the support surface moves or when visual information becomes inaccurate. Delays between sensory detection and the production of

corrective motor responses may further compromise postural stability.
Sensory mismatch can increase uncertainty in the estimation of body orientation. If corrective motor commands are generated from an inaccurate or delayed estimate, the response may be inappropriate in magnitude, direction, or timing. Excessive corrections may displace the body beyond the desired equilibrium position, whereas insufficient or delayed responses may fail to counteract the perturbation. Repeated corrective errors can therefore produce increased postural sway, oscillatory behaviour, delayed balance recovery, and, under sufficiently challenging conditions, a loss of postural stability.
In healthy individuals, sensory mismatch does not necessarily result in persistent instability. The central nervous system can dynamically modify the relative contribution assigned to each sensory input through sensory reweighting. When visual information becomes unreliable, its contribution may be reduced while vestibular or somatosensory information is given greater weight. Similarly, when the support surface becomes unstable and proprioceptive information from the ankles becomes less reliable, greater reliance may be placed on vestibular and visual cues. This reweighting process allows postural control to remain effective across different environments and experimental conditions [3, 11, 12].
Sensory reweighting is accompanied by the adaptation of internal models and predictive postural responses. With repeated exposure to a perturbation, healthy individuals can learn its temporal and spatial characteristics, anticipate its destabilising effects, and modify the timing and magnitude of muscular activation. Consequently, instability is often greatest during the initial exposure or immediately after a change in sensory conditions. As the central nervous system updates its predictions and identifies the most reliable sensory information, postural responses generally become more appropriate and efficient. Nevertheless, adaptation requires time, and transient instability may occur when the sensory environment changes rapidly or when the conflict exceeds the individual's ability to reorganise postural control.

1.2.1 Sensory Mismatch, Postural Instability, and Motion Sickness

Motion sickness represents a relevant application of sensory mismatch theory. According to the sensory conflict framework, symptoms arise when the pattern of visual, vestibular, and somatosensory information differs from the pattern expected on the basis of previous experience and internal predictions [14, 15]. During sea travel, for example, vestibular and somatosensory systems detect the movement of the vessel, while visual information obtained from the interior of the vessel may suggest a relatively stationary environment. In visually induced motion sickness or virtual reality, the opposite condition may occur: optic flow indicates self-motion, while vestibular and somatosensory signals indicate that the body is stationary.
The inability to resolve this mismatch can affect both perceptual orientation and postural regulation. Corrective responses may be generated in relation to visually perceived motion rather than actual body motion, producing in-

appropriate or destabilising adjustments. Prolonged exposure may lead to disorientation, dizziness, nausea, autonomic symptoms, and reduced postural stability. Susceptibility varies considerably between individuals, partly because of differences in sensory reliance, previous exposure, adaptation rate, and the ability to reweight conflicting sensory information.
A related but distinct explanation is provided by the postural instability theory of motion sickness. According to this framework, motion sickness develops following a prolonged inability to maintain stable control of the body in an unfamiliar motion environment [16]. Changes in postural sway and movement organisation may therefore precede the conscious onset of nausea and other symptoms. Experimental studies using moving visual environments and virtual reality have shown that alterations in postural activity can occur before participants report motion sickness, although the relationship between instability and symptom development is not identical across all individuals and experimental conditions [17]. Sensory conflict and postural instability should therefore be considered as related mechanisms: conflicting sensory information challenges the estimation of body orientation, while the inability to adapt effectively to this conflict may result in persistent postural instability and motion sickness.

1.2.2 Postural Instability in Neurological and Neurodegenerative Disorders

The mechanisms used by healthy individuals to resolve sensory mismatch may be altered by neurological, sensory, or musculoskeletal disorders. Instability can arise from reduced sensory accuracy, abnormal central integration, impaired prediction, inappropriate sensory weighting, delayed motor responses, or insufficient musculoskeletal output. Vestibular disorders, peripheral neuropathies, cerebellar diseases, ageing-related sensory decline, and neurodegenerative conditions can therefore affect postural control through different components of the same sensorimotor system.
In vestibular disorders, inaccurate or asymmetric vestibular information may conflict with visual and somatosensory inputs, particularly during head movements or in environments containing moving visual stimuli. Individuals may compensate by increasing their reliance on vision or somatosensory information, but this strategy can become ineffective when these alternative inputs are also unreliable. Cerebellar disorders, in contrast, primarily affect the timing, coordination, prediction, and adaptation of postural responses. This can lead to dysmetria, excessive sway, oscillatory corrections, and difficulty learning from repeated perturbations [18, 19].
Postural impairment is also observed in several neurodegenerative disorders. In Alzheimer's disease and other dementias, balance deficits may reflect the combined effects of cognitive decline, impaired visuospatial processing, reduced attentional resources, and executive dysfunction. These alterations become particularly evident when postural control must be performed simultaneously with another cognitive or motor task [20, 21]. In Huntington's disease, progressive basal ganglia and cortical degeneration contributes to involuntary movements,

impaired motor coordination, increased gait variability, and reduced stability [22, 23].
Parkinson's disease represents a particularly relevant model for investigating the relationship between sensory mismatch, central integration, and postural instability. Degeneration of basal ganglia circuits affects the automatic selection and scaling of postural responses, while alterations in proprioceptive processing can reduce the accuracy of information concerning body position and movement [24–26]. Increased reliance on visual information may partly compensate for impaired proprioceptive processing, but it can also make postural control more vulnerable when visual information is absent, inaccurate, or conflicting.
People with Parkinson's disease may retain some capacity to modify sensory weighting, but this adaptation may be less efficient, slower, or more dependent on the specific experimental condition [27]. The combination of altered sensory processing, reduced automaticity, impaired anticipatory adjustments, delayed corrective responses, and limited flexibility in changing motor strategies may therefore increase instability during unexpected perturbations or multisensory conflict. Although severe postural instability is traditionally associated with advanced Parkinson's disease, subtle abnormalities in sway, sensory integration, and anticipatory control may already be present during the early stages. Postural control is consequently a valuable functional domain for identifying early alterations and investigating how neurodegeneration modifies the interaction between sensory information, central integration, and motor output.

1.3 Quantitative Assessment of Postural Control

Postural control can be evaluated through clinical scales, observational tests, and instrumental measurements. Clinical tests provide important information about functional balance and fall risk; however, their results may depend on examiner judgement and may not detect subtle alterations in postural regulation. Instrumental assessment enables the objective and continuous quantification of postural behaviour through biomechanical, neuromuscular, kinematic, and neurophysiological signals.
Among the available instrumental methods, force-platform posturography is generally considered the reference laboratory method for the quantitative assessment of postural sway during standing. A force platform records the ground reaction forces and moments generated at the interface between the feet and the support surface, from which the position of the centre of pressure (CoP) can be calculated. The resulting CoP signal provides a sensitive measure of the mechanical output of the postural-control system [28–30].
Nevertheless, the force platform does not directly measure all the physiological mechanisms involved in balance regulation. CoP analysis describes the resultant biomechanical behaviour produced by sensory integration and motor control, but it does not independently identify which sensory, muscular, or neural mechanisms generated that behaviour. For this reason, stabilometric measurements can be combined with electromyography, kinematic measurements, inertial

sensors, electroencephalography, and other physiological signals to obtain a more complete characterisation of postural control.

1.3.1 Force-Platform Stabilometry

Force-platform stabilometry is a form of static posturography used for the quantitative analysis of postural sway while an individual maintains a standing position. In its conventional form, the participant stands as still as possible under controlled conditions, such as with the eyes open or closed, while the displacement of the CoP is continuously recorded. Dynamic or perturbation-based posturography extends this approach by introducing mechanical, visual, or multisensory perturbations to evaluate reactive responses, sensory integration, and adaptation.

A laboratory force platform typically records three orthogonal ground reaction forces,

$$\mathbf{F}(t) = \begin{bmatrix} F_x(t) & F_y(t) & F_z(t) \end{bmatrix}^T, \tag{1.1}$$

and three corresponding moments,

$$\mathbf{M}(t) = \begin{bmatrix} M_x(t) & M_y(t) & M_z(t) \end{bmatrix}^T. \tag{1.2}$$

The vertical component F_z primarily reflects body-weight support, while the horizontal components F_x and F_y reflect shear forces generated during postural corrections. Assuming that the measurement origin is located a vertical distance h below the platform surface, the CoP coordinates can be estimated as

$$x_{\mathrm{CoP}}(t) = \frac{hF_x(t) - M_y(t)}{F_z(t)} \tag{1.3}$$

$$y_{\mathrm{CoP}}(t) = \frac{M_x(t) + hF_y(t)}{F_z(t)} \tag{1.4}$$

When the coordinate origin is defined at the platform surface, $h = 0$, the equations reduce to

$$\begin{aligned} x_{\mathrm{CoP}}(t) &= -\frac{M_y(t)}{F_z(t)}, \\ y_{\mathrm{CoP}}(t) &= \frac{M_x(t)}{F_z(t)}. \end{aligned} \tag{1.5}$$

The exact signs and correspondence between the x–y axes and the mediolateral and anteroposterior directions depend on the coordinate convention adopted by the force-platform manufacturer.

The CoP represents the point of application of the resultant ground reaction force on the support surface. It should not be confused with the centre of mass (CoM). The CoM describes the weighted average position of the body's mass, whereas the CoP reflects the resultant interaction between body mechanics

and the neuromuscular actions transmitted to the support surface to regulate CoM motion. During quiet standing, the CoP generally moves around the CoM projection and produces the corrective forces required to prevent the body from falling.
The temporal evolution of the CoP in the mediolateral and anteroposterior directions is commonly referred to as the *stabilogram*. The corresponding two-dimensional representation of the CoP trajectory on the horizontal plane is also frequently called the *statokinesigram*. Although these terms are not used consistently throughout the literature, both representations describe the continuous corrective activity occurring during standing [28, 30].
Reliable stabilometric assessment requires the experimental conditions to be carefully standardised. Relevant factors include trial duration, sampling frequency, filtering procedures, foot position, visual target, distance from the target, footwear, arm position, number of repetitions, and the characteristics of the support surface. International recommendations indicate that static stabilometric recordings should last at least 25 seconds and should be acquired at a sampling frequency of at least 50 Hz, although longer trials or higher sampling frequencies may be necessary for specific time- or frequency-domain analyses [31].

1.3.2 Quantitative Parameters Derived from the Stabilogram

Let the sampled CoP trajectory be represented by

$$\mathbf{p}_i = \begin{bmatrix} x_i & y_i \end{bmatrix}^T, \qquad i = 1, \dots, N, \tag{1.6}$$

where x_i and y_i represent the mediolateral and anteroposterior CoP coordinates, respectively.
One of the most common measures is the total CoP path length, calculated as the cumulative Euclidean distance between consecutive samples:

$$L = \sum_{i=2}^{N} \sqrt{(x_i - x_{i-1})^2 + (y_i - y_{i-1})^2}. \tag{1.7}$$

The mean CoP velocity is obtained by dividing the total path length by the recording duration T:

$$v_{\text{mean}} = \frac{L}{T}. \tag{1.8}$$

Mean velocity reflects the overall amount and rate of corrective postural activity and is considered one of the most reliable and sensitive conventional stabilometric measures [30, 32].
Directional variability can be quantified using the root mean square displacement. For the mediolateral direction,

$$\text{RMS}_x = \sqrt{\frac{1}{N} \sum_{i=1}^{N} (x_i - \bar{x})^2} \tag{1.9}$$

where

$$\bar{x} = \frac{1}{N}\sum_{i=1}^{N} x_i \tag{1.10}$$

Similarly, for the anteroposterior direction,

$$\mathrm{RMS}_y = \sqrt{\frac{1}{N}\sum_{i=1}^{N} (y_i - \bar{y})^2} \tag{1.11}$$

The displacement range can be calculated separately for each direction:

$$R_x = \max(x_i) - \min(x_i), \tag{1.12}$$

$$R_y = \max(y_i) - \min(y_i). \tag{1.13}$$

These measures describe the maximum spatial excursion of the CoP along the mediolateral and anteroposterior axes.

The spatial dispersion of the two-dimensional trajectory is frequently represented by a confidence ellipse. If λ_1 and λ_2 are the eigenvalues of the covariance matrix of the CoP coordinates, the area of a 95% confidence ellipse can be estimated as

$$A_{95} = \pi \chi^2_{2,0.95} \sqrt{\lambda_1 \lambda_2} \tag{1.14}$$

where $\chi^2_{2,0.95}$ is the 95th percentile of a chi-squared distribution with two degrees of freedom. Different ellipse algorithms and definitions have been adopted in posturographic studies; therefore, the calculation method should always be explicitly reported [30, 33].

Additional analyses may include directional sway, mean radial displacement, sway density, frequency-domain power, mean or median frequency, entropy, stabilogram-diffusion analysis, and other nonlinear measures. These parameters provide complementary information about the magnitude, velocity, spatial organisation, frequency content, and temporal complexity of postural sway.

Although increased path length, velocity, RMS displacement, or ellipse area is often associated with poorer postural steadiness, CoP magnitude should not be interpreted as a direct and universal measure of instability. A larger CoP trajectory may reflect reduced balance control, but it may also indicate an active exploratory or compensatory strategy. Conversely, reduced sway may result from increased muscular stiffness or co-contraction rather than more efficient postural control. The interpretation of stabilometric parameters must therefore consider the experimental task, sensory conditions, population, and accompanying physiological measurements.

1.3.3 Complementary Quantitative Measurements

Complementary measurements can be integrated with force-platform stabilometry to identify the mechanisms underlying the observed CoP trajectory.

Electromyography provides information about the timing, amplitude, frequency content, and coordination of muscle activation. In postural-control experiments, EMG can identify ankle, hip, and trunk strategies; quantify muscle-response latency following perturbations; and detect changes in co-contraction or neuromuscular recruitment. The simultaneous analysis of CoP and EMG makes it possible to relate the resulting mechanical sway to the muscular commands responsible for postural correction.
Motion-capture systems and inertial measurement units provide kinematic information about body-segment displacement, joint angles, trunk motion, and approximate CoM behaviour. These measurements are particularly relevant because similar CoP trajectories may be generated by different combinations of ankle, hip, trunk, or stepping strategies.
Electroencephalography provides complementary information about cortical processes associated with sensory integration, attention, error detection, adaptation, and motor planning. EEG is especially useful during unpredictable perturbations, sensory conflict, virtual-reality exposure, and cognitively demanding balance tasks. However, because movement-related and muscular artefacts can strongly affect EEG recordings, its interpretation requires careful acquisition, preprocessing, and integration with biomechanical measurements.
Consequently, force-platform stabilometry should be considered the primary quantitative method for characterising postural sway, whereas EMG, kinematic measurements, inertial sensors, and EEG provide complementary information about the neuromuscular and neural mechanisms underlying the measured postural response.

1.4 Aim and Thesis Structure

The primary aim of this thesis is to investigate how postural control is maintained and adapted under challenging sensory and mechanical conditions, and to determine whether these mechanisms are altered in individuals with early-stage Parkinson's disease. Particular attention is given to the ability to integrate changing sensory information, generate appropriate postural responses, adapt to repeated perturbations, and recover once the destabilising condition has ended.
By integrating complementary measurements, the thesis investigates whether early-stage Parkinson's disease is associated with altered postural sway, modified muscular recruitment, reduced adaptability to changing sensory conditions, or abnormal cortical organisation during postural challenge. The analysis also considers how these responses evolve before, during, and after perturbation, since postural-control impairment may be reflected not only in the magnitude of instability, but also in the ability to anticipate, adapt to, and recover from destabilising conditions.
Overall, this thesis aims to characterise postural instability as a multidimensional alteration arising from the interaction between sensory integration, motor coordination, and cortical dynamics. The combined analysis of centre-of-pressure

behaviour, muscle activation, and brain activity is intended to identify subtle alterations in postural control that may not be detectable through clinical observation or through a single measurement modality.
Following this introductory chapter, Chapter 2 provides an overview of Parkinson's disease, including its pathophysiology, clinical manifestations, diagnostic approaches, biomarkers, therapeutic strategies, and the relevance of postural-control impairment. Chapter 3 describes the experimental procedures, data-acquisition systems, signal-processing methods, statistical analyses, and ethical considerations. The subsequent chapters present the experimental studies included in the thesis, focusing on biomechanical, neuromuscular, and cortical responses to postural challenge. The general discussion integrates the findings across the different measurement modalities, while the final chapters summarise the principal contributions, limitations, and future perspectives of the work.

Chapter 2

Parkinson's Disease

Parkinson's disease (PD) is a progressive neurological syndrome characterized by both motor and non-motor manifestations. Its typical motor signs include tremor, rigidity, bradykinesia, stooped posture, slow voluntary movements, and reduced facial expression. Diagnosis may require time, since early manifestations can be subtle and may be mistakenly attributed to aging [34]. Globally, PD represents an increasing clinical burden: disability and mortality associated with the disease are rising faster than for any other neurological disorder, and its prevalence has doubled over the past 25 years, with more than 8.5 million people estimated to be living with PD worldwide in 2019 [35]. Although updated diagnostic criteria have improved clinical accuracy, the identification of objective parameters for diagnosis, follow-up, and treatment monitoring remains an important challenge.

PD is a chronic, slowly progressive, and heterogeneous disease affecting motor, autonomic, behavioral, and cognitive functions. Although it is classically recognized as a movement disorder, non-motor manifestations may appear years before motor symptoms and can strongly affect quality of life. For this reason, PD is now considered a multisystem disorder rather than a purely motor disease. Clinical progression varies across patients in terms of age at onset, dominant symptoms, rate of progression, response to dopaminergic therapy, and development of motor and non-motor complications, supporting the need for multimodal assessment approaches.

The pathophysiology of PD is mainly associated with progressive dysfunction of neural circuits involved in motor control. The basal ganglia, including the caudate nucleus, putamen, and globus pallidus, play a central role in the planning, initiation, and execution of voluntary movement [36]. In PD, motor impairment is primarily related to a progressive and permanent reduction in dopamine production [37]. Dopamine loss, mainly caused by degeneration of dopaminergic neurons in the substantia nigra pars compacta, disrupts the balance between direct and indirect basal ganglia pathways and contributes to bradykinesia, rigidity, tremor, and postural instability.

Another major pathological feature is the abnormal accumulation of alpha-

synuclein (αSyn). Altered expression, aggregation, or impaired clearance of αSyn can affect intracellular processes and promote neurodegeneration [38]. For this reason, αSyn has also been investigated as a potential biomarker for PD [39]. Aggregated αSyn is closely associated with Lewy bodies and Lewy neurites, which are distinctive neuropathological hallmarks of idiopathic PD [40].

2.1 Risk Factors and Disease Etiology

The causes of PD are not fully understood and are thought to involve a complex interaction among genetic susceptibility, aging, sex-related biological factors, environmental exposures, and lifestyle determinants. Genetic research in PD began with the identification of mutations in the α-synuclein gene [41]. Later, rare familial and early-onset forms were associated with mutations in Parkin (PARK-2), PINK1 (PARK-6), DJ-1 (PARK-7), LRRK2 (PARK-8), and GBA, which encodes glucocerebrosidase [42–44]. However, most cases are sporadic, although approximately 20% of patients report a family history of PD.

Aging is the strongest known risk factor. PD prevalence varies according to age, sex, ethnicity, genetic background, and environmental context [45]. The disease affects approximately 1–3% of individuals over 60 years of age, and its global burden is expected to increase substantially with population aging [35]. PD is also considered one of the fastest-growing neurological disorders and a major cause of disability worldwide [46]. Men are affected more frequently than women [47, 48], although women may show distinct symptom profiles, mortality rates, progression patterns, and responses to pharmacological treatment or deep-brain stimulation [49–51].

Environmental and lifestyle factors may also influence PD risk. Traffic-related pollution and other environmental pollutants have been associated with increased PD prevalence [52]. Other proposed risk factors include oxidative stress, traumatic brain injury, dairy product consumption, and higher intake of red meat, seafood, alcohol, or beverages containing high-fructose corn syrup [53]. Conversely, tobacco smoking and caffeine consumption have shown an inverse association with PD risk, possibly through monoamine oxidase inhibition and adenosine receptor antagonism [54]. Physical activity, ibuprofen use, and calcium channel blockers have also been investigated, although their associations appear less consistent [55]. Overall, PD etiology is multifactorial, and further research is needed to clarify causal mechanisms and improve prevention, diagnosis, and treatment strategies [56].

2.2 Clinical Manifestations

PD is clinically characterized by heterogeneous motor and non-motor symptoms. The cardinal motor manifestations include bradykinesia, resting tremor, rigidity, and, in more advanced stages, postural instability [57]. Symptoms are often asymmetric at onset, with one side of the body more affected than the other

[58]. Bradykinesia, defined as slowness in voluntary movement execution, is one of the most disabling symptoms of PD [59, 60], whereas akinesia refers to difficulty initiating spontaneous movements [61, 62]. Resting tremor is common but not universal, may be asymmetric, and can vary during disease progression [63–66]. Rigidity consists of involuntary increased muscle tone and may affect the limbs, neck, or trunk [63–66].

Postural instability typically emerges later and primarily affects axial control [67–69]. It is associated with impaired postural reflexes, reduced balance recovery, and increased fall risk. Gait disturbances include reduced arm swing, flexed posture, shortened stride length, impaired turning, and freezing of gait [69–71]. Freezing is a major contributor to falls [72]. In advanced disease, patients may also develop motor fluctuations, such as wearing-off, nocturnal akinesia, unpredictable off phases, and motor blocks [73]. Dyskinesias are involuntary movements commonly related to long-term levodopa therapy [74, 75].

Non-motor symptoms are also central to PD and may precede motor signs by several years. They include autonomic dysfunction, olfactory impairment, sleep disorders, mood and anxiety disturbances, cognitive impairment, fatigue, pain, and speech or swallowing problems [76–79]. Speech impairment may include hypophonia, reduced modulation, monotone speech, or altered speech rhythm [76–79], while dysphagia usually occurs later and may increase aspiration and pneumonia risk [80]. Autonomic dysfunction may include orthostatic hypotension [81, 82], and olfactory dysfunction often precedes motor symptoms [76–79]. Sleep disorders, including insomnia, excessive daytime sleepiness, and REM sleep behavior disorder, are frequent [76–79]; insomnia may be related to nocturnal rigidity and bradykinesia [83], while excessive daytime sleepiness can strongly affect daily functioning [84]. Depression and anxiety are also common [85–87]. Cognitive impairment can involve attention, visuospatial abilities, and executive functions [86, 87]; when it appears within one year of motor onset, Lewy body disease should be considered [88, 89]. Fatigue and pain further contribute to disease burden [74].

2.3 Diagnosis, Staging, and Clinical Assessment

2.3.1 Clinical Diagnosis and Disease Staging

PD was first described by James Parkinson in 1817 as “shaking palsy”, and the term Parkinson’s disease later entered clinical use through Jean-Martin Charcot and the Salpêtrière school [90, 91]. Although the main clinical signs had long been recognized, formal diagnostic criteria were introduced only in the late twentieth century, before which diagnostic accuracy was limited [92]. The first widely used criteria were the United Kingdom Parkinson’s Disease Society Brain Bank criteria [93], followed by criteria proposed by Gelb and colleagues based on clinically possible and clinically probable PD [94]. In 2015, the Movement Disorder Society introduced updated criteria defining Parkinsonism as bradykinesia combined with rest tremor, rigidity, or both, with diagnosis based on supportive criteria, absolute exclusion criteria, and red

flags [95]. These criteria define clinically established and clinically probable PD and improve diagnostic assessment by integrating motor and non-motor manifestations [96].
PD staging is commonly based on clinical observation, with the Hoehn-Yahr system primarily describing disease severity according to motor manifestations [97, 98]. Disease progression can be broadly divided into pre-clinical, prodromal, early, middle, and advanced stages. The early stage may include mild tremor, slight gait difficulty, unilateral symptoms, and reduced facial expression, usually without major interference with daily life [98]. The middle stage is associated with greater balance and coordination impairment, while the advanced stage is characterized by severe disability and major difficulties in standing and walking [98].

2.3.2 Clinical and Functional Assessment

Clinical and functional tests are used to evaluate mobility, balance, endurance, resistance, and flexibility in PD [99]. These include balance scales, gait tests, endurance tests, strength assessments, and flexibility measures. Overall, these tools support a multidimensional characterization of gait, balance, and physical function, but may not fully capture subtle postural-control alterations.

2.3.3 Biomarkersand and Instrumental Assessment

Biomarkers are useful for investigating predisposition to PD, supporting diagnosis, evaluating prognosis, and monitoring disease progression [100]. Biological samples such as blood, urine, and skin are potential sources of biochemical biomarkers [101]. Biomarkers are objectively measured indicators of biological or pathological processes and may be classified as trait, state, or rate biomarkers [100, 102]. Biomarker development may follow candidate-based or unbiased discovery approaches [100]. Among the most studied biomarkers in PD is α-synuclein [103, 104], whose relevance is supported by its role in PD genetics and neuropathology [41].
Non-invasive neuroimaging techniques provide information about brain structure and function [105]. In PD, PET, SPECT, MRI, and EEG are commonly used to investigate structural, functional, and neurophysiological alterations [106]. PET can support diagnosis and estimate disease progression using radioactive tracers, while SPECT and DaTscan can assess dopamine transporter availability and dopaminergic integrity [106, 107]. Although DaTscan is not required in all patients, it may be useful when symptoms overlap with other neurological disorders or treatment response is unclear [107]. MRI may detect structural changes suggestive of Parkinsonian pathology [106]. EEG can detect neurophysiological alterations, and Waninger et al. reported differences between PD patients and controls in the anterior cingulate and temporal lobe, with beta-coherence alterations correlated with UPDRS scores and dopamine transporter activity [108].

2.3.4 Assessment Across Disease Progression

Because the clinical manifestations and assessment priorities of PD evolve throughout the disease course, no single examination can adequately characterize all phases of the disorder. Clinical evaluation and standardized rating scales remain central, but additional assessments may be required according to the presence of prodromal manifestations, diagnostic uncertainty, postural instability, motor complications, cognitive decline, autonomic dysfunction, or swallowing impairment. Table 2.1 summarizes the main clinical and instrumental assessments used across the progression of PD, distinguishing routinely performed evaluations from symptom-driven examinations and methods that are currently used mainly in research. The reported disease phases and Hoehn–Yahr stages should be regarded as approximate clinical categories, since progression is heterogeneous and individual assessments are not restricted to a single stage.

Table 2.1: **Clinical and instrumental assessments across Parkinson's disease progression.** The table summarizes the clinical manifestations and the main assessments used throughout the progression of Parkinson's disease. Hoehn–Yahr stages are approximate indicators of motor disability and do not represent rigid boundaries between disease phases.

Disease phase and approximate stage	**Typical clinical presentation**	**Main clinical assessments**	**Additional, instrumental, or research assessments**
At-risk or preclinical H&Y not applicable	No clinically detectable parkinsonism. Increased risk may be associated with pathogenic genetic variants, family history, environmental exposure, or biological markers.	Medical and family history, neurological examination, genetic counselling, and targeted genetic testing in selected familial or early-onset cases.	Longitudinal neurological monitoring, molecular imaging, advanced MRI, and α-synuclein seed-amplification assays in cerebrospinal fluid or peripheral tissues. Biological staging systems are currently intended primarily for research rather than routine population screening [109, 110].

Continued on the next page

Table 2.1 continued from the previous page

Disease phase and approximate stage	**Typical clinical presentation**	**Main clinical assessments**	**Additional, instrumental, or research assessments**
Prodromal H&Y not applicable	Possible REM sleep behaviour disorder, hyposmia, constipation, autonomic dysfunction, mood disturbances, or subtle motor abnormalities without established parkinsonism.	Targeted clinical history, neurological examination, non-motor symptom questionnaires, olfactory testing, REM sleep behaviour disorder screening, orthostatic blood pressure measurement and brief cognitive assessment.	Video-polysomnography for suspected REM sleep behaviour disorder, formal autonomic testing, and DAT-SPECT in selected diagnostically uncertain cases. Research approaches include the MDS prodromal probability criteria, digital assessment of gait, voice, sleep, and movement, and α-synuclein assays [109, 111, 112].
Early clinically manifest PD Approximately H&Y 1–2	Unilateral or bilateral bradykinesia, rigidity, and/or resting tremor without clinically evident postural instability. Activities of daily living are generally preserved.	Clinical evaluation according to the MDS diagnostic criteria, MDS–UPDRS, Hoehn–Yahr staging, assessment of treatment response, non-motor symptoms, activities of daily living, and cognitive screening such as the MoCA [95, 113, 114].	Structural MRI for differential diagnosis and DAT-SPECT when the diagnosis remains uncertain. Functional assessments may include the Timed Up and Go, 10-Metre Walk Test, and Mini-BESTest. Research approaches include force-platform posturography, centre-of-pressure analysis, instrumented gait, wearable sensors, surface EMG, and EEG during motor or postural tasks [112, 115].

Continued on the next page

Table 2.1 continued from the previous page

Disease phase and approximate stage	Typical clinical presentation	Main clinical assessments	Additional, instrumental, or research assessments
Middle or moderate PD Approximately H&Y 2.5–3	Bilateral motor involvement with emerging postural instability, impaired balance, falls, freezing of gait, increasing activity limitations, and possible motor fluctuations or dyskinesias.	Repeated MDS–UPDRS and Hoehn–Yahr assessment, evaluation in defined medication states, fall history, Timed Up and Go, Mini-BESTest or Berg Balance Scale, Freezing of Gait Questionnaire, activities-of-daily-living scales, and quality-of-life questionnaires [113, 114].	ON/OFF and dyskinesia diaries, orthostatic blood-pressure assessment, neuropsychological evaluation, and speech and swallowing screening. FEES or VFSS may be performed when dysphagia is suspected. Instrumental approaches include continuous wearable monitoring, posturography, gait analysis, stride variability, trunk stability, and quantitative muscle-activation assessment [112, 115, 116].
Advanced or complex PD Frequently H&Y 4–5	Severe mobility impairment, recurrent falls, freezing, prolonged OFF periods, troublesome dyskinesias, cognitive or psychiatric complications, autonomic dysfunction, dysphagia, and increasing caregiver dependence.	MDS–UPDRS, including Part IV, Hoehn–Yahr stage, Schwab and England Activities of Daily Living Scale, PDQ-39, motor-fluctuation diaries, medication review, and cognitive, psychiatric, nutritional, falls, and caregiver assessments [113, 114].	Screening for advanced therapies using indicators such as the 5–2–1 criteria, levodopa challenge, multidisciplinary neurological, neuropsychological, and neurosurgical assessment, and MRI for deep-brain-stimulation planning. FEES or VFSS may be used for dysphagia, whereas home-based technologies can monitor ON/OFF periods, dyskinesias, freezing, falls, sleep, and daily mobility [112, 116, 117].

Abbreviations: DAT-SPECT, dopamine-transporter single-photon emission computed tomography; EEG, electroencephalography; EMG, electromyography; FEES, fibreoptic endoscopic evaluation of swallowing; H&Y, Hoehn–Yahr; MDS–UPDRS, Movement Disorder Society–Unified Parkinson's Disease Rating Scale; MoCA, Montreal Cognitive Assessment; MRI, magnetic resonance imaging; PDQ-39, 39-item Parkinson's Disease Questionnaire; VFSS, videofluoroscopic swallowing study.

Note: Assessments are not exclusive to a single disease phase and should be selected according to the patient's clinical presentation. Clinical examination and longitudinal reassessment remain central throughout the disease course. Imaging, biological biomarkers, neurophysiological recordings, and digital measures are generally used for differential diagnosis, symptom-specific evaluation, treatment selection, or research purposes.

As summarized in Table 2.1, clinical examination and standardized scales provide the foundation for diagnosis and longitudinal monitoring, whereas neuroimaging, biological biomarkers, neurophysiological recordings, and digital technologies generally provide complementary information to support diagnosis, characterize disease progression, and quantify treatment-related or functional changes. Overall, the assessment of PD becomes progressively more multidimensional as motor, cognitive, autonomic, and functional complications emerge.

2.3.5 Therapeutic Approaches

Current PD treatments include supportive care, physical and occupational therapy, pharmacological treatment, and surgery. Levodopa®, or L-dopa, remains the main pharmacological treatment and aims to compensate for dopamine deficiency in the striatum. Most patients respond well to treatment [118], although treatment may become less effective over time, with increasing disability and reduced independence [119]. Nevertheless, newer therapeutic protocols have improved the quality of life for many patients with PD [118].

2.4 Postural Control Impairment in Early-Stage Parkinson's Disease

Although postural instability is traditionally associated with more advanced stages of PD, subtle alterations in balance regulation may already be present in early-stage disease. Patients in the first years of the disease may show inefficient motor coordination, reduced ability to adapt postural strategies, and difficulties maintaining the base of support under destabilizing conditions. These impairments may contribute to balance loss and falls even before the development of severe postural instability or before reaching Hoehn-Yahr stage III [120].

Early postural impairment may also involve inefficient ankle and hip strategies, suggesting compromised vestibular, proprioceptive, and sensorimotor integration mechanisms. Sensitive multimodal assessment protocols may therefore help identify subtle postural-control deficits and support targeted rehabilitation strategies. Interventions addressing postural weakness and impaired

sensory integration may contribute to compensating for altered vestibular and sensorimotor control mechanisms in PD [121].

Taken together, these findings indicate that postural-control alterations are clinically relevant even in early-stage PD, before severe balance disability becomes evident. Since conventional clinical scales may not fully capture subtle changes in balance regulation, instrumental assessment can provide complementary information on motor strategies, neuromuscular activation, and cortical involvement during postural tasks. For this reason, the following chapter introduces the main instrumental approaches used for early-PC assessment, including center of pressure, electromyography, and electroencephalography.

Chapter 3

BioVRSea: A Multimodal Paradigm for Quantitative Postural-Control Assessment

3.1 The BioVRSea Paradigm

The methodological foundations of the BioVRSea system originate from earlier investigations of postural control in which balance perturbations were induced through vibratory proprioceptive stimulation of the calf muscles while postural sway and cortical activity were recorded synchronously [122, 123]. In these studies, participants stood on a force platform while repeated mechanical vibrations challenged the proprioceptive contribution to upright stance. This experimental framework made it possible to characterise postural adaptation, defined as the initial modification of the motor response following the introduction of a perturbation, and habituation, reflected by the progressive adjustment of the response during repeated stimulation. Changes in postural performance were quantified through force-platform measurements, while electroencephalography was used to investigate the corresponding variations in cortical activity.
The first investigation combined posturographic measurements with high-density EEG spectral analysis, demonstrating that adaptation and habituation to repeated proprioceptive perturbations were accompanied by changes in cortical spectral power. The results also showed that visual information substantially influenced cortical recruitment: the eyes-open condition produced more widespread changes in EEG spectral power than the eyes-closed condition during both adaptation and habituation [122]. A subsequent EEG source-connectivity investigation extended these findings by examining the functional organisation and dynamic reconfiguration of the cortical networks involved in postural control. In the alpha band, the eyes-open condition was characterised predominantly by stronger frontal connectivity, whereas the absence of visual cues was associated with greater recruitment of right temporo-parietal and sensorimotor regions. Furthermore, the flexibility of cortical regions surrounding the right

temporo-parietal junction was associated with the complexity of postural sway, highlighting the importance of dynamic cortical reconfiguration in balance regulation [123].
Building on the methodological and physiological findings of both investigations [122, 123], the novel BioVRSea setup extends the study of postural adaptation from an isolated proprioceptive perturbation to a controlled multisensory environment. The system combines immersive virtual reality (VR) with a moving platform to reproduce controlled sea-motion conditions and evaluate postural-control responses during the simultaneous manipulation of visual, vestibular, and somatosensory information, as shown in Fig. 3.1. The moving platform generates controlled mechanical perturbations, while the immersive visual environment reproduces the perception of being on a small boat, creating a sensory-conflict condition that resembles exposure to maritime motion.

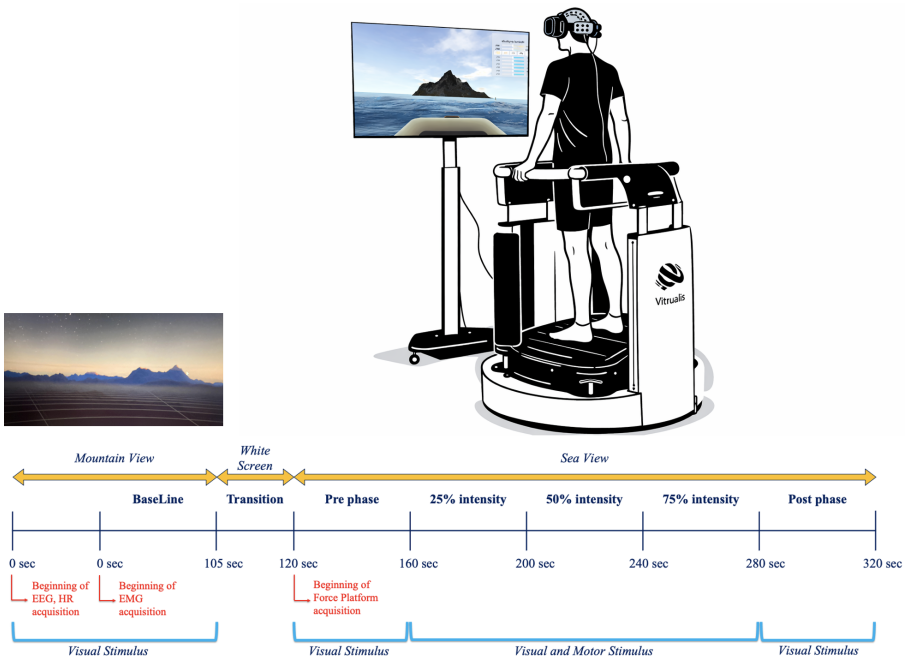


Figure 3.1: **Schematic representation of the BioVRSea experimental setup and protocol.** Participants stood on the instrumented moving platform while wearing a virtual-reality headset and multimodal acquisition equipment. The protocol included a 105-s baseline with a static mountain scene, a 15-s white-screen transition, and a 40-s pre-motion phase with sea visualization and no platform movement. This was followed by three 40-s motion phases at 25%, 50%, and 75% intensity and a final 40-s post-motion phase with the platform stationary. EEG, heart-rate, and EMG recordings began at baseline, while force-platform acquisition started during the pre-motion phase.

One of the first functional applications of BioVRSea involved North Atlantic

sailors. In this context, the system was not employed as a training platform, but as an experimental paradigm to investigate postural-control adaptation in individuals routinely exposed to demanding maritime conditions. Owing to their professional experience and repeated exposure to sea motion, sailors represented a highly adapted reference population for evaluating the postural responses elicited by the simulated maritime environment. This application therefore provided an initial demonstration of the ability of BioVRSea to characterise postural adaptation strategies under ecologically relevant multisensory perturbations.

3.1.1 Motion Sickness and Sensory-Conflict Framework

Following the initial maritime application, BioVRSea was further adapted as an experimental paradigm for the evaluation of motion sickness and postural control in the general population. Motion sickness is a common condition experienced during passive transportation and is generally described as a sensation of sickness or discomfort, with symptoms such as nausea, vomiting, sweating, facial pallor, and dizziness. According to the sensory-conflict theory, motion sickness can arise from a mismatch between visual, vestibular, and somatosensory inputs [124, 125]. This mismatch may occur during passive locomotion, such as travelling by car or boat, when vestibular information does not correspond to the expected visual input. A similar conflict can also be induced in VR environments, where visual motion is perceived while the vestibular system does not provide a corresponding motion signal.
Within the BioVRSea paradigm, sensory conflict is experimentally reproduced by combining sea-wave visual stimulation with controlled platform motion. The virtual environment and moving platform can be configured by the operator according to the experimental protocol. Simulated sea-wave frequencies can be adjusted between 0.5 and 3 Hz, while the wave-amplitude setting can be varied from 0 to 2. The intensity of the corresponding physical platform movement can be scaled up to 75% or 100% of the maximum available motion. Physiological responses are acquired through a synchronized multimodal recording system comprising a 64-channel EEG system for cortical activity, six wireless surface EMG sensors for bilateral lower-limb muscle activity, and a force platform for the measurement of CoP displacement. The EMG sensors are distributed bilaterally over the tibialis anterior, lateral gastrocnemius, and soleus muscles, allowing the muscular responses of both legs to be monitored throughout the experimental conditions. This integrated acquisition system enables the simultaneous evaluation of the temporal evolution of cortical, neuromuscular, and postural responses. The configuration of the EEG, EMG, and CoP acquisition systems and the corresponding sensor placement are illustrated in Fig. 3.2.
Previous studies have also reported associations between motion-sickness severity and physiological biosignals, including EEG, skin conductance, heart rate, blood pressure, and body temperature [126]. Therefore, BioVRSea allows motion-sickness symptoms to be evaluated alongside postural-control responses and biosignal dynamics, supporting the construction of individualized multi-

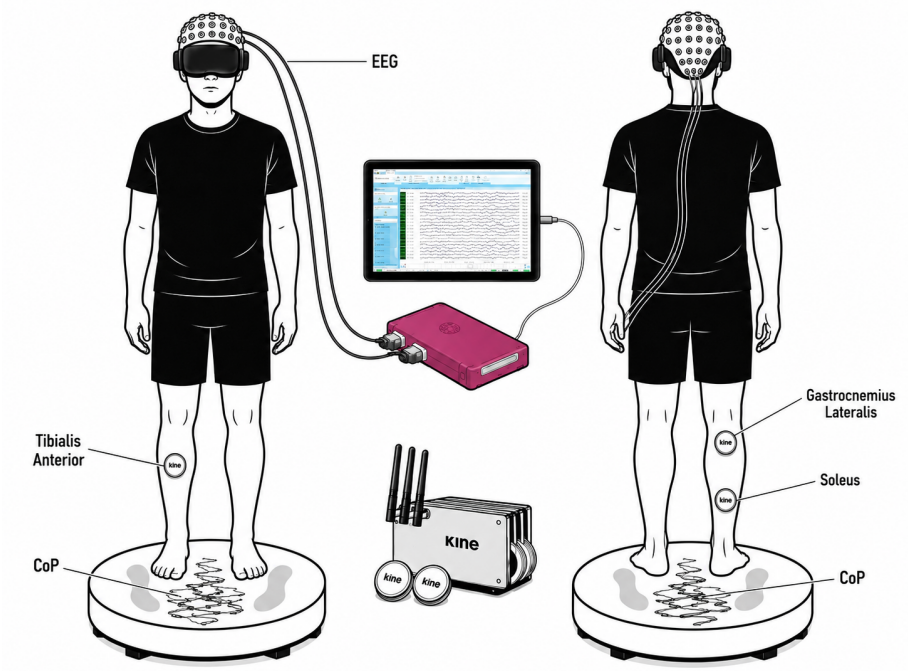


Figure 3.2: **BioVRSea multimodal acquisition system and sensor placement.** Anterior and posterior views illustrate the 64-channel EEG cap worn together with the virtual-reality headset, the bilateral placement of six wireless surface EMG sensors over the tibialis anterior, lateral gastrocnemius, and soleus muscles, and the force-platform measurement of centre-of-pressure (CoP) displacement. The EEG amplifier and wireless EMG acquisition unit are also shown.

metric profiles that integrate lifestyle information, symptom reports, participant characteristics, and objective physiological features.

The experimental protocol, schematically represented in Fig. 3.3, was divided into six consecutive segments: baseline (BL), pre-phase (PRE), three moving-platform phases corresponding to 25%, 50%, and 75% of the maximal wave amplitude, and post-phase (POST). During BL, participants stood quietly on the platform, with their arms relaxed at their sides, while observing a static mountain-view scene, with the platform still. This phase was followed by PRE, during which participants continued standing without holding the support bars while observing the sea-wave visual simulation. During this phase, the platform remained still, and only visual stimulation was provided.

After the initial visual-stimulation phase, participants were instructed to hold onto the bars positioned in front of them. The platform then started to move in synchrony with the sea-wave scene displayed in the VR goggles, producing combined visual and motor stimulation. Platform movement was progressively

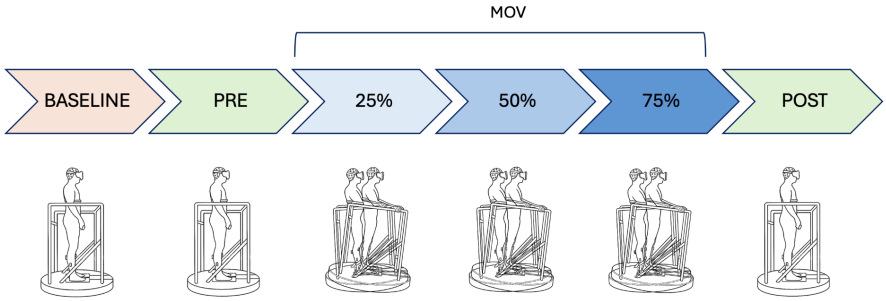


Figure 3.3: **Schematic representation of the BioVRSea experimental protocol.** The protocol consists of baseline (BL), pre-phase (PRE), three moving-platform phases corresponding to 25%, 50%, and 75% of the maximal wave amplitude, and post-phase (POST). The three moving-platform stimulation phases are collectively referred to as the MOV phase.

increased across three consecutive stimulation phases corresponding to 25%, 50%, and 75% of the maximal wave amplitude, each lasting 40 seconds. These three moving-platform phases are collectively referred to as the MOV phase. During this central part of the protocol, participants held the bars while continuing to observe the sea simulation.
At the end of the 75% phase, the platform motion ceased, and the POST phase began. Participants were asked to release the bars, relax their arms along their bodies, and remain standing as still as possible for the final 40 seconds of the experiment. During this phase, the sea-wave visual stimulus continued while the platform remained still, allowing the assessment of postural readaptation immediately after motor stimulation. The PRE and POST phases were particularly relevant for evaluating how different populations maintained unassisted standing under sensory-conflict conditions before and after exposure to the complex postural-control task generated by the combined moving platform and VR scene [127].
Throughout the protocol, multiple biosignals were recorded, including EEG, EMG, CoP, and cardiac activity. This design allows the assessment of postural responses during static visual exposure, visual sensory conflict, combined visual-motor stimulation, and postural readaptation after platform motion. Several recent studies have highlighted the relevance of the BioVRSea setup for cohort differentiation and pathological assessment [128, 129].

Questionnaire Before the experimental session, each participant completed a structured questionnaire designed to collect demographic, clinical, lifestyle, neurological, motion-sickness-related, and family-history information. The questionnaire included general background variables such as age, gender, height, weight, handedness, physical activity, nicotine use, caffeine intake, alcohol consumption, self-perceived health status, visual impairments, restricted mobility, vestibular or dizziness-related disorders, migraine, hypertension, previous

motion sickness, family history of migraine or motion sickness, and current medication use. Participants also answered questions adapted from Golding's Motion Sickness Susceptibility Questionnaire (MSSQ) [130], which assessed previous experiences of motion sickness across different transport and recreational conditions, including cars, buses, trains, aircraft, small boats, ships, playground swings, roundabouts, and funfair rides.

Based on the questionnaire responses, several descriptive indices previously applied in studies using the BioVRSea system can be derived [129]. The Lifestyle Index summarizes general lifestyle and health-related factors, including Body Mass Index (BMI), physical activity, and nicotine, caffeine, and alcohol consumption, all of which may influence overall physiological condition. The Proneness Index quantifies individual susceptibility to motion sickness by considering how frequently participants reported feeling sick or nauseated in different transport and recreational situations. In addition, symptom changes induced by the VR exposure can be summarized using indices calculated from the difference between symptom ratings collected before and after the experiment. The Physiological/Vegetative (PHY) index is based on symptoms mainly related to autonomic responses, including general discomfort, increased salivation, sweating, and nausea. The Neurological/Muscle Strain (NEURO) index includes symptoms more closely related to neurological or strain-related responses, such as general discomfort, fatigue, headache, blurred vision, and dizziness.

Immediately before and after exposure to the BioVRSea virtual-reality environment, participants rated their current symptoms using a four-point severity scale ranging from 0 to 3, corresponding to no symptoms, mild symptoms, moderate symptoms, and severe symptoms. The assessed symptoms included general discomfort, fatigue, headache, eye strain, difficulty concentrating, increased salivation, sweating, nausea, blurred vision, and dizziness. These pre–post ratings can also be used to calculate the BioVRSea Effect Index (BVSEI), which quantifies whether participants experienced one or more symptom changes following the VR simulation. This index allows participants to be classified according to the presence or absence of a measurable subjective response to the BioVRSea stimulation.

Although motion-sickness-related indices are not the primary focus of the present thesis, they provide relevant contextual information for the interpretation of individual responses to the BioVRSea paradigm and have been used in previous studies involving this system. This information is particularly relevant when studying populations with neurological or neurodegenerative conditions, in which altered sensory integration and impaired postural stability may influence both balance control and subjective symptom responses during visually and mechanically demanding tasks.

3.1.2 Initial Application in Seafarers

The first application of the BioVRSea paradigm was conducted in seafarers, a population repeatedly exposed to unstable support surfaces and complex visual, vestibular, and somatosensory demands. This study was first presented

at the CMBBE 2024 Symposium and subsequently expanded in the IEEE MetroXRAINE 2025 proceedings. In this thesis, the study serves as the initial functional application of BioVRSea, demonstrating that the paradigm can detect postural control adaptation in individuals exposed to challenging real-world environments. Since the experiment reproduced boat-like motion through the combined use of virtual reality and a moving platform, professional sailors provided an ecologically relevant reference population. Their extensive experience and training in unstable maritime environments allowed them to serve as a high-performance benchmark for postural adaptation, offering a more informative comparison than healthy controls without specific exposure to such conditions.

The study compared 21 male sailors with a matched group of 21 healthy male controls. The sailors had spent three weeks at sea and were tested immediately upon returning to shore, allowing assessment of postural responses following recent and prolonged maritime exposure. The control subgroup was selected from a larger cohort of healthy participants using Mahalanobis distance matching based on height, weight, and body mass index to reduce potential anthropometric bias between groups. All participants had no history of neurological conditions or balance disorders.

Center-of-pressure analysis showed that seafarers exhibited a more dynamic postural control profile than healthy controls. As illustrated in Fig. 3.4, the mean CoP ellipses differed between groups during both the adaptation and habituation phases, with the major axis reflecting anteroposterior sway and the minor axis reflecting mediolateral sway.

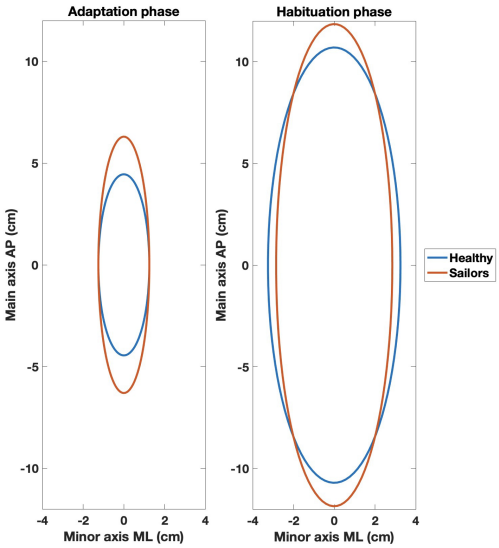


Figure 3.4: **Center-of-pressure ellipses in the initial seafarer application of BioVRSea.** Mean CoP ellipses are shown for healthy controls and sailors during the adaptation and habituation phases. The major axis represents anteroposterior sway, whereas the minor axis represents mediolateral sway.

During the adaptation phase, sailors showed higher total excursion and mean velocity in the anteroposterior direction, together with increased entropy and complexity measures. These findings suggest that the greater sway observed in sailors should not be interpreted simply as impaired stability, but rather as a flexible postural strategy shaped by repeated exposure to unstable maritime environments. Electromyographic analysis provided complementary evidence of neuromuscular adaptation. Although several EMG features showed trends toward significance before correction, only the skewness of the right soleus during the adaptation phase remained statistically significant after Bonferroni correction. As shown in Fig. 3.5, sailors displayed more positive skewness values than healthy controls. Since positive skewness indicates predominantly low-intensity activity interrupted by occasional high-intensity bursts, this result suggests a selective, ankle-based strategy rather than generalized lower-limb overactivation. Overall, the seafarer study provided an initial demonstration that BioVRSea is sensitive to experience-dependent postural-control strategies. Importantly, the findings indicate that increased sway is not necessarily pathological, but may reflect adaptive flexibility when it occurs in individuals trained by repeated exposure to unstable environments. This observation was important for the subsequent clinical application of BioVRSea because it established the paradigm as a multimodal framework capable of distinguishing adaptive postural strategies from altered or constrained postural responses, such as those investigated later in Parkinson's disease.

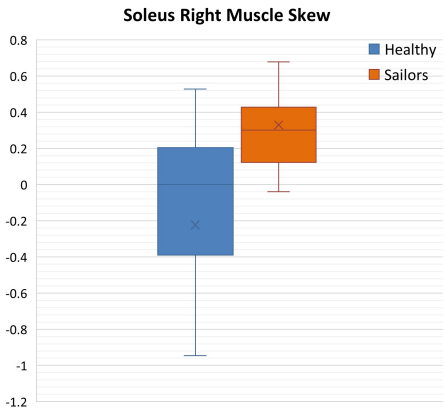


Figure 3.5: **Right soleus skewness during the adaptation phase.** Boxplots show the distribution of right soleus EMG skewness in healthy controls and sailors. Sailors showed higher skewness values, suggesting a pattern of low-intensity background activity combined with intermittent high-intensity corrective bursts during BioVRSea stimulation.

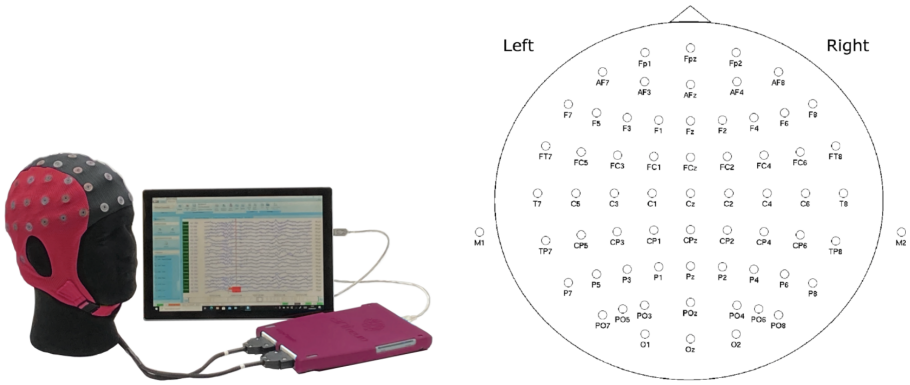
3.1.3 Data Acquisition

3.1.3.1 Virtual Reality System

The virtual environment was generated using software from Virtualis (Clapiers, France) and displayed through VIVE Focus VR goggles (HTC, New Taipei, Taiwan). The VR scenarios were designed to provide controlled visual stimulation during the different phases of the BioVRSea protocol. The VR goggles allowed participants to experience the visual scene immersively while maintaining a standing posture on the platform. Head motion was tracked through the headset's integrated sensors, enabling real-time interaction with the virtual environment and preserving the natural relationship between head movements and visual perspective.

3.1.3.2 Electroencephalography

EEG data were recorded using a 64-channel WaveGuard EEG cap (CA-201; ANT Neuro, Hengelo, The Netherlands) connected to the ANT Neuro eego amplifier (EE-2XX; ANT Neuro, Hengelo, The Netherlands), as shown in Fig 3.6a. Signals were acquired with a sampling frequency of $F_s = 4096$ Hz. Electrode placement followed the international 10–10 system (Fig. 3.6b).



(a) EEG setup (b) Channels location

Figure 3.6: **EEG acquisition system and electrode montage.** (a) EEG recording setup including the electrode cap, acquisition unit, and computer interface used for real-time monitoring of the recorded signals. (b) Spatial distribution of the EEG electrodes according to the extended 10–10 system, showing the left and right hemispheric positions and the mastoid electrodes M1 and M2.

The EEG cap was connected to the amplifier, which interfaced with a tablet for data acquisition. The amplifier design supports reliable coupling between the cap and the recording system through very high input impedance (> 1 GΩ) and active shielding technology. These features allow stable EEG recording

even when electrode–scalp impedance values are relatively high. Electrode contact was ensured by applying conductive gel to each electrode using a blunt-needle syringe, in order to reduce impedance between the scalp and the electrodes. Electrode impedances below 40 kΩ were considered acceptable for data acquisition. This threshold is consistent with the specifications of the ANT Neuro eego amplifier used in the BioVRSea setup, for which high-quality EEG signals can be maintained even at relatively high impedance levels [131]. In addition, the preprocessing pipeline was designed to attenuate noise related to electrode-contact variability, ensuring that data quality remained adequate for subsequent analyses, including source reconstruction.

Processing A standardized preprocessing pipeline was applied across all EEG studies to improve signal quality while preserving physiologically relevant neural activity. EEG preprocessing was performed using the EEGLAB MATLAB toolbox. The pipeline aimed to reduce non-neural contributions, including ocular artifacts, movement-related noise, and power-line interference. Each recording was visually inspected to ensure signal quality and to adapt preprocessing steps when required. EEG recordings were downsampled from the original acquisition frequency to 1024 Hz. Signals were then band-pass filtered between 1 and 45 Hz to retain the frequency components of interest while removing slow signal drifts and high-frequency noise. Channels exhibiting abnormal activity, including flat signals or low correlation ($< 60\%$) with neighboring channels, were identified and removed. Initial artifact attenuation was performed using the Artifact Subspace Reconstruction (ASR) algorithm [132]. Following artifact reduction, Independent Component Analysis (ICA) was performed using the PICARD algorithm [133]. This approach was selected because of its robustness and computational efficiency when processing high-density EEG recordings acquired during dynamic experimental conditions. Independent components associated with non-neural sources, including ocular and muscular artifacts, were identified and rejected. Previously removed noisy channels were subsequently reconstructed through interpolation. Mastoid electrodes (M1 and M2), together with PO5 and PO6 electrodes, which were more susceptible to neck-related muscular activity during postural tasks, were excluded from further analyses. Finally, EEG data were interpolated to a common 61-channel configuration and re-referenced using the average reference method. After preprocessing, EEG signals were analyzed using complementary approaches in both the temporal and spectral domains. Time-domain analyses were performed to investigate variations in signal amplitude, temporal dynamics, and EEG microstate characteristics, whereas frequency-domain analyses were conducted to characterize oscillatory activity within conventional EEG frequency bands, including delta, theta, alpha, beta, and gamma ranges. Analyses were performed both at the single-electrode level and by grouping electrodes according to their corresponding cortical regions, allowing the investigation of localized and region-specific patterns of neural activity. Table 3.1 summarizes the EEG frequency bands and cortical regions considered in this thesis.

Table 3.1: **EEG frequency bands and cortical regions.** Summary of the functional relevance of the EEG frequency bands and cortical regions considered in the analyses.

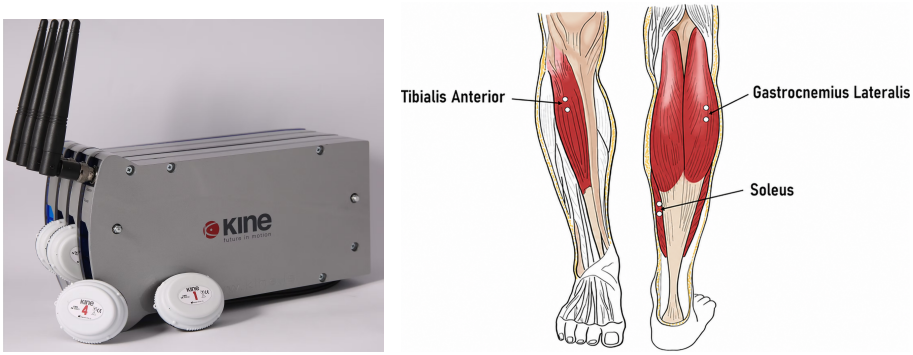
Name	Significance
FREQUENCY BANDS	
DELTA	The slowest EEG activity, predominantly associated with deep sleep and large-scale cortical synchronization. During wakefulness, delta activity may reflect slow regulatory processes, attentional engagement, and the integration of internal and external information. Interpretation during postural tasks requires caution because this frequency range can also be influenced by eye movements, body movement, and signal drift.
THETA	Associated with working memory, cognitive control, error monitoring, emotional processing, and spatial orientation. Increased theta activity may indicate greater cognitive effort and attentional demand during challenging balance conditions or during the adaptation to unfamiliar sensory environments.
ALPHA	Prominent during relaxed wakefulness, particularly with the eyes closed. Alpha activity is involved in cortical inhibition, sensory gating, and the regulation of attentional resources. Alpha suppression, or desynchronization, is commonly associated with increased visual, cognitive, and sensorimotor engagement during postural control.
BETA	Associated with active cortical processing, sustained attention, motor planning, and the maintenance of the current sensorimotor state. Changes in beta synchronization and desynchronization are related to movement preparation, movement execution, and the cortical regulation of postural adjustments.
LOW GAMMA	Higher-frequency activity associated with local cortical processing, multisensory integration, feature binding, and the coordination of complex sensorimotor information. Low-gamma modulation may reflect the integration of visual, vestibular, and proprioceptive inputs during dynamic postural control, although this band is particularly sensitive to contamination from cranial and neck-muscle activity.
CORTICAL REGIONS	
FRONTAL	Higher-order cognitive functions, including attention, planning, judgment, inhibition, emotional regulation, and executive control
TEMPORAL R&L	Associative functions, including memory processing, emotion, and auditory-related processing
PARIETAL	Somatosensory processing and integration of sensory information from muscles and skin
OCCIPITAL	Visual processing and visual association functions involved in object recognition and spatial interpretation

The investigated frequency bands represent different components of neural oscillatory activity associated with distinct functional processes, including slow-wave activity (delta), cognitive and sensorimotor processing (theta and alpha), active cortical engagement (beta), and higher-frequency integration processes (gamma). Cortical regions were grouped into frontal, temporal, parietal, and occipital areas to evaluate activity associated with executive processing, associative functions, somatosensory integration, and visual processing, respectively.

3.1.3.3 Electromyographic Data Acquisition and Pre-Processing

Lower-limb muscle activity was recorded using six wireless KineLive EMG sensors (Kiso ehf, Reykjavik, Iceland), sampled at $F_s = 1600$ Hz, as shown in Fig. 3.7a. Sensors were positioned bilaterally over the tibialis anterior (TA), gastrocnemius lateralis (GL), and soleus (S) muscles, resulting in recordings from the right and left TA, GL, and S muscles (Fig. 3.7b). These muscles were

selected because of their role in ankle stabilization and postural control during quiet standing and platform-induced perturbations. The sensors were placed on the skin surface over the corresponding muscle bellies to capture activation patterns associated with postural adjustments across the experimental protocol. The EMG signals were divided into four experimental phases: BL, PRE, MOV, and POST, based on predefined time intervals.



(a) Wireless surface electromyography acquisition system

(b) Lower-leg muscles monitored during electromyographic recording

Figure 3.7: **EMG acquisition system and sensors placement.** (a) The image shows the Kine wireless EMG device and sensor units used for recording lower-limb muscle activity during the experimental protocol. (b) The tibialis anterior, gastrocnemius lateralis, and soleus are highlighted, with white markers indicating approximate electrode placement sites.

Processing EMG data processing was performed in MATLAB. Signals were bandpass filtered using a fourth-order Butterworth filter (20–500 Hz) to retain the relevant neuromuscular frequency components. Power line interference and its harmonics at 50 Hz were attenuated using a series of notch filters. Amplitude thresholding was then applied to identify and remove extreme values, and spline interpolation was used to reconstruct missing segments.
The processed EMG signals were rectified, and a 100-ms moving window was used to compute the root mean square envelope. Normalization was performed by scaling both the filtered and enveloped signals to the maximum peak amplitude observed across all phases for each subject and muscle. This approach ensured comparability between phases while preserving within-subject variability.
Finally, time-domain and frequency-domain features were extracted from the preprocessed signals to characterize muscular responses during static visual stimulation, combined visual-motor stimulation, and postural readaptation following platform motion. Spectral analysis was conducted using both Fast Fourier Transform and Welch's method to extract power spectral density, peak

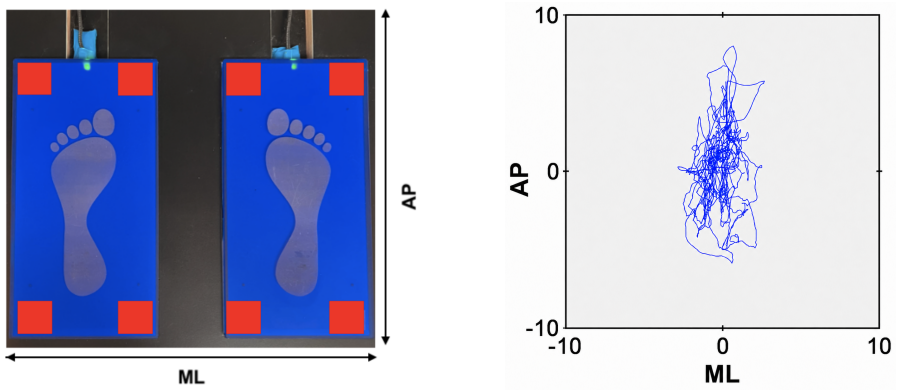
frequency, and median frequency. The EMG features extracted from the signals are detailed in Table 3.2.

Table 3.2: **EMG features extracted from the preprocessed signals.** The table summarizes the time-domain and frequency-domain parameters used to characterize lower-limb muscle activity across the experimental phases.

Name	Definition
	TIME PARAMETERS
AAC	Average Amplitude Change
AE	Average Energy
ASM	Absolute Value of the Summation of the Exponential Root
ASS	Absolute Value of the Summation of the Square Root
CV	Coefficient of Variation
DAMV	Difference Absolute Mean Value
DASDV	Difference Absolute Standard Deviation Value
DVARV	Difference Absolute Standard Deviation Value
EMAV	Enhanced Mean Absolute Value
EWL	Enhanced Wavelength
FZC	New Zero Crossing
KURT	Kurtosis
IEMG	Integrated EMG
IQR	Interquartile Range
LCV	Log Coefficient of Variation
LD	Log Detector
LDAMV	Log Difference Absolute Mean Value
LDASDV	Log Difference Absolute Standard Deviation
L-Moments	L-mean: Mean of the sorted signal L-scale: Scale or dispersion of the data L-skewness: Asymmetry via linear combinations L-kurtosis: Peakedness or flatness of distribution
LTKEO	Log Teager Kaiser Energy Operator
MAD	Mean Absolute Deviation
MAV	Mean Absolute Value
MFL	Maximum Fractal Length
MN	Mean
MD	Median
MMAV	Modified Mean Absolute Value
MMAV2	Modified Mean Absolute Value 2
MSR	Mean Value of the Square Root
Poincaré	S1: Short-term variability from Poincaré Plot S2: Long-term variability from Poincaré Plot RatioSD: Ratio variability
RMS	Root Mean Square
SD	Standard Deviation
SKEW	Skewness
SSI	Single Square Integral
TM	Temporal Moment
VAR	Variance
VARE	Variance of EMG
VO	V-Order
WL	Waveform Length
	FREQUENCY PARAMETERS
PT	Total Power
Pmax	Maximum Power
Fmax	Maximum Frequency
FMD	Median Frequency
FMN	Mean Frequency
Fkurt	Frequency Kurtosis
Fskew	Frequency Skewness

3.1.3.4 Center of Pressure Data Acquisition and Pre-Processing

Postural sway was assessed using a force platform integrated into the BioVRSea moving platform (Virtualis, Clapiers, France). The platform consisted of two independent foot platforms, each equipped with force sensors positioned beneath the support surface. Four force sensors were used to record the distribution of vertical forces under the feet at a sampling frequency of $F_s = 90$ Hz. These measurements were used to estimate the center of pressure (CoP), which represents the point of application of the resultant ground-reaction force and provides an indirect measure of postural sway. During the experiment, the moving platform was synchronized with the virtual sea scenario displayed on the VR headset, enabling assessment of postural responses under controlled sensory-conflict conditions.



(a) Force Platform (b) Sway pattern

Figure 3.8: **Force-platform configuration and representative center-of-pressure trajectory.** (a) Top view of the two independent foot platforms integrated into the BioVRSea moving platform, with the force-sensor locations highlighted in red. The anteroposterior (AP) and mediolateral (ML) directions are indicated. Vertical force measurements were acquired at a sampling frequency of $F_s = 90$ Hz and used to estimate the center of pressure (CoP). (b) Representative CoP trajectory in the AP–ML plane, illustrating postural sway during the experimental conditions. The platform was synchronized with the virtual sea scenario displayed through the VR headset, enabling the assessment of postural responses under controlled sensory-conflict conditions.

Processing CoP trajectories were computed along the anteroposterior (AP) and mediolateral (ML) directions throughout the experimental protocol. The resulting stabilogram represented the projection of the participant's body sway onto the support surface and was used to quantify postural control during baseline, visual stimulation, combined visual-motor stimulation, and postural readaptation.

AP and ML CoP components were extracted, smoothed with a Savitzky-Golay filter, and converted to centimeters using the platform dimensions. To reduce inter-subject variability, CoP signals were preprocessed through centering and normalization. Centering involved subtracting the mean from each ML and AP time series, yielding zero-mean trajectories used to compute spatiotemporal features, including total excursion, mean and root mean squared distances, mean sway velocity, root distance, and RMS values in both directions. Additional features included trajectory extremes, expressed as magnitude and angle in cardinal directions, statistical measures, including standard deviations of CoP magnitude and direction, and geometric descriptors derived from ellipse fitting using Principal Component Analysis.
Normalization was performed by applying z-score scaling to the CoP time series within each phase, separately for each subject. The first difference of the normalized signals was then used to compute entropy-based features, including Sample Entropy, Multiscale Entropy, and Complexity Indices, both univariate and multivariate. The CoP features extracted from the signals are detailed in Table 3.3.

Table 3.3: **CoP features extracted from the preprocessed signals.** The table summarizes the time-domain, entropy-based, geometric, fractal, and spectral parameters used to characterize postural sway across the experimental phases.

Name	Definition
TIME PARAMETERS	
TOTEX	Total excursion on the support plane
TOTEX-ML	Total excursion on the mediolateral plane
TOTEX-AP	Total excursion on the anteroposterior plane
RD	Square root distance between a point and the plane origin
MDIST-ML	Mean distance in the mediolateral direction
MDIST-AP	Mean distance in the anteroposterior direction
MVELO	Mean velocity on the support plane
MVELO-ML	Mean velocity on the mediolateral plane
MVELO-AP	Mean velocity on the anteroposterior plane
RDIST	Root mean square distance with respect to the origin
RDIST-ML	Root mean square distance in the mediolateral direction
RDIST-AP	Root mean square distance in the anteroposterior direction
ML-SampEn	Mediolateral Sample Entropy
AP-SampEn	Anteroposterior Sample Entropy
ML-CI	Mediolateral Complexity Index
AP-CI	Anteroposterior Complexity Index
Ellipse Area	Area of the 95% confidence ellipse
Ellipse Angle	Angle between the main axis of the 95% confidence ellipse and the mediolateral axis
Ellipse Main Axis Length	Length of the main axis of the 95% confidence ellipse
Ellipse Minor Axis Length	Length of the minor axis of the 95% confidence ellipse
SD AP	Standard deviation in the anteroposterior direction
SD ML	Standard deviation in the mediolateral direction
SD Magnitude	Standard deviation of the distance of points with respect to the origin
SD Direction	Standard deviation of the angle difference between successive points with respect to the mediolateral axis
Magnitude Entropy	Sample Entropy of the distance of points with respect to the origin
Direction Entropy	Sample Entropy of the angle difference between successive points with respect to the mediolateral axis

Continued on next page

Table 3.3: **CoP features extracted from the preprocessed signals.** Continued.

Name	Definition
Multivariate CI	Sum of Sample Entropy values computed across increasing time scales on the multivariate ML-AP series
Antero Magnitude	Magnitude of the furthest point in the anterior portion of the plane
Antero Angle	Angle of the furthest point in the anterior portion of the plane
Postero Magnitude	Magnitude of the furthest point in the posterior portion of the plane
Postero Angle	Angle of the furthest point in the posterior portion of the plane
Left Magnitude Maximum	Magnitude of the furthest point in the left portion of the plane
Left Angle	Angle of the furthest point in the left portion of the plane
Right Magnitude Maximum	Magnitude of the furthest point in the right portion of the plane
Right Angle	Angle of the furthest point in the right portion of the plane
RMS AP	Root mean square of displacement in the anteroposterior direction
RMS ML	Root mean square of displacement in the mediolateral direction
Fractal Higuchi ML	Fractal dimension computed using the Higuchi method on the mediolateral trajectory
Fractal Higuchi AP	Fractal dimension computed using the Higuchi method on the anteroposterior trajectory
SPECTRAL FEATURES	
Total Power	Total power of the signal in the frequency domain, computed as the area under the PSD curve
Mean Frequency	Weighted average frequency based on the power distribution
Median Frequency	Frequency dividing the spectrum into two equal-power halves
Spectral Variance	Variance of the power distribution around the mean frequency
Peak Frequency	Frequency at which the maximum power occurs
Total Power ML	Total spectral power in the mediolateral axis
Mean Frequency ML	Mean frequency in the mediolateral axis
Median Frequency ML	Median frequency in the mediolateral axis
Spectral Variance ML	Spectral variance in the mediolateral axis
Peak Frequency ML	Peak frequency in the mediolateral axis
Total Power AP	Total spectral power in the anteroposterior axis
Mean Frequency AP	Mean frequency in the anteroposterior axis
Median Frequency AP	Median frequency in the anteroposterior axis
Spectral Variance AP	Spectral variance in the anteroposterior axis
Peak Frequency AP	Peak frequency in the anteroposterior axis

3.1.4 Statistical Analysis

Electroencephalography dynamic functional connectivity The statistical analysis was conducted to investigate the effects of the BNSs and subject group on occurrence, duration, and coverage across different phases of the experimental protocol. The study utilized a Linear Mixed Model (LMM) approach to account for the hierarchical structure of the data, where repeated measures within subjects were nested within the levels of the BNS factor. The primary objective was to ascertain any significant main effects and interactions between the subject group (PD vs. CTR) and the BNSs.
Model fit was assessed by examining model summary statistics, including coefficients, standard errors, and p-values derived from likelihood ratio tests. Additionally, an analysis of variance (ANOVA) was performed to assess the overall significance of the fixed effects in the model. To further elucidate significant effects identified by the primary analysis, post-hoc pairwise comparisons were conducted using estimated marginal means. These comparisons aimed to delineate differences in the specific metrics between specific levels of the BNSs

factor within each subject group across different experiment phases. To mitigate the risk of Type I errors arising from multiple pairwise comparisons, p-values were adjusted using the Benjamini-Hochberg method. This method controls the False Discovery Rate (FDR) and helps maintain the overall integrity of statistical inference.
Results were visually represented through empirical cumulative distribution functions and pairs plots to illustrate the distributional properties of the data and highlight significant differences between experimental conditions.

Electroencephalography and Center of Pressure Statistical analyses of EMG and CoP features were performed to identify differences between the subject groups (PD and CTR; Sailors and CTR) across the experimental phases. For each feature, data normality was assessed using the Shapiro–Wilk test with a significance level of $\alpha = 0.05$. Features that satisfied the normality assumption were analyzed using independent two-sample t-tests, whereas features that violated normality were analyzed using the Mann–Whitney U test.
To account for multiple comparisons, Bonferroni correction was first applied to the p-values obtained from the univariate statistical tests, adjusting the significance threshold according to the number of comparisons performed within each dataset. In addition, the Benjamini–Hochberg false discovery rate procedure was applied to the combined set of p-values to obtain corresponding q-values. This procedure was used to reduce the likelihood of type I errors while retaining sensitivity to potentially relevant group differences across EMG and CoP features.

3.2 Ethical Approval and Consent

The studies included in this thesis were conducted using data collected from three participant cohorts: healthy control volunteers, experienced sailors recruited through Samherji hf. (Akureyri, Iceland), and individuals with Parkinson's disease.
Prior to participation, all individuals received written information describing the aims, procedures, and requirements of the study. Written informed consent was obtained from all participants before any experimental procedures were performed. All research activities were conducted in accordance with the ethical principles of the Declaration of Helsinki and in compliance with applicable Icelandic statutory requirements. The study protocol was approved by the Icelandic National Bioethics Committee (approval No. VSN-20-101). A subsequent amendment was approved to include the Parkinson's disease cohort (Amendment No. VSN-20-101-V2).
This work was supported by RANNIS, the Icelandic Research Fund through the Grant of Excellence No. 239612-051, and by the Research Fund of Landspitali University Hospital. Their financial support is gratefully acknowledged.

Chapter 4

Multimodal Assessment of Postural Control Adaptation in Early-Stage Parkinson's Disease

The material presented in this chapter is adapted from the peer-reviewed article "Adaptation strategies and neurophysiological response in early-stage Parkinson's disease: BioVRSea approach," published in *Frontiers in Human Neuroscience* in 2023. The original study was the first application of the BioVRSea system to the investigation of postural control in early-stage PD.
The chapter focuses on assessing postural-control adaptation during a complex sensory-conflict task. Specifically, it examines how individuals with early-stage PD responded to visual and mechanical stimulation compared with healthy controls through the analysis of CoP, EMG, and EEG signals. By integrating postural, muscular, and cortical responses, the original study investigated whether BioVRSea could reveal altered adaptation strategies and neurophysiological patterns associated with early-stage PD.

4.1 Introduction

The general clinical characteristics of PD, its diagnostic framework, the physiological mechanisms underlying postural control, and the BioVRSea paradigm have been described in the preceding chapters. The present chapter therefore focuses specifically on the rationale for using a controlled multisensory challenge to investigate postural adaptation in individuals with early-stage PD.
PD is characterized by progressive motor and non-motor alterations, with bradykinesia, rigidity, tremor, gait impairment, and postural instability among its principal motor manifestations [34, 99]. Its global burden has increased markedly over recent decades [134], while the identification of early-stage disease remains challenging because subtle manifestations may overlap with age-related changes [135, 136]. Clinical assessment therefore integrates disease staging and established diagnostic criteria [98, 137], together with quantitative and

instrumental approaches intended to improve the objective characterization of the disease.

A range of potential biological and neurophysiological markers has consequently been explored. These include blood-based molecular profiles [138], structural, metabolic, and dopaminergic neuroimaging [106, 139], and transcranial sonography [140]. EEG provides complementary information on neurophysiological activity and on alterations in cortical and cortico-subcortical organization [108]. Oscillatory activity within the delta, theta, alpha, and beta frequency bands has been investigated as a potential marker of neurological dysfunction [141–143], with resting-state studies in PD generally indicating a shift toward slower activity, including increased delta and theta activity and reduced alpha and beta activity [144–150]. However, resting-state recordings provide limited information about how these neural dynamics change when postural regulation is actively challenged.

This distinction is particularly relevant because postural control depends on the continuous integration and reweighting of visual, vestibular, and somatosensory information together with appropriate muscular and central nervous-system responses. EEG studies performed during postural perturbations have shown task-related changes particularly across frontal, central, and parietal regions, involving oscillatory activity associated with attention, postural-error processing, sensory integration, and corrective motor responses [122, 151–154]. The importance of sensory reweighting is also illustrated by studies in visually impaired individuals, who may exhibit greater postural sway and increased dependence on vestibular and proprioceptive information in the absence of visual feedback [13]. Together, these observations indicate that abnormalities in postural regulation may become more apparent when the nervous system is required to adapt to changing or conflicting sensory conditions.

Although overt postural instability is generally associated with more advanced PD, subtle impairments in balance regulation, sensory integration, and adaptive motor responses may already occur during early-stage disease [98, 99]. Controlled perturbation tasks may therefore expose abnormalities that remain difficult to identify through conventional clinical assessment.

BioVRSea provides such a challenge by combining immersive virtual-reality stimulation with moving-platform perturbation while simultaneously recording CoP, EMG, and EEG signals [128, 129]. This multimodal design allows biomechanical, muscular, and cortical responses to be examined within the same experimental protocol, providing an integrated characterization of adaptation to conflicting visual, vestibular, and somatosensory information. The technical characteristics, experimental phases, and acquisition procedures of BioVRSea are described in Chapter 3 and are therefore not repeated here.

The present study aimed to characterize the postural-adaptation strategies adopted by individuals with early-stage PD and healthy controls during the BioVRSea task. Specifically, we investigated changes in CoP, EMG, and EEG responses across the experimental phases to determine whether controlled visual and mechanical perturbations could reveal subtle group-specific alterations in postural regulation and neurophysiological adaptation.

4.2 Materials and Methods

4.2.1 Participants

Nine early-stage (recently diagnosed) PD participants (6 male, 3 female, between 56 and 76 years of age) and 29 healthy subjects (17 male, 12 female, between 50 and 73 years old) took part in the BioVRSea experiment. A few of them showed physical evidence of early-stage PD, such as weak tremor or onset of postural instability. All were taking the drug Levodopa as part of their treatment.

4.2.2 Statistical Analysis

The Shapiro-Wilk test and visual inspection of each variable's distribution were used to assess data normality. Statistical comparisons between the healthy and PD groups in both the PRE and POST phases were carried out using the t-test with Welch's correction for the normally distributed variables and the Mann-Whitney U-test for the non-normally distributed variables, with a significance value of $p < 0.05$. Effect sizes were calculated through the non-parametric Cliff's delta using the R package 'effsize' [155]. Cliff's delta ranges from +1 if all observations in the first group are larger than all observations in the second group, to -1 if all observations in the first group are smaller than all observations in the second group [156].

4.3 Results

The following results were reported for the analysis of the PRE and POST phases of the experiment to distinguish between the PD and healthy groups based on their biosignal responses. The analysis identified group differences across several of the investigated domains.
The protocol simulated the visual and motor experience of being on a boat, and some participants experienced symptoms of seasickness. Just under half of PD subjects experienced actual discomfort with various symptoms (reported on questionnaires), and a smaller percentage of them reported a self-assessment of motion sickness in daily life.

EMG The right TA muscle showed several statistically significant features in the POST phase, with a p-value ($p < 0.05$). The right side could be considered the dominant leg in the group. Significant changes were also found in the left soleus (MN - mean, p=0.003, cliff delta = -0.64) in the POST phase and the right soleus, which had one significant feature (MD -median, p=0.007, cliff delta = -0.586) in the PRE phase.

CoP Sway Profile Fig. 4.1 highlights the CoP evolution between PD and healthy subjects on two of its main characteristics: area and axis length of the sway ellipse. Sway was greater in healthy than in PD participants.

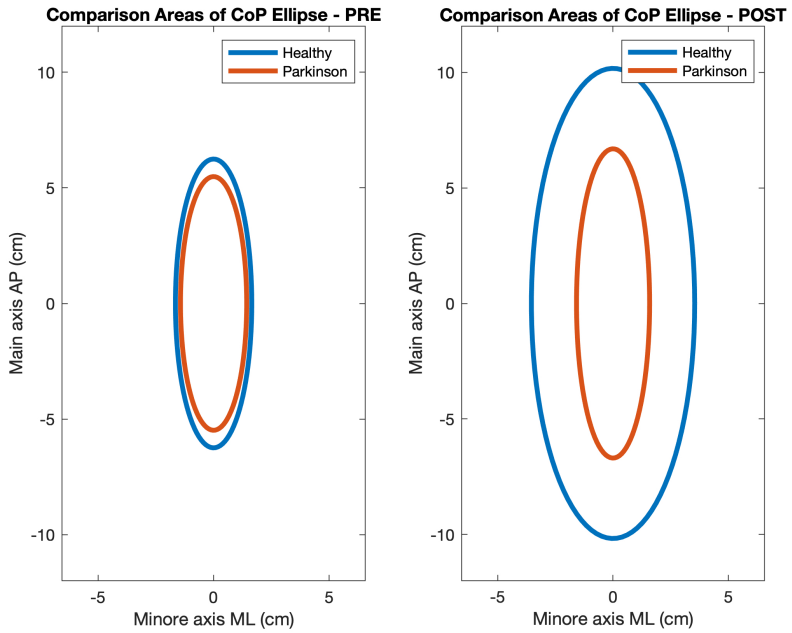


Figure 4.1: **Comparison of center of pressure ellipse areas between Parkinson's disease and healthy control groups.** Ellipse areas are shown for the PRE and POST phases of the experiment

Direction Entropy (Nats) was the only significant CoP feature ($p < 0.05$) in the PRE phase, whereas the most relevant statistically significant POST-phase measures of postural control included ellipse area and its main and minor axes, radial-distance measures (RD and RDIST), antero-posterior and medio-lateral sway variability (SD AP, SD ML, and SD magnitude), and medio-lateral entropy and complexity measures (ML-SampEn, ML-CI, and Multivariate CI).

EEG The topological plots were computed for all frequency bands during the phases of the acquisition. Each of them displays the difference of power spectral density between PD and healthy cohorts, only for the statistically significant electrodes ($p \leq 0.05$, represented by a green point in the figure). Theta and alpha bands presented several significant electrodes in different locations of the brain. In the theta band, significant electrodes were found mostly in the temporal lobe (T7, T8, C6, FT7), one in the frontal lobe (AF3), and one in the occipital lobe (PO6). In the alpha band, significant electrodes were found mostly in the temporal lobe (FC5, T7, T8, FT8), one in the parietal lobe (P4), and one in the occipital lobe (PO6). They highlight the differences in brain activity in the two phases and underline the significant difference in the POST

phase of the experiment between the PD and Healthy groups.

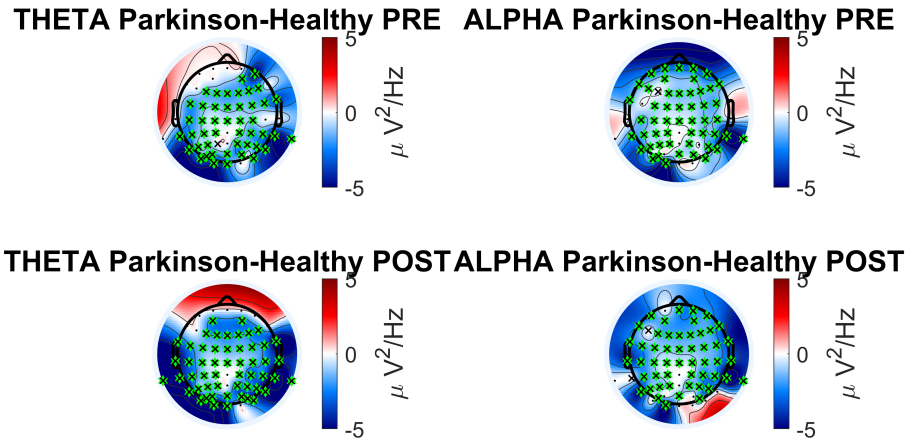


Figure 4.2: **Theta and alpha absolute power spectral density comparison.** Absolute PSD values are compared between participants with Parkinson's disease and healthy controls.

Chapter 5

Dynamic Alpha-Band Functional Connectivity During Postural Control Assessment in Parkinson's Disease

This chapter is based on material adapted from the peer-reviewed article "Exploring Dynamic Alpha Band Connectivity in Parkinson's Disease During a Virtual Reality Postural Control Task," published in *Brain Topography* in 2026. The original study extended the BioVRSea-based investigation of postural control in PD by focusing specifically on EEG activity and dynamic alpha-band functional connectivity during a virtual-reality postural-control task.
The chapter examines how brain connectivity patterns differed between individuals with PD and healthy controls during the BioVRSea paradigm. EEG signals were used to extract dynamic functional connectivity states, referred to as brain network states (BNSs), to characterize task-related changes in cortical organization. By focusing on alpha-band connectivity, the original study investigated whether altered brain-network dynamics reflected impaired visuomotor integration, attentional control, and postural-control regulation in PD.

5.1 Introduction

The clinical characteristics of PD, the challenges associated with its early identification, and the role of quantitative methods in its assessment have been discussed in the preceding chapters. Briefly, PD affects both motor and non-motor function and progressively compromises the ability to respond to increasingly demanding motor tasks [34, 157, 158]. Because early manifestations may overlap with age-related or other neurological changes [159], a broad range of complementary quantitative approaches has been investigated, including gait analysis [160, 161], structural and functional neuroimaging [162–164], near-infrared spectroscopy [165], and EEG [166–168]. Rather than revisiting these

diagnostic approaches, the present chapter focuses specifically on the dynamic cortical organization underlying postural control.

EEG is particularly suited to this objective because its temporal resolution allows rapid neural changes associated with motor and cognitive processes to be examined during active behaviour. Alterations in oscillatory activity and functional organization have been investigated as potential markers of early PD [169–171], but much of this evidence derives from resting-state recordings. Postural-control tasks provide a different perspective by requiring the nervous system to continuously integrate sensory information and generate appropriate motor responses [172–175]. These processes are particularly relevant in PD, in which impaired motor and cognitive contributions to balance are associated with postural instability and increased fall risk [176, 177].

Among the oscillatory components involved in these processes, alpha activity is of particular interest. Previous studies have associated alpha-band modulation with balance maintenance and postural adjustments [178–180]. Changes in alpha power have been related to differences in postural stability and attentional demand [181–184], while alpha coherence between cortical regions has been implicated in sensory processing and motor planning [153, 185]. Importantly, PD has also been associated with disrupted synchronization and functional connectivity between sensorimotor and parietal regions involved in the integration of sensory information and motor responses [186]. These observations suggest that examining alpha activity at the network level may provide information that cannot be obtained from regional spectral measures alone.

The BioVRSea paradigm provides a suitable context in which to investigate these dynamics under an active multisensory challenge. Its experimental design and acquisition procedures have already been described in Chapter 3 and in the preceding study and are therefore not repeated here. Previous investigations have established its applicability to postural-control assessment [128, 187] and to the development of physiological predictive models across different conditions [127, 188, 189]. More specifically, its application in early-stage PD revealed differences in theta- and alpha-band power between patients and healthy controls during the postural-control task [190]. These findings motivated a transition from the analysis of oscillatory activity itself to the investigation of how distributed cortical regions dynamically interact throughout the task.

Dynamic functional-connectivity analysis enables this interaction to be characterized through recurring Brain Network States (BNSs) [191]. BNSs represent transient patterns of functional connectivity that emerge and reorganize in response to changing behavioural and environmental demands [192, 193]. This framework is particularly relevant to postural control, which depends on coordinated activity across networks involved in sensorimotor integration, attention, and motor planning. Alterations in such functional organization have previously been reported in PD [194], while established large-scale networks, including sensorimotor, salience, executive-control, and default-mode systems, have been associated with cognitive and motor functions relevant to balance regulation [195–198]. Dynamic analysis can therefore complement conventional connectivity measures by examining not only which regions interact, but also how

network configurations evolve throughout a postural challenge.
Building on these observations, the present study applied source-level dynamic EEG analysis to characterize alpha-band BNSs during the BioVRSea task. Methodological procedures previously shown to provide reliable reconstruction of EEG functional networks were adopted [199]. By comparing the temporal organization of these states between individuals with early-stage PD and healthy controls, we aimed to determine whether altered alpha-band network dynamics reflected impairments in visuomotor integration, attentional control, and postural regulation that were not captured by conventional measures alone.

5.2 Materials and methods

5.2.1 Participants

Participants were recruited between 18/01/2022 and 03/10/2023. Informed consent was obtained from all participants before their inclusion in the study. The Icelandic National Bioethics Committee approved the study protocol with the consent *VSN-20–101* for the healthy cohort and extended it to include the Parkinson's cohort under amendment *VSN-20–101-V2*. The study involved 42 participants: 20 PD patients (54–82 years old, mean age=65.35) and 22 age-matched healthy control (CTR) individuals (55–72 years old, mean age=62.78). Table 5.1 shows that neither the t-test for age nor the chi-squared test for gender revealed any significant differences, indicating homogeneity in the population characteristics between the two groups.

Table 5.1: **Age and gender distribution in PD and CTR groups.** No significant differences were found (t-test for age, chi-squared test for gender)

	PD (n=20)	**CTR (n=22)**	**p-value**
Age			0.182
Mean ± SD	65.4 ± 4.50	62.8 ± 4.27	
Min-Max	54-82	55-72	
Gender (%)			0.817
Female	8 (40%)	12 (54.5%)	
Male	12 (60%)	10 (45.5%)	

Participants in the PD group had a diagnosis of early-stage PD, and they were on levodopa medication. All patients were tested while on their ON medication, as confirmed by the absence of visible motor symptoms during the experimental session. The mean disease duration at the time of testing was approximately 1–2 months, confirming that all patients were evaluated very early after diagnosis. The Hoehn and Yahr (H/Y) scale [200] was used to classify disease stage, with values ranging from 1 to 3. Following clinical evaluation, 11 patients showed no signs of cognitive decline, while the remaining participants were classified as having mild cognitive impairment (MCI). None

were diagnosed with Parkinson's dementia. Consistent with both the medical screening performed before participation and our direct observations during data acquisition, none of the patients exhibited visible tremor, dyskinesia, or other involuntary movements throughout the BioVRSea experiment. All participants completed the full experiment and responded to both the pre- and post-experiment questionnaires. From these responses, we observed no cognitive issues or impairments.

5.2.2 Data processing: Connectivity analysis to dynamic network computation

Several preliminary steps were required before computing the dynamic brain networks, as described in Fig. 5.1. EEG source connectivity is a valuable method for identifying brain networks linked to specific cognitive functions, as demonstrated by Hassan et al. [199].

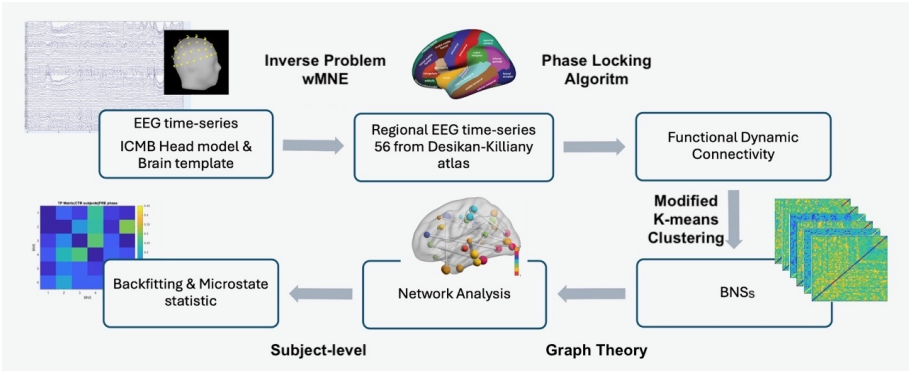


Figure 5.1: **Workflow description.** EEGs were recorded using 64 electrodes during the BioVRSea experiment. The cortical sources were reconstructed by solving the inverse problem using the wMNE method. After source reconstruction, the signals were divided into 56 brain Regions of Interest (ROIs) derived from the Desikan–Killiany atlas, originally composed of 68 ROIs. The reduction to 56 ROIs was performed to address the spatial resolution limitations of EEG source estimation by aggregating anatomically related regions, and to ensure methodological consistency with the network analysis by selecting ROIs according to their assignment to the seven canonical Resting-State Networks (RSNs). Functional connectivity matrices were computed between the 56 regional time series using the PLV method across five frequency bands (Delta, Theta, Alpha, Beta, Gamma). Connectivity matrices were first obtained separately for the PD and CTR groups, then concatenated before being input into the k-means++ clustering algorithm. This clustering process identified distinct Brain Network States (BNSs), followed by network analysis at the subject level to compute metrics for group comparisons.

The first step was the reconstruction of brain sources from the signals recorded on

the scalp. In fact, estimating connectivity directly from the sensor level is limited by low spatial resolution and the effects of volume conduction. These issues can cause false correlations in connectivity measurements, as signals from different electrodes may originate from the same neural source. As a result, connectivity at the sensor level does not accurately reflect functional interactions between brain areas. To address this, we used EEG source localization techniques to reconstruct cortical activity, which involves solving the complex EEG inverse problem. The neural sources for artifact-free EEG data were estimated using the following equation.

$$S = GD + N \tag{5.1}$$

where $S(t)$ represents the EEG signals recorded at M electrodes, G is the lead field matrix that models how sources contribute to the scalp potentials, $D(t)$ denotes the unknown brain activity at P source locations, and $N(t)$ accounts for noise and modeling errors. To solve the inverse problem, we used the *Weighted Minimum Norm Estimate (wMNE)*, given by the formula:

$$D_{wMNE} = (G^T W G + \lambda I)^{-1} G^T W S \tag{5.2}$$

where G is the lead field matrix, W is a depth-weighting matrix, λ is a regularization parameter, and S represents the EEG signals.
We used the ICBM MRI template with three-layer segmentation (scalp, outer skull, and inner skull) from the OpenMEEG plugin within the Brainstorm toolbox. The Boundary Element Method (BEM) was employed to model the head volume conductor, validated by prior research [123, 201, 202]. The initial 45 seconds of the EEG were used to construct the noise covariance matrix, while the remaining 273 seconds were allocated for source reconstruction.
The signals were then divided into 56 brain regions of interest (ROIs) derived from the Desikan-Killiany atlas [203], which originally contains 68 ROIs, aiming for a lower number of ROIs, to address the low spatial resolution issue of EEG and the effect on the accuracy of source estimation [204–206]. Moreover, to ensure consistency with the network analysis performed in this study, those ROIs were selected based on their assignment to the seven canonical RSNs, emphasizing the functional response of brain dynamics to BioVRSea. This resulted in a final set of 56 ROIs (Appendix ROI–Node–RSN Mapping).
Functional connectivity between the EEG time series of the 56 ROIs was calculated across multiple frequency bands (Delta: 1-4 Hz, Theta: 4-8 Hz, Alpha: 8-13 Hz, Beta: 13-30 Hz, Gamma: 30-45 Hz) using the Phase-Locking Value (PLV) algorithm with a sliding window approach (50% overlap and window size of six cycles) [207]. The combination of wMNE and PLV has demonstrated strong performance in capturing meaningful brain-network dynamics in the alpha band during complex postural-control tasks [191, 199].
The PLV computation produced 56x56 square dynamic matrices for each band. The number N, representing the total number of computed connectivity matrices, is detailed in Appendix Phase-Locking Value (PLV) Calculation. Specifically, for the alpha band, 953 matrices were created. Each matrix element $A_{i,j}$ represents

the strength of the connections from node i to node j, referred to as an *edge* in graph theory-based analysis (Table 5.2).

Table 5.2: **Dynamic Connectivity Variables.** A list of the number of matrices (N) calculated for each frequency band. The dimension (n) of each matrix is based on the number of ROIs, with each element ($A_{i,j}$) representing the connectivity between the respective regions

Variable	Description	Band	Value
N	Number of dynamic connectivity matrices	Alpha	953
		Beta	1953
		Delta	226
		Gamma	3407
		Theta	544
n	Dimension of dynamic connectivity matrices	56×56	
$A_{i,j}$	Element of one connectivity matrix	–	

BNS segmentation was performed on this dataset using a clustering algorithm to identify stable periods over time. The analysis was based on functions from the EEGLab Microstate toolbox, originally designed for EEG voltage topography. We adapted the microstate analysis pipeline described by Poulsen et al. to extract BNSs from functional connectivity data [208]. The optimal number of classes was determined based on goodness-of-fit metrics, including Global Explained Variance (GEV) criterion [208, 209].

For the clustering process, we transformed the symmetric connectivity matrices into vectors of size $(n \times (n-1)/2) = 1540$ by extracting the upper triangular elements, excluding the diagonal. Each vector was then concatenated across all time points, resulting in a subject-specific matrix of dimensions 1540×953, where each column represents a time window, and each row corresponds to a specific connection within the network. These matrices were concatenated among subjects and served as input for the modified k-means (k-means++) clustering algorithm [210], which has been successfully used in other previous studies on the dynamic functional connectivity of EEG and fMRI [211, 212]. Clustering was performed with the following parameters: the number of clusters varied from 2 to 10 (K_{range}), the number of random initializations (rep) was set to 100, and the maximum number of iterations (iter) was 1000, with a default convergence threshold of 10^{-6}.

A meta-criterion was applied to obtain the optimal number of clusters [211, 213, 214], which was determined to be six. Specifically, the meta-criterion was implemented using the CVIK Toolbox [215], a MATLAB framework that integrates 28 Cluster Validity Indices (e.g., Silhouette, Davies–Bouldin, Dunn, PBM, S_{Dbw}) and multiple proximity measures to automatically determine the optimal number of clusters based on index consensus.

Each identified cluster was defined as a BNS, representing the temporal evolution of brain connectivity. K-means++ was run multiple times with different pa-

rameters to ensure the robustness of the clustering results. The BNSs obtained from each clustering iteration were then compared using Pearson correlation analysis to assess the consistency of the identified patterns. A strong correlation indicated high similarity between BNSs across different clustering runs, validating the reliability of the extracted states (Table 5.3).

Table 5.3: **Pearson correlation of the six Brain Network States across different clustering runs.** The optimal number of clusters ($K = 6$) was determined using the meta-criterion based on multiple internal Cluster Validity Indices (CVIs). Modified k-means clustering was then repeated four times with different parameter configurations. Cluster #1, defined by the parameters $K_{\text{range}} = 2{:}10$, rep = 100, ite = 1000, was used as the reference for comparison. We therefore computed the Pearson correlation between the corresponding cluster maps obtained in different runs to evaluate the similarity and stability of the clustering results

Clusters	**Parameters**	**Pearson correlation**					
		BNS1	**BNS2**	**BNS3**	**BNS4**	**BNS5**	**BNS6**
Cluster #2	K_{range}=2:10; rep=100; ite=1000	1	1	1	1	1	1
Cluster #3	K_{range}=3:7; rep=100; ite=1000	−1	1	0.99	0.99	0.99	1
Cluster #4	K_{range}=3:7; rep=200; ite=1000	1	1	1	0.99	0.99	1

The topological visualization of the six BNSs was conducted, and they were labeled based on the most prevalent RSNs, as detailed in Subsection Data processing: Association of BNSs with RSNs. Each BNS was characterized by distinct spatial distributions and temporal dynamics that correspond to specific cognitive and functional processes. This allowed for a more intuitive interpretation of the BNSs in relation to established RSNs, facilitating comparisons between the two groups in our study.
As a final step, we computed the back-fitting at the subject level using Global Map Dissimilarity (GMD) to identify the best-fitting BNSs throughout the experiment. The smoothing process involved rejection based on small-segment criteria of five matrices [191, 208, 209]. For the identified BNSs, we calculated several common metrics used in microstate analysis, including Global Field Power (GFP), occurrence per second (occurrence), average duration (duration), percentage of time occupied (coverage), global explained variance (GEV), and the transition probabilities (TP). These metrics were subjected to statistical analysis between the two groups. A comprehensive description of these metrics is provided in Appendix Computational Methods for BNSs metrics.

5.2.3 Data processing: Association of BNSs with RSNs

Each BNS vector was reshaped into a 56×56 symmetric matrix representing the corresponding functional network. Based on some studies [196, 216], each of the 56 nodes was assigned to one of seven RSNs: Default Mode Network (DMN), Dorsal Attention Network (DAN), Salience Network (SAN), Motor Network (MOT), Auditory Network (AUD), Visual Network (VIS), and Other. The node-RSN affiliations are detailed in Appendix (ROI–Node–RSN Mapping). Using the Brain Connectivity Toolbox [217], the strength of each node was calculated, representing the sum of the weights of all links connected to that node. Subsequently, we determined the strength of each RSN by summing the values of nodes associated with the specific RSN and normalizing this sum by dividing it by the number of nodes within the RSN. To identify the dominant RSN for each BNS, we considered those with a value exceeding the sum of the average and standard deviation of the strengths of the seven RSNs. We utilized BrainNet Viewer [218] for visualization, where each ROI was represented by a color corresponding to its specific RSN. Each network was displayed with a sparsity of 0.01.

5.3 Results

5.3.1 BNSs presence

Following the back-fitting process, we initially identified distinct patterns in the presence of BNSs between individuals with PD and CTR subjects across the experimental phases (Fig. 5.2).

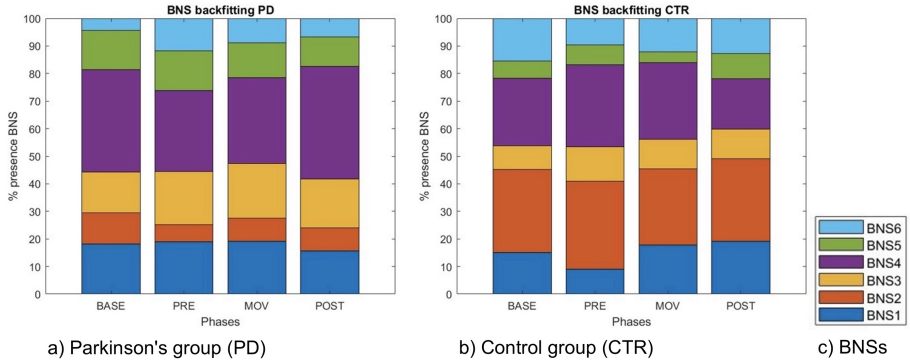


Figure 5.2: **Percentage representation of Brain Network States.** Distribution of Brain Network States (BNSs) across different experimental time phases for (a) PD patients and (b) the CTR group. Each bar represents the frequency of a specific BNS during the respective phase, illustrating how often each state was engaged throughout the experiment. (c) Lists the identified BNSs.

All BNSs appeared in each phase for both cohorts, but their relative frequencies varied. Specifically, BNS1 was slightly more frequent in the PD group, except during the POST phase, where it was higher in the CTR group. The trend of BNS1 in the PD group remained consistent across all phases except for the POST phase, whereas in the CTR group, it differed in the PRE phase. BNS2 was consistently less frequent in the PD group across all phases. Conversely, BNS3 and BNS5 were consistently more prominent in the PD group. BNS4 was more frequent in the PD group except during the PRE phase, while BNS6 showed a higher presence in the CTR group except during the PRE phase.

5.3.2 Correlations between questionnaire scores and brain state metrics

The correlation analysis between questionnaire indices and BNS metrics uncovered several significant relationships specific to BNS3. For the CTR group, a notable Spearman correlation was found between the occurrence metric and the NEURO index ($\rho = 0.27$, $p < 0.01$). Both groups showed significant correlations between NEURO scores and the metrics of coverage and duration within BNS3. In the CTR group, the correlation of duration with NEURO was $\rho = 0.24$ ($p < 0.02$), and for coverage, $\rho = 0.26$ ($p < 0.01$). Similarly, in the PD group, the duration-NEURO correlation was $\rho = 0.21$ ($p < 0.05$), and the coverage-NEURO correlation was $\rho = 0.22$ ($p < 0.05$). These findings indicated that both groups demonstrated significant associations between the NEURO index and the metrics of duration and coverage. However, the occurrence metric exhibited a unique correlation pattern that appeared only within the CTR group.

5.3.3 Statistical analysis of BNSs

We investigated the following parameters of the BNSs: occurrence, duration, coverage, and TP. Statistical analysis revealed significant variations in BNS2 coverage during the PRE (adjusted p-value = 0.019) and MOV (adjusted p-value = 0.036) phases following FDR correction with $\alpha < 0.05$ (Fig. 5.3), consistent with an initial trend observed in these phases. For BNS4, a similar trend was observed in the BL and POST phases, although it did not remain significant after correction (Appendix Statistical Result of Coverage).
No statistically significant results were observed for occurrence; however, a trend was evident in BNS2 during the PRE and MOV phases (Appendix Statistical Result of Occurrence). For duration, no statistically significant results were found; however, a trend was noted in BNS5 during the BL phase and in BNS4 during the POST phase. TP analysis indicated that, in individuals with PD, transitions from BNS1 to BNS4 and from BNS4 to BNS1 consistently exhibited significantly higher probabilities compared to the CTR group. Conversely, transitions from BNS4 to BNS1 and BNS3 to BNS4 in CTR subjects displayed higher probabilities than those in the PD group starting from the PRE phase. In PD, activation within the same BNSs occurred later during the POST phase

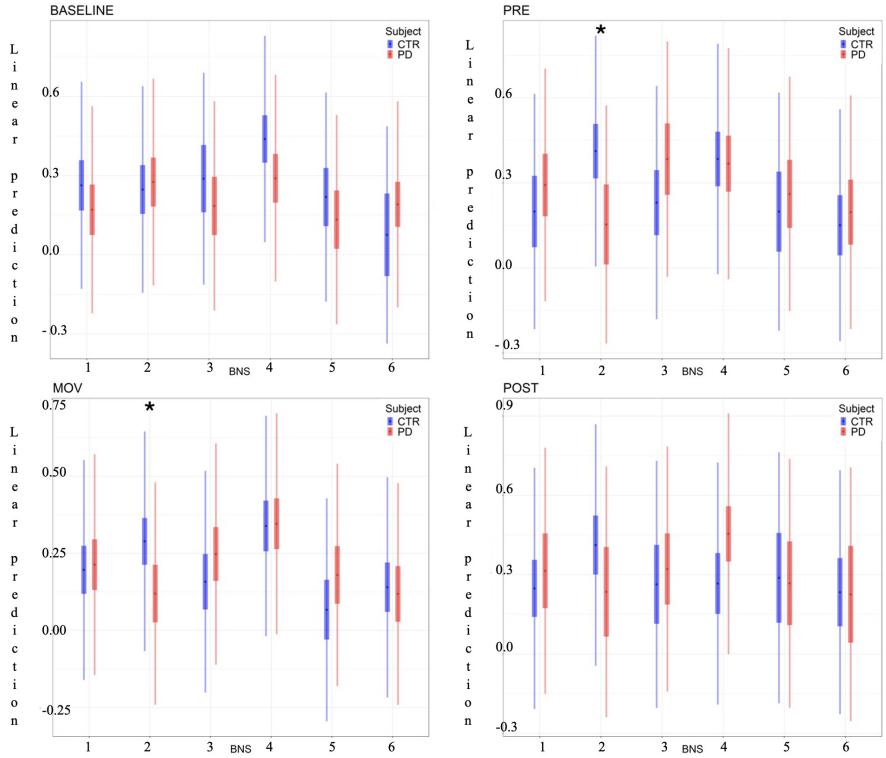


Figure 5.3: **Linear Mixed Model analysis.** Coverage for each Brain Network States (BNSs) across all experimental phases in PD patients and CTR. Coverage refers to the proportion of total activity distributed across the six identified BNSs, indicating how dominant each BNS was relative to the others during each phase. Significant differences between groups, corrected using the False Discovery Rate (FDR) method, are highlighted: * $p < 0.05$.

(Fig. 5.4, Appendix Statistical Result of Duration).

The statistical findings are summarized in Table 5.4, which provides an overview of the main statistical outcomes for each BNS metric and experimental phase.

5.3.4 Association between BNSs and RSNs

Fig. 5.5 displays the network nodes, with the size of each node representing its strength, corresponding to the overall connectivity of that node. For visualization purposes, a sparsity threshold of 0.01 was applied, displaying only the strongest connections. This approach highlighted the most significant interactions, using color-coding to distinguish different RSNs. In BNS1, the VIS predominated, with nodes concentrated in the left hemisphere, particularly in the parietal and occipital lobes. The SAN was also prominent, with nodes

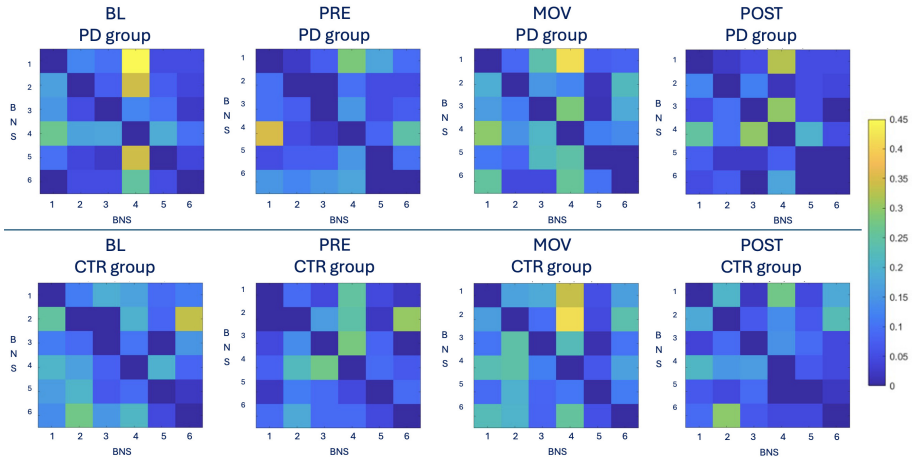


Figure 5.4: **Transition Probability matrices.** PD and CTR subjects across baseline (BL), pre-motor stimulus (PRE), movement-stimulus (MOV), and post-motor stimulus (POST) phases. Each heatmap represents the likelihood of transitioning between different Brain Network States (BNSs) within each phase, with lighter colors indicating higher transition probabilities. These matrices highlight the patterns of state transitions and the differences between groups in terms of network dynamics.

distributed across the frontal and right parietal lobes. In the remaining five BNSs, the DAN was the dominant RSN. BNS2 featured the DAN primarily in the parietal lobe, with nodes of similar sizes spread across the interhemispheric fissure, followed by the SAN in the frontal lobe. BNS3 included the DMN in the frontal lobe, with balanced node strength between the left and right hemispheres, and the AUD in the parietal lobe. BNS4 comprised the DMN, with node strength balanced across the interhemispheric fissure in the parietal

Table 5.4: **Summary of main statistical outcomes for each Brain Network States metric and experimental phase.** Linear Mixed Model (LMM) analysis with False Discovery Rate (FDR) correction ($\alpha < 0.05$). Significant results are highlighted in bold, while non-significant trends are also indicated for clarity

Metric	Phase	BNS	Group difference (PD vs. CTR)	adjusted p-value
Coverage	PRE	BNS2	PD < CTR	**0.019**
Coverage	MOV	BNS2	PD < CTR	**0.036**
Coverage	BL	BNS4	PD > CTR	n.s.
Coverage	POST	BNS4	PD > CTR	n.s.
Occurrence	PRE	BNS2	CTR > PD	n.s.
Occurrence	MOV	BNS2	CTR > PD	n.s.
Duration	BL	BNS5	PD > CTR	n.s.
Duration	POST	BNS4	CTR > PD	n.s.

lobe, while being exclusively present in the right hemisphere in the frontal lobe. Additionally, the VIS network was mainly localized in the left occipital lobe for the BNS4. BNS5 was similar to BNS4, with larger node sizes across the interhemispheric fissure and in the frontal lobe for the DAN, whereas the SAN was present in both hemispheres across the interhemispheric fissure. Finally, BNS6 involved both the DMN and the SAN, similar to BNS5, but with the DMN absent in the right hemisphere of the parietal lobe.

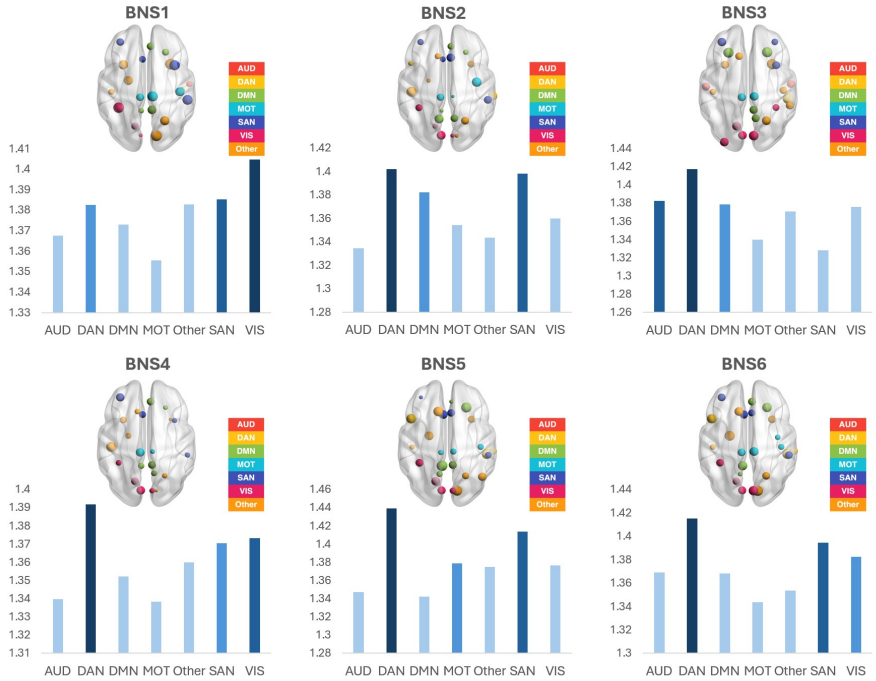


Figure 5.5: **Prevalence of Resting Network States in each Brain Network State.** Calculated as the sum of the node strength values for each Region of interest (ROI) associated with the specific Resting Network State (RSNs). Each Brain Network State (BNS) is visualized with nodes sized proportionally to their strength (the sum of connections at each node), and edges are shown based on their connectivity, with a sparsity threshold of 0.01 applied to filter weak connections. Different colors represent distinct RSNs, facilitating clear visual differentiation of the dominant networks in each BNS. This visualization highlights the key RSNs contributing to the overall network dynamics across experimental phases.

Chapter 6

Frequency-Specific Brain Network Dynamics During Postural Control Assessment in Parkinson's Disease

The material presented in this chapter is adapted from the manuscript "Dynamic connectivity patterns in Parkinson's disease: A new framework for postural control assessment with BioVRSea," currently under review in the *Brain Topography* Journal. The study extended previous BioVRSea-based investigations of postural control in Parkinson's disease by characterizing Brain Network State dynamics across the delta, theta, and beta frequency bands, providing further insight into large-scale cortical-network reorganization during visuomotor postural control.

6.1 Introduction

The preceding chapters established the relevance of postural-control dysfunction in PD, including its potential emergence before severe clinical instability becomes evident [34, 157–159]. They also introduced EEG as a means of investigating the rapid neural dynamics underlying motor regulation and sensorimotor integration [166–168], and demonstrated the utility of the BioVRSea paradigm for studying these processes during controlled multisensory postural challenges [128, 187]. The present chapter therefore does not revisit these general principles, but addresses a more specific question arising from the previous connectivity analysis: whether alterations in dynamic cortical organization in early-stage PD are specific to the alpha band or extend across other oscillatory regimes.

This question is relevant because different frequency bands contribute complementary information about the neural processes supporting postural and motor control. Delta oscillations (1–4 Hz) have been associated with large-scale coordination and integrative mechanisms during demanding sensorimotor conditions.

Theta activity (4–8 Hz) is linked to attentional engagement, cognitive control, and error monitoring, whereas beta oscillations (13–30 Hz) are closely related to motor planning, execution, and the maintenance of sensorimotor states. In PD, abnormalities across these oscillatory regimes have been associated with impaired motor regulation and reduced neural flexibility [169–171]. Considering these frequency bands separately may therefore reveal whether postural dysfunction is associated with a common disruption of network organization or with distinct frequency-dependent mechanisms.

The previous chapter approached cortical organization through Brain Network States (BNSs), recurring configurations of functional connectivity that capture the temporal reorganization of large-scale networks during changing task demands [191]. The conceptual basis of this framework has already been described and is not repeated here. Importantly, dynamic network organization reflects interactions among systems involved in attention, sensorimotor integration, executive processing, and motor regulation [192–198]. Examining the temporal expression of these configurations across distinct frequency bands therefore provides a means of assessing whether the neural flexibility required for adaptation to postural perturbation is altered in a frequency-dependent manner in PD.

This analysis directly extends our previous investigation of alpha-band connectivity during the same BioVRSea task, which identified PD-related differences in the organization and temporal expression of cortical network states [219]. While those findings demonstrated the sensitivity of dynamic alpha-band connectivity to early-stage PD, they could not determine whether the observed alterations represented an alpha-specific phenomenon or one component of a broader reorganization of oscillatory network dynamics.

Accordingly, the present study extended the BNS analysis to the delta, theta, and beta frequency bands in individuals with early-stage PD and CTR. By comparing the coverage, duration, and occurrence of the identified states across the BioVRSea experimental phases, we aimed to characterize complementary and frequency-specific alterations in large-scale cortical-network dynamics during postural regulation. The technical characteristics, experimental phases, acquisition procedures, and general BNS framework have been described in the preceding chapters and are therefore not repeated here.

6.2 Materials and Methods

6.2.1 Participants

Participants were enrolled between 18/01/2022 and 03/10/2023 after providing written informed consent. The study was approved by the Icelandic National Bioethics Committee (healthy cohort: *VSN-20–101*; Parkinson's cohort: amendment *VSN-20–101-V2*). A total of 42 individuals took part in the experiment: 20 people with PD (54–82 years, mean age = 65.35) and 22 age-matched CTR (55–72 years, mean age = 62.78). Neither age nor gender differed significantly between the groups, confirming comparable demographic characteristics. Patients were in the early stages of PD and were receiving levodopa. All were

assessed in the ON medication state, with no observable motor symptoms during testing. Disease duration at the time of participation was short (approximately 1–2 months post-diagnosis). Disease staging based on the Hoehn and Yahr scale [200] ranged from 1 to 3. Clinical evaluation indicated that 11 patients had no cognitive deficits, while the others exhibited mild cognitive impairment; none met criteria for Parkinson's dementia. No tremor, dyskinesia, or other involuntary movements were observed during the BioVRSea session. All participants completed the full protocol as well as the pre- and post-experiment questionnaires, which did not indicate any cognitive difficulties.

6.2.2 Data processing: Connectivity analysis and dynamic network computation

The overall methodological pipeline adopted in the present study followed the framework previously validated in [219], where detailed descriptions of preprocessing, source reconstruction, dynamic connectivity estimation, clustering procedures, and robustness analyses are provided. The workflow of the present implementation, schematically illustrated in Fig. 6.1, adhered to the same validated analytical strategy.

EEG sensor data were projected into source space using the wMNE solution [199] implemented on a three-layer BEM head model (ICBM template; OpenMEEG). Noise covariance was computed from the first 45 seconds of recording, and source activity from the remaining signal was then parcellated into 56 regions. These ROIs were derived by functionally grouping parcels from the Desikan–Killiany atlas [203] to reduce redundancy, improve source estimation reliability [204–206], and ensure consistency with the seven canonical Resting State Networks (RSNs) described in previous work [196, 216].

Functional connectivity was estimated between the 56 regional signals using the Phase Locking Value (PLV) [207] in Beta, Delta, and Theta bands, adopting a sliding-window approach (six-cycle window, 50% overlap). The mathematical formulation is provided in the Supplementary Material 11.1.2. The combination of wMNE and PLV has shown strong performance in capturing meaningful network dynamics during PC and cognitive tasks [191, 199]. This procedure produced a time series of 56×56 PLV matrices for each subject.

For clustering, each connectivity matrix was vectorized by extracting its upper-triangular values, and these vectors were concatenated across all time windows and all individuals. Dynamic BNSs were extracted using the modified k-means (k-means++) algorithm [210], which is widely applied in EEG and fMRI dynamic connectivity studies [208, 211, 212].

The number of clusters was determined through a meta-criterion integrating multiple internal validity indices [211, 213, 214]. This meta-analysis was performed using the CVIK toolbox [215], which aggregates 28 Cluster Validity Indices (e.g., Silhouette, Dunn, Davies–Bouldin, PBM, S_{Dbw}) and several distance measures. The consensus consistently identified optimal clusters. To ensure stability, clustering was repeated with different initialization parameters, and the resulting centroids were compared across runs using Pearson correlation.

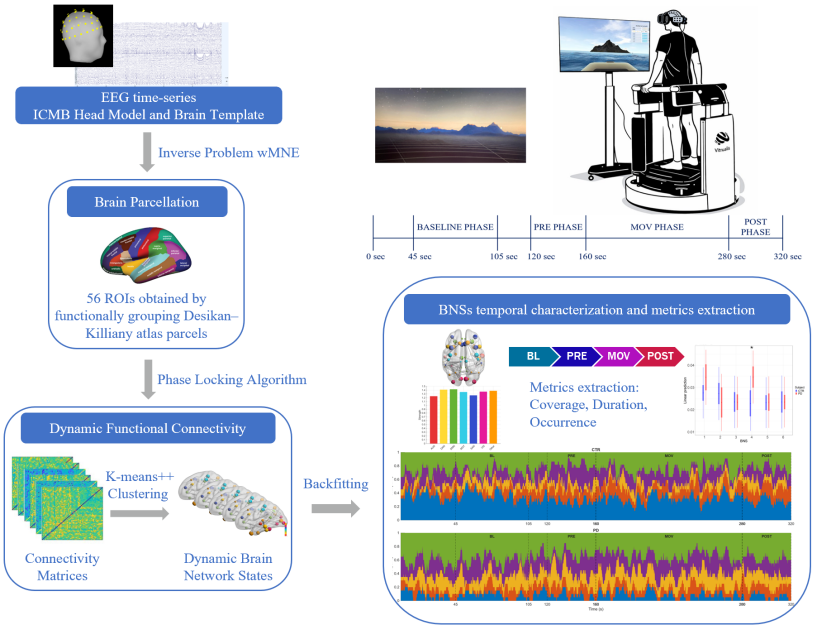


Figure 6.1: **BioVRSea EEG-processing workflow.** EEG was recorded using 64 electrodes, and cortical sources were reconstructed with wMNE and mapped to 68 Desikan–Killiany regions, subsequently aggregated into 56 ROIs. PLV-based functional connectivity matrices were computed across the delta, theta, and beta bands for PD and CTR groups, concatenated, and clustered using k-means++ to identify BNSs. Subject-level network metrics were then extracted for between-group comparisons.

Each cluster centroid was then reshaped into a 56×56 connectivity pattern and labelled according to the RSNs contributing most strongly to its topology. The temporal activation of each BNS at the subject level was obtained through back-fitting using Global Map Dissimilarity [208, 209], followed by temporal smoothing to remove segments shorter than five windows [191].
Following back-fitting, BNS temporal sequences were segmented into the four experimental phases. Within each phase, the presence of each BNS was computed as the proportion of time points assigned to that state relative to the total number of samples in that phase. Subject-level values were then averaged within each group and expressed as percentages for visualization. In addition to this phase-specific characterization, we extracted global BNS-inspired metrics computed over the entire recording, namely coverage, duration, and occurrence rate. These complementary metrics were used for statistical comparisons between groups to assess differences in both temporal distribution and dynamical stability of brain states.

6.2.3 Data processing: Association of BNSs with RSNs

Each BNS centroid was reshaped into a 56×56 symmetric matrix to represent its functional connectivity pattern. Following previous work [196, 216], every node was assigned to one of seven large-scale RSNs: Default Mode Network (DMN), Dorsal Attention Network (DAN), Salience Network (SAN), Motor Network (MOT), Auditory Network (AUD), Visual Network (VIS), or Other. The detailed ROI-to-RSN mapping is provided in Supplementary Material, Section 11.1.1. Node strength was computed using the Brain Connectivity Toolbox [217] as the sum of all weighted connections linked to each ROI. RSN strength was then obtained by aggregating the strengths of nodes belonging to that RSN and normalizing by the number of nodes in the respective network. To determine the dominant RSN of each BNS, we identified networks whose strength exceeded the mean plus one standard deviation across all seven RSNs. Visualization was performed using BrainNet Viewer [218], with each ROI colored according to its RSN affiliation and networks displayed using a sparsity threshold of 0.04.

6.3 Results

The results are presented for the delta, theta, and beta frequency bands, focusing on the association between BNSs and RSNs, followed by the statistical analysis of BNS temporal metrics. Additional analyses, including time-resolved BNS occupancy descriptive visualizations, phase-wise BNS presence across frequency bands, and detailed spatial characterization of BNSs, are provided in the Supplementary Material (Sections 11.3.1 and 11.3.2).

6.3.1 Delta

6.3.1.1 Association between BNSs and RSNs

BNS1 was characterized by dominant contributions from DAN and SAN, with a distributed topology spanning anterior and posterior regions (Fig. 6.2, Tab. 6.1). BNS2 showed a DAN-dominant configuration with widespread bilateral distribution across frontal, temporal, and occipital regions (Fig. 6.2, Tab. 6.1). BNS3 exhibited a globally integrated profile with relatively balanced contributions across RSNs, including AUD, DAN, and DMN, reflecting a distributed large-scale configuration (Fig. 6.2, Tab. 6.1). BNS4 was dominated by DAN and VIS networks, displaying a posterior-centered topology anchored by midline and occipital regions, consistent with a large-scale attentional–visual integration state (Tab. 6.1). BNS5 showed a relatively uniform profile across RSNs, with a slight predominance of DAN, indicating a broadly distributed integrative configuration (Fig. 6.2, Tab. 6.1). BNS6 was characterized by strong contributions from DAN, SAN, and VIS, with a distributed topology spanning frontal and posterior regions (Fig. 6.2, Tab. 6.1).

6.3.1.2 Statistical analysis of BNSs

To further characterize the temporal expression of these network configurations, we investigated *coverage*, *duration*, and *occurrence* using LMMs with FDR correction. In the *Delta* band, a significant group effect emerged for *Occurrence* in *BNS4* during the *BL* phase, with PD showing higher values than CTR (Fig. 6.3, Supplementary Material 11.3.4). Notably, BNS4 corresponds to the posterior attentional–visual integration state described above, suggesting that PD patients more frequently engage this large-scale DAN–VIS configuration at baseline.

6.3.2 Theta

6.3.2.1 Association between BNSs and RSNs

BNS1 was dominated by DAN, SAN, and VIS, forming a continuous anterior–posterior organization with strong frontal (DAN–SAN–DMN), central (MOT–DMN–SAN), and posterior (VIS–SAN–Other) interactions, consistent with a large-scale integrative configuration (Fig. 6.4, Tab. 6.2). BNS2 showed a relatively uniform profile with slight DAN predominance and widespread connectivity linking frontal, central, and posterior regions, including a prominent right-hemisphere DMN–Other interaction and reduced inferior–posterior coupling. BNS3 exhibited a DAN-dominant and asymmetric organization, with connectivity concentrated in lateral temporal and inferior–posterior regions and sparse superior–central interactions, particularly in the right hemisphere (Fig. 6.4, Tab. 6.2). BNS4 reflected a globally integrated, DMN-centered configuration, with major hubs in PCC, precuneus, and frontal regions, strongly coupled with motor and attentional systems, forming a large-scale bilaterally symmetric network (Fig. 6.4, Tab. 6.2). BNS5 was characterized by VIS–DAN dominance and a right-lateralized anterior-to-posterior connectivity pattern linking frontal, temporal, and posterior occipital regions, consistent with visuospatial integration (Fig. 6.4, Tab. 6.2).

6.3.2.2 Statistical analysis of BNSs

In the *Theta* band, *Duration* in *BNS4* during the *PRE* phase remained significant after FDR correction, with higher values observed in PD compared to CTR (Fig. 6.5, Supplementary Material 11.3.4). Given that BNS4 reflects a DMN-centered, globally integrated configuration, this result indicates a prolonged engagement of this large-scale default-mode–driven state during the preparatory phase in PD.

6.3.3 Beta

6.3.3.1 Association between BNSs and RSNs

BNS1 showed a globally distributed configuration dominated by DMN and DAN, with strong integration across posterior visual, sensorimotor, and asso-

ciative regions, forming a largely symmetric large-scale network state (Fig. 6.6, Tab. 6.3). BNS2 reflected a DMN-centered integrative state, with prominent midline hubs (PCC, precuneus, ACC) strongly coupled with posterior visual and lateral associative cortices, indicating large-scale interaction between internally oriented and visual systems (Fig. 6.6, Tab. 6.3). BNS3 exhibited a relatively balanced configuration with a slight DAN–VIS predominance, characterized by posterior and sensorimotor clustering and broadly distributed connectivity, which was slightly reduced in the right hemisphere (Fig. 6.6, Tab. 6.3). BNS4 combined a symmetric sensorimotor core with modest DMN and DAN contributions, including a mild right-lateralized attentional component (Fig. 6.6, Tab. 6.3). BNS5 was characterized by strong DAN and AUD contributions, with a predominantly posterior occipital organization and limited involvement of other regions, consistent with a sensory-driven configuration (Fig. 6.6, Tab. 6.3).

6.3.3.2 Statistical analysis of BNSs

In the *Beta* band, significant group differences emerged during the *BL* phase after FDR correction (Fig. 6.7, Supplementary Material 11.3.4). Specifically, *Coverage* and *Duration* in *BNS1* were higher in controls (CTR > PD), whereas *Occurrence* in *BNS2* was higher in PD patients (PD > CTR).
Notably, BNS1 corresponds to the globally distributed DMN–DAN integrative state described above, indicating a more stable and sustained engagement of this large-scale configuration in controls. In contrast, BNS2 reflects a DMN-centered integrative network linking internal and visual processing systems; its increased occurrence in PD suggests a shift toward more frequent recruitment of this alternative configuration at baseline.

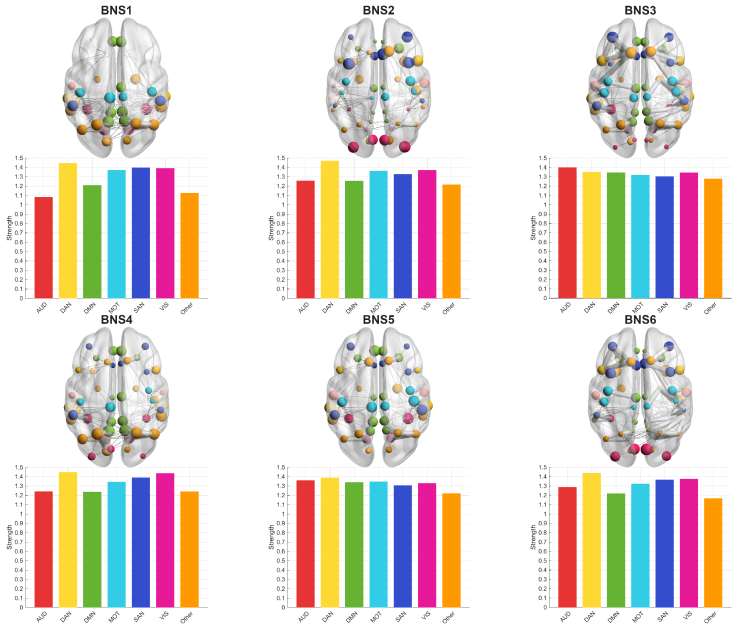


Figure 6.2: **Delta: Prevalence of RSNs in each BNS.** Calculated as the sum of the node strength values for each ROI associated with each RSN. Each BNS is displayed with nodes sized proportionally to their strength, while edges are shown using a sparsity threshold of 0.04. Colors represent distinct RSNs: AUD (red), DAN (yellow), DMN (green), MOT (cyan), SAN (blue), VIS (magenta), and Other (orange).

BNS	AUD	DAN	DMN	MOT	SAN	VIS	Other
BNS1	1.083	**1.446**	1.210	1.371	1.399	1.392	1.127
BNS2	1.258	**1.472**	1.257	1.364	1.328	1.372	1.217
BNS3	**1.401**	1.352	1.346	1.319	1.304	1.344	1.280
BNS4	1.243	**1.448**	1.237	1.344	1.390	1.437	1.242
BNS5	1.361	**1.389**	1.341	1.347	1.306	1.331	1.222
BNS6	1.289	**1.439**	1.222	1.324	1.367	1.376	1.168

Table 6.1: **Delta mean strength values for each BNS across networks.** The highest value per BNS is highlighted in bold.

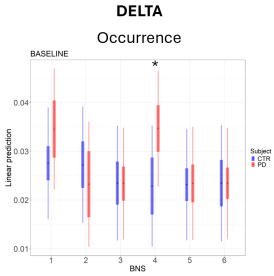


Figure 6.3: **LMM analysis.** Linear mixed-model analysis revealed significant between-group differences in BNS dynamics. In the *delta* band, the PD group showed a higher *occurrence* of BNS4 during BL.

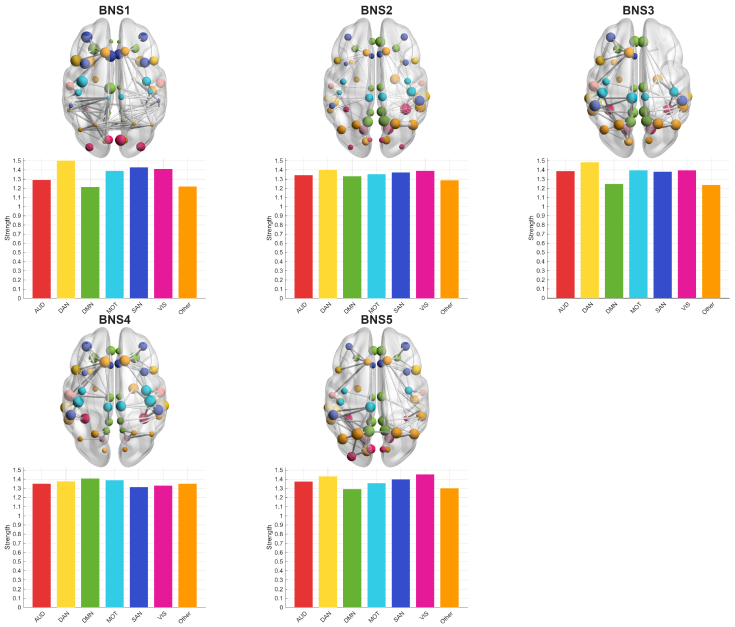


Figure 6.4: **Theta: Prevalence of RSNs in each BNS.** Prevalence was calculated as the sum of the node-strength values of the ROIs associated with each RSN. Node size is proportional to strength, while edges are displayed using a sparsity threshold of 0.04. Colors represent AUD (red), DAN (yellow), DMN (green), MOT (cyan), SAN (blue), VIS (magenta), and Other (orange).

BNS	AUD	DAN	DMN	MOT	SAN	VIS	Other
BNS1	1.291	**1.503**	1.215	1.390	1.429	1.412	1.219
BNS2	1.345	**1.401**	1.332	1.354	1.373	1.391	1.287
BNS3	1.387	**1.484**	1.247	1.395	1.381	1.395	1.236
BNS4	1.351	1.376	**1.408**	1.389	1.314	1.330	1.350
BNS5	1.373	1.431	1.292	1.356	1.397	**1.453**	1.300

Table 6.2: **Theta mean strength values for each BNS across networks.** The highest value for each BNS is highlighted in bold.

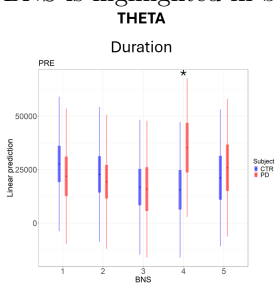


Figure 6.5: **LMM analysis.** Linear mixed-model analysis revealed significant between-group differences in BNS dynamics. In the *theta* band, PD showed a longer *duration* of BNS4 during PRE. The reported effect survived FDR correction ($*p < 0.05$).

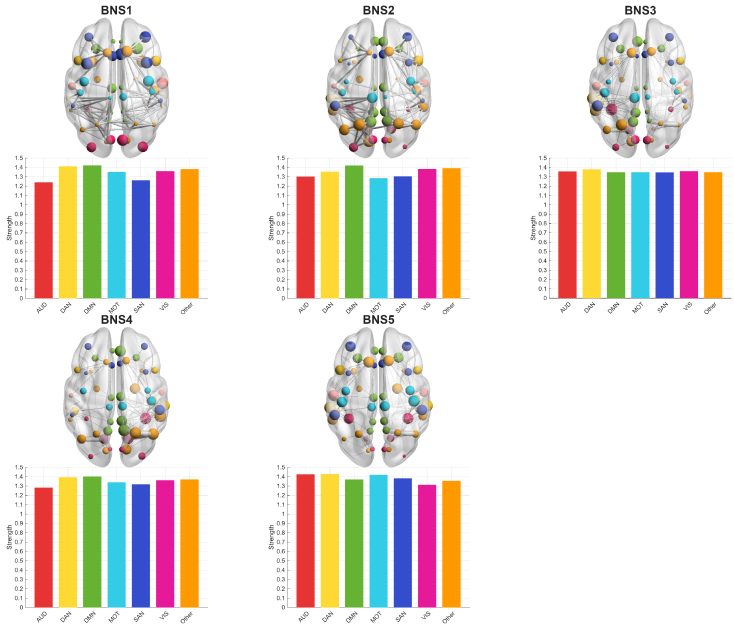


Figure 6.6: **Beta: Prevalence of RSNs in each BNS.** Prevalence was calculated as the sum of the node-strength values of the ROIs associated with each RSN. Node size is proportional to strength, while edges are displayed using a sparsity threshold of 0.01. Colors represent AUD (red), DAN (yellow), DMN (green), MOT (cyan), SAN (blue), VIS (magenta), and Other (orange).

BNS	AUD	DAN	DMN	MOT	SAN	VIS	Other
BNS1	1.241	1.412	**1.422**	1.351	1.263	1.360	1.382
BNS2	1.303	1.355	**1.420**	1.286	1.304	1.384	1.391
BNS3	1.358	**1.380**	1.349	1.348	1.347	1.360	1.350
BNS4	1.283	1.393	**1.401**	1.340	1.318	1.363	1.369
BNS5	1.426	**1.428**	1.369	1.418	1.383	1.314	1.355

Table 6.3: **Beta mean strength values for each BNS across networks.** The highest value for each BNS is highlighted in bold.

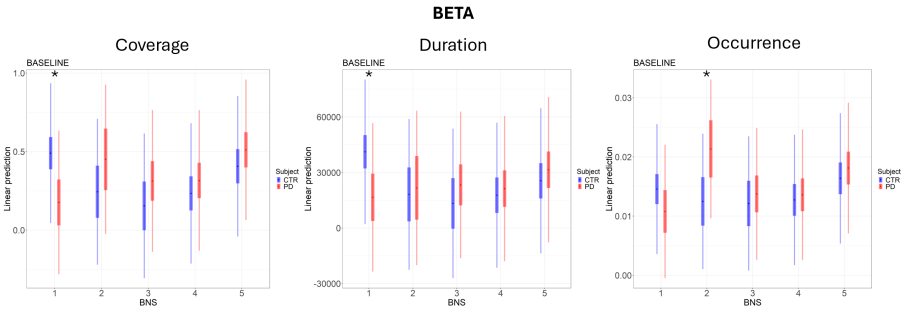


Figure 6.7: **LMM analysis.** During BL in the *beta* band, CTR showed greater *coverage* and *duration* of BNS1, whereas PD showed greater *occurrence* of BNS2. All effects remained significant after FDR correction ($*p < 0.05$).

Chapter 7

Postural Control Constraints and Muscle Activation Patterns in Parkinson's Disease

The material presented in this chapter is based on the study "Multimodal Assessment of Postural Control in Parkinson's Disease Using BioVRSea: Insights from CoP and Muscle Activation Patterns," submitted to MEDICON 2026, and will be published in the IFMBE Proceedings by *Springer Nature*. The chapter focuses on the application of the BioVRSea paradigm to the assessment of postural control in PD, using CoP and EMG signals acquired during a virtual-reality postural-control task.
The chapter focuses on the application of the BioVRSea paradigm to the assessment of postural control in PD, using CoP and EMG signals acquired during a virtual-reality postural-control task. It presents the comparison of postural responses to controlled visual and mechanical perturbations between individuals with PD and healthy controls. CoP features were used to characterize postural sway, spatial dispersion, directional variability, and post-perturbation readaptation, whereas EMG features were used to examine muscle-specific activation patterns in the tibialis anterior, gastrocnemius lateralis, and soleus muscles. By integrating posturographic and neuromuscular measures, the study explored whether PD was associated with a constrained postural strategy, reduced adaptability, and altered lower-limb muscle organization during balance-challenging conditions.

7.1 Introduction

The preceding chapters have characterized postural-control alterations in PD from multimodal and neurophysiological perspectives. Postural control depends on the continuous integration of visual, vestibular, and somatosensory information and on the ability to adapt motor responses to changing environmental demands [1, 4, 11]. In PD, this adaptive process may be compromised even be-

fore severe postural instability becomes clinically evident [95, 220, 221]. Deficits in sensorimotor integration can alter responses to perturbation and the processing of proprioceptive information [222], while quantitative assessment may reveal abnormalities that remain difficult to identify through clinical observation alone [223].
Clinical and functional assessments such as the MDS-UPDRS, Berg Balance Scale, and Timed Up and Go test remain important for evaluating motor and balance impairment, but may have limited sensitivity to subtle or early postural alterations [98, 224, 225]. Objective posturographic measures provide a complementary perspective by quantifying the spatial and temporal characteristics of balance regulation [32, 226]. In particular, CoP analysis can characterize the magnitude, dispersion, and directional organization of postural sway, while EMG provides information about the muscular strategies underlying these responses. Their combined analysis can therefore help determine whether altered postural behaviour in PD reflects not only greater instability, but also a more constrained or less adaptable neuromuscular strategy.
Virtual-reality approaches provide controlled conditions in which these responses can be examined during multisensory challenges [227, 228]. The BioVRSea paradigm and its experimental procedures have already been described in the preceding chapters and are therefore not repeated here. Previous BioVRSea investigations have demonstrated its ability to reveal PD-related alterations across cortical, postural, and physiological domains [190, 219, 229]. The present study extends these observations by focusing specifically on how exposure to mechanical perturbation influences subsequent biomechanical and lower-limb muscular behaviour.
For this purpose, particular attention was given to the PRE and POST phases of the BioVRSea protocol. These phases were performed under equivalent external conditions, with visual stimulation present and the motion platform stationary, but differed in their temporal relationship to the mechanical perturbation: PRE preceded platform movement, whereas POST immediately followed it. Comparison of these conditions therefore provides a means of examining the persistence of perturbation-induced adaptations after the mechanical stimulus has ceased. The present study compared individuals with PD and healthy controls using CoP measures of postural sway, spatial dispersion, and directional variability together with EMG features from the tibialis anterior, gastrocnemius lateralis, and soleus muscles. By integrating these measures, we aimed to determine whether PD was associated with constrained postural regulation, altered muscle-activation strategies, and reduced post-perturbation readaptation.

7.2 Material and Methods

7.2.1 Participants

This study initially included two cohorts: 54 patients with PD and 382 healthy controls. Before analysis, some PD participants were excluded because one or

both of the signals of interest were either missing or affected by acquisition issues that prevented reliable feature extraction. As a result, the final PD cohort included fewer subjects than originally recruited. To improve group comparability, a statistical selection procedure based on the Mahalanobis distance was applied to the pool of healthy controls. Height and weight were used as matching variables to identify the subset of controls most similar to the PD group from an anthropometric standpoint, thereby reducing potential bias associated with body-size differences between cohorts. Following signal quality screening and the matching procedure, the final study population consisted of 39 patients with PD and 39 healthy controls.

7.3 Results

7.3.1 Center of Pressure

After Bonferroni correction, only a limited subset of COP features reached statistical significance in the PRE phase, whereas a substantially larger number of features were significant in the POST phase. In PRE, significant group differences were observed for global displacement and velocity measures, namely TOTEX, which reflects the total excursion of the COP trajectory on the support plane ($p = 2.47 \times 10^{-2}$) Fig. 7.1, TOTEX AP, which represents the total excursion along the antero-posterior axis ($p = 1.31 \times 10^{-2}$), MVELO, which reflects the mean COP velocity on the support plane ($p = 2.47 \times 10^{-2}$) Fig. 7.1, and MVELO AP, which represents the mean velocity along the antero-posterior axis ($p = 1.31 \times 10^{-2}$).
Significant differences were also found for directional extreme-point measures, including Antero Magnitude, corresponding to the magnitude of the furthest point in the anterior portion of the plane ($p = 1.90 \times 10^{-8}$), Postero Magnitude, corresponding to the magnitude of the furthest point in the posterior portion of the plane ($p = 2.13 \times 10^{-6}$), and Right Magnitude, corresponding to the magnitude of the furthest point in the right portion of the plane ($p = 2.09 \times 10^{-4}$).
In the POST phase, significance extended to a broader set of features. These included global measures such as TOTEX ($p = 3.14 \times 10^{-6}$), TOTEX ML, which reflects total excursion along the medio-lateral axis ($p = 4.39 \times 10^{-5}$), TOTEX AP ($p = 4.13 \times 10^{-6}$), MVELO ($p = 3.14 \times 10^{-6}$), MVELO ML, which reflects mean velocity along the medio-lateral axis ($p = 4.39 \times 10^{-5}$), and MVELO AP ($p = 4.13 \times 10^{-6}$); distance-based metrics including RD, which represents the square-root distance between a COP point and the origin ($p = 1.28 \times 10^{-5}$), MDIST ML, which reflects the mean distance in the medio-lateral direction ($p = 1.73 \times 10^{-4}$), MDIST AP, which reflects the mean distance in the antero-posterior direction ($p = 3.41 \times 10^{-5}$), RDIST, which represents the root mean square distance from the origin ($p = 7.11 \times 10^{-6}$), RDIST ML, which reflects the root mean square distance in the medio-lateral direction ($p = 9.25 \times 10^{-5}$), and RDIST AP, which reflects the root mean square distance in the antero-posterior direction ($p = 2.15 \times 10^{-5}$); variability measures such as SD AP, which reflects the standard deviation in the antero-posterior direction ($p = 2.15 \times 10^{-5}$),

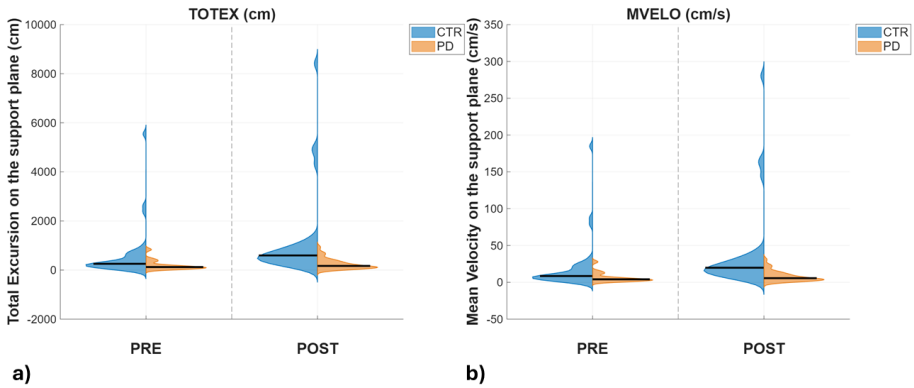


Figure 7.1: **CoP Total Excursion and Mean Velocity** ***a)*** Total CoP Excursion (TOTEX) for the control group (CTR, blue) positioned to the left and Parkinson's disease group (PD, orange) positioned to the right within each assessment phase, namely PRE and POST phases. Black horizontal lines represent the median values. Across the two phases, the control group showed a broader distribution and higher median values than the Parkinson group. ***b)*** Mean CoP Velocity (MVELO) for the control group (CTR, blue) positioned to the left and the Parkinson's disease group (PD, orange) positioned to the right within each assessment phase, namely PRE and POST. Black horizontal lines represent the median values. Across the two phases, the control group showed a broader distribution and higher median values than the Parkinson group.

SD ML, which reflects the standard deviation in the medio-lateral direction ($p = 9.25 \times 10^{-5}$), and SD Magnitude, which reflects the standard deviation of the distance of COP points with respect to the origin ($p = 2.52 \times 10^{-6}$); and spatial descriptors including EllipseArea, which reflects the area of the 95% confidence ellipse ($p = 5.42 \times 10^{-6}$), EllipseMainAxisLength, which reflects the length of the major axis of the 95% confidence ellipse ($p = 7.50 \times 10^{-6}$), and EllipseMinorAxisLength, which reflects the length of the minor axis of the 95% confidence ellipse ($p = 3.08 \times 10^{-5}$). Directional features also remained highly significant in POST, with Antero Magnitude ($p = 1.12 \times 10^{-11}$) and Postero Magnitude ($p = 3.38 \times 10^{-11}$).

A subset of features remained statistically significant across both phases, specifically TOTEX, TOTEX AP, MVELO, MVELO AP, Antero Magnitude, and Postero Magnitude. Overall, these variables describe the extent and velocity of COP displacement, particularly along the antero-posterior axis, as well as the most extreme anterior and posterior sway excursions. This pattern is visually illustrated in Fig. 7.2, where CTR participants exhibit larger sway areas than PD participants, with a clear elongation along the antero-posterior direction and an increase from PRE to POST.

For these features, a consistent group effect was observed at the subject level,

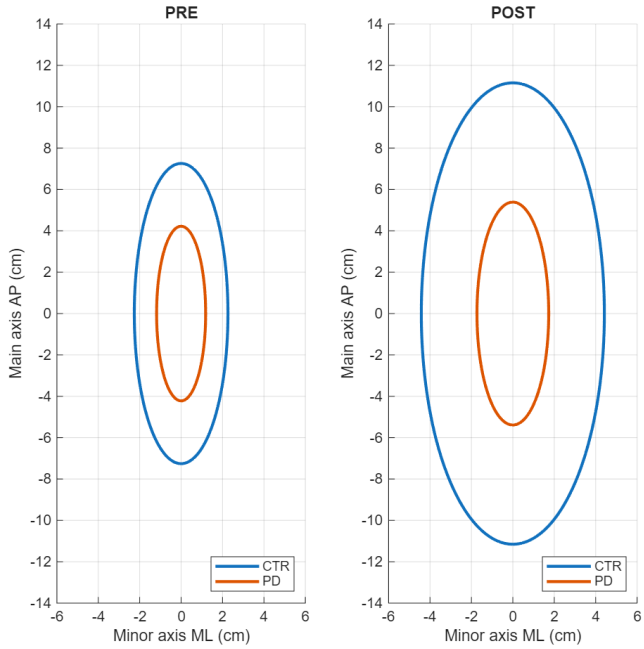


Figure 7.2: **Mean center-of-pressure (CoP) ellipses for the control group (CTR) and Parkinson's disease group (PD) across the PRE, MOV, and POST phases.** Ellipses are shown in the mediolateral (ML, minor axis) and anteroposterior (AP, main axis) directions. Across all phases, the CTR group exhibited larger sway ellipses than the PD group, with the greatest ellipse area observed during the POST phase

with higher values in CTR than in PD in both phases. In the PRE phase, mean values for CTR versus PD were: TOTEX (570.82 vs 188.31 cm), TOTEX AP (498.57 vs 173.26 cm), MVELO (19.02 vs 6.27 cm/s), and MVELO AP (16.61 vs 5.77 cm/s). Similarly, directional components showed marked differences, with Antero Magnitude (10.84 vs 2.23) and Postero Magnitude (8.30 vs 2.07). In the POST phase, the same pattern was preserved and amplified: TOTEX (1100.03 vs 242.51 cm), TOTEX AP (889.68 vs 221.76 cm), MVELO (36.65 vs 8.08 cm/s), and MVELO AP (29.65 vs 7.39 cm/s). Directional measures also increased in magnitude in CTR while remaining low in PD, with Antero Magnitude (14.40 vs 2.79) and Postero Magnitude (15.25 vs 2.75). Across both phases, CTR participants consistently exhibited larger sway excursions and higher velocities than PD participants, as shown in Fig. 7.2. This effect was particularly pronounced along the anterior-posterior axis and in directional sway components. Overall, features related to sway magnitude and velocity were the only metrics that remained robustly significant across both phases, whereas spatial, variability, and distance-based features became significant only in the POST phase, suggesting increased sensitivity of these measures under

more demanding or later-stage conditions.

7.3.2 Electromyography

7.3.2.1 Soleus

The analysis of electromyographic features of the soleus muscle revealed a limited number of significant differences between CTR and PD, with a highly selective and phase-specific pattern (Table 7.1). Significant effects were predominantly observed in the left soleus (SL), while the right soleus (SR) showed only a small number of isolated differences. Overall, the majority of features did not reach statistical significance across phases, indicating a generally preserved activation profile. In the *Baseline* phase, a small set of frequency-domain features differed between groups, including median frequency (FMD) and Welch-based descriptors (Fkurt Welch, Fskew Welch, FMN Welch, FMD Welch), as well as low-frequency power (P 0–100) and signal skewness (SKEW). Notably, significant features were observed in both the left and right soleus, although not necessarily the same metrics on each side. During the *PRE* phase, no features were statistically significant, indicating no detectable group differences in soleus activity during the anticipatory stage. In the *POST* phase, significant differences emerged in variability-related measures, including coefficient of variation (CV), as shown in Fig.7.3a, logarithmic coefficient of variation (LCV), standard deviation (SD), as illustrated in Fig.7.3b, and variance (VAR), primarily in the left soleus.

7.3.2.2 Gastrocnemius Lateralis

The analysis of electromyographic features of the gastrocnemius lateralis revealed extensive and consistent differences between CTR and PD across all experimental phases, with a markedly higher number of significant features compared to the soleus muscle (Table 7.2). Significant effects were observed bilaterally (GLL and GLR) and across a wide range of feature domains, including time-domain, frequency-domain, variability, and nonlinear descriptors, indicating a global alteration in the activation patterns of the gastrocnemius lateralis. In the *Baseline* phase, numerous features were already significantly different between groups. These included frequency-related measures (e.g., low-frequency power bands P 0–100 and P 100–200, Welch-based spectral features), as well as time-domain amplitude and variability metrics such as RMS, MAV, IEMG, variance (VAR), standard deviation (SD), waveform length (WL), and interquartile range (IQR). In addition, several nonlinear descriptors, including approximate entropy (AE), higher-order moments (ASM, ASS), and L-moment-based features, were significantly different. During the *PRE* phase, no features reached statistical significance, suggesting that differences in gastrocnemius lateralis activity were not detectable during the anticipatory stage of the task. In the *POST* phase, several features remained significant, although fewer than in Baseline. These included variability-related measures (CV, LCV, VAR), as shown in Fig.7.4a,c, distribution-based descriptors (kurtosis), and selected amplitude features such

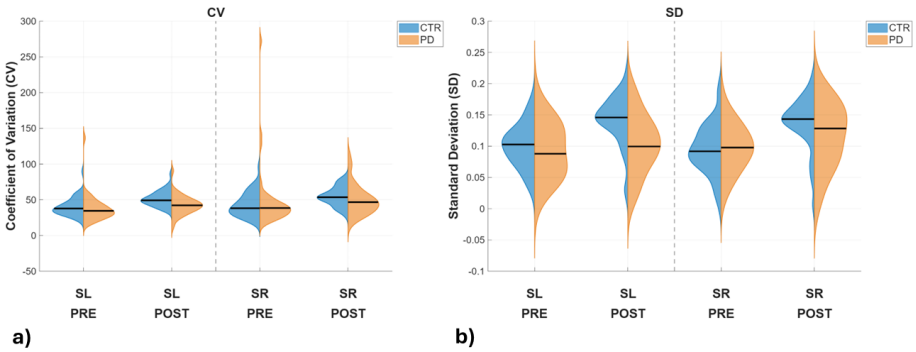


Figure 7.3: **EMG coefficient of variation and standard deviation** ***a)*** EMG coefficient of variation (CV) for Soleus Left (SL) and Soleus Right (SR) in the PRE and POST phases. CTR (blue) is shown on the left and PD (orange) on the right within each phase. Black horizontal lines indicate the median. A significant inter-group difference was found for SL in the POST phase. ***b)*** EMG standard deviation (SD) for SL and SR in the PRE and POST phases. CTR (blue) is shown on the left and PD (orange) on the right within each phase. Black horizontal lines indicate the median. A significant inter-group difference was found for SL in the POST phase, with higher variability in CTR than in PD.

as IEMG (Fig.7.4b) and waveform length (WL). Nonlinear features (e.g., ASS) also remained significant.

7.3.2.3 Tibialis Anterior

The analysis of electromyographic features of the tibialis anterior revealed a substantial number of significant differences between CTR and PD, with a pattern that was highly phase-specific and strongly lateralized (Table 7.3). Most of the significant effects were observed during the Baseline phase, in both the left tibialis anterior (TAL) and right tibialis anterior (TAR), whereas the PRE phase showed no significant differences. During MOV, significant effects were found almost exclusively in the right tibialis anterior, while the POST phase showed only a limited number of significant results. In the *Baseline* phase, both TAL and TAR exhibited numerous significant differences across multiple feature domains. These included frequency-related measures, such as low-frequency band powers (P 0–100 and P 100–200), Welch-based spectral features, and mean frequency (MN), together with time-domain and variability-related features including SD1, SD2, AAC, DAMV, DASDV, DVARV, EMAV, IEMG, IQR, MAD, MAV, RMS, SD, VAR, SSI, VARE, VO, and waveform length (WL). In addition, nonlinear and distribution-based descriptors were also significant,

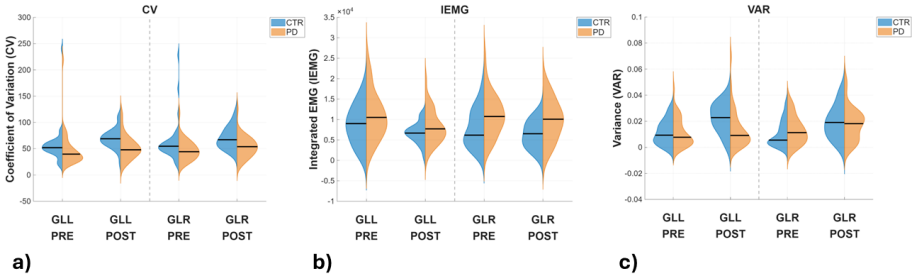


Figure 7.4: **EMG coefficient of variation, integrated EMG, and variance.** CTR (blue, left) and PD (orange, right) are compared in PRE and POST, with black horizontal lines indicating medians. ***a)*** CV for GLL and GLR, showing higher POST medians and dispersion in CTR. ***b)*** IEMG for GLL and GLR, showing higher medians and a broader upper distribution in PD. ***c)*** VAR for GLL and GLR, with higher POST median and dispersion for GLL in CTR.

including approximate entropy (AE), ASM, ASS, and L-moment scale, skewness, and kurtosis. On the right side, further baseline differences were observed for frequency kurtosis and skewness (Fkurt and Fskew). In the *PRE* phase, no features reached statistical significance for either TAL or TAR, indicating that no detectable group differences emerged during the anticipatory stage. In the *POST* phase, only a small number of features remained significant, all confined to the right side, including MAD, SD, and VAR, as shown in Fig.7.5. No significant effects were observed in the left tibialis anterior during this phase.

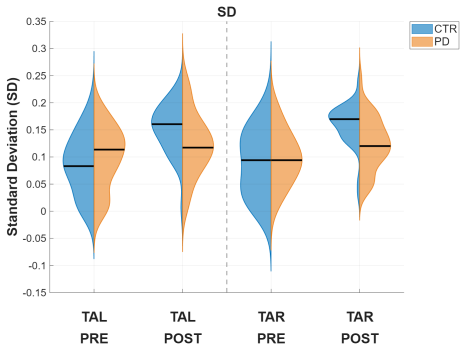


Figure 7.5: **EMG Standard Deviation (SD) for the Tibialis Anterior Left (TAL) and Right (TAR).** The control group (CTR, blue) is positioned to the left and the Parkinson's disease group (PD, orange) to the right within each phase, namely PRE and POST. Black horizontal lines represent the median values. In the POST phase, the CTR group exhibited significantly higher median SD and broader dispersion in both muscles compared to the more constrained PD profile.

Table 7.1: Statistical significance across phases (Bonferroni-corrected, $p < 0.05$) for S muscle.

Feature	**SL**			**SR**		
	Baseline	**PRE**	**POST**	**Baseline**	**PRE**	**POST**
P 0 100	4.98×10^{-2}					
P 100 200						
FMD	2.57×10^{-3}					
Pmax						
Fmax						
Fkurt						
Fskew						
SD1						
SD2						
RatioSD	7.04×10^{-3}			4.16×10^{-2}		
AAC						
Fkurt welch	1.14×10^{-2}			4.81×10^{-2}		
Fskew welch	6.76×10^{-3}			3.59×10^{-2}		
PT welch						
Pmax welch						
FMN welch	2.98×10^{-2}					
FMD welch	2.08×10^{-3}			3.64×10^{-2}		
PT trapz welch						
P 0 100 welch						
P 100 200 welch						
AE						
ASM						
ASS						
CV			3.59×10^{-2}			
DAMV						
DASDV						
DVARV						
EMAV						
EWL						
FZC	2.66×10^{-2}					
KURT						
IEMG						
IQR						
LCV			3.59×10^{-2}			
LD						
LDAMV						
LDASDV						
LTKEO						
MAD						
MAV						
MFL						
MN						
MD						
MMAV						
MMAV2						
MSR						
RMS						
SD			1.07×10^{-2}			
SKEW	9.73×10^{-3}					
SSI						
TM						
VAR			1.18×10^{-2}			
VARE						
VO						
WL						
L moments mean						
L moments scale						
L moments Skewness						
L moments Kurtosis						

Table 7.2: Statistical significance across phases (Bonferroni-corrected, $p < 0.05$) for GL muscle.

Feature	**GLL**			**GLR**		
	Baseline	**PRE**	**POST**	**Baseline**	**PRE**	**POST**
P 0 100	2.36×10^{-3}			3.44×10^{-5}		
P 100 200	1.23×10^{-2}			6.47×10^{-4}		
FMD						
Pmax						
Fmax				1.62×10^{-2}		
Fkurt						
Fskew						
SD1	1.23×10^{-2}			9.33×10^{-4}		
SD2	3.78×10^{-3}			1.10×10^{-4}		
RatioSD						
AAC	1.44×10^{-2}			5.14×10^{-4}		
Fkurt welch						
Fskew welch						
PT welch						
Pmax welch	3.33×10^{-3}			1.28×10^{-4}		
FMN welch	4.47×10^{-2}			5.28×10^{-3}		
FMD welch						
PT trapz welch	3.33×10^{-3}			1.28×10^{-4}		
P 0 100 welch	2.17×10^{-3}			4.23×10^{-5}		
P 100 200 welch	1.01×10^{-2}			6.47×10^{-4}		
AE	2.36×10^{-3}			1.64×10^{-4}		
ASM	8.98×10^{-3}			1.35×10^{-4}		
ASS	8.28×10^{-3}			1.41×10^{-4}		3.19×10^{-3}
CV			3.80×10^{-2}			1.80×10^{-2}
DAMV	1.44×10^{-2}			5.14×10^{-4}		
DASDV	1.23×10^{-2}			9.33×10^{-4}		
DVARV	1.23×10^{-2}			9.33×10^{-4}		
EMAV	1.14×10^{-2}			1.35×10^{-4}		
EWL	2.13×10^{-2}			4.26×10^{-4}		3.33×10^{-3}
FZC						
KURT			4.64×10^{-2}			
IEMG	4.29×10^{-3}			2.53×10^{-4}		4.47×10^{-2}
IQR	1.69×10^{-2}			7.78×10^{-4}		
LCV			7.64×10^{-3}			7.04×10^{-3}
LD	1.19×10^{-2}			2.92×10^{-4}		
LDAMV	1.44×10^{-2}			5.14×10^{-4}		
LDASDV	1.23×10^{-2}			9.33×10^{-4}		
LTKEO	1.14×10^{-2}			6.47×10^{-4}		
MAD	2.47×10^{-3}			3.27×10^{-5}		
MAV	9.35×10^{-3}			1.41×10^{-4}		
MFL	1.19×10^{-2}			8.91×10^{-4}		
MN	4.86×10^{-3}			2.78×10^{-4}		
MD	2.57×10^{-3}			3.94×10^{-3}		
MMAV	7.33×10^{-3}			1.48×10^{-4}		
MMAV2	3.47×10^{-3}			1.16×10^{-4}		
MSR	1.80×10^{-3}			4.07×10^{-4}		
RMS	2.36×10^{-3}			1.64×10^{-4}		
SD	7.10×10^{-4}			5.91×10^{-6}		
SKEW						
SSI	2.93×10^{-3}			1.05×10^{-4}		
TM	6.47×10^{-4}			7.04×10^{-5}		
VAR	7.10×10^{-4}		3.86×10^{-2}	5.91×10^{-6}		
VARE	3.33×10^{-3}			1.22×10^{-4}		
VO	3.33×10^{-3}			1.22×10^{-4}		
WL	4.11×10^{-3}			1.22×10^{-3}		
L-moments mean						
L-moments scale	5.75×10^{-5}			3.03×10^{-6}		
L-moments Skewness	6.69×10^{-5}			2.42×10^{-6}		
L-moments Kurtosis	6.69×10^{-5}			2.29×10^{-6}		

Table 7.3: Statistical significance across phases (Bonferroni-corrected, $p < 0.05$) for TA muscle.

Feature	**TAL**			**TAR**		
	Baseline	**PRE**	**POST**	**Baseline**	**PRE**	**POST**
P 0 100	1.40×10^{-3}			3.21×10^{-4}		
P 100 200	1.34×10^{-3}			4.07×10^{-4}		
FMD						
Pmax						
Fmax						
Fkurt				7.04×10^{-3}		
Fskew				1.44×10^{-2}		
SD1	1.53×10^{-3}			2.19×10^{-4}		
SD2	1.53×10^{-3}			1.56×10^{-4}		
RatioSD						
AAC	7.78×10^{-4}			3.06×10^{-4}		
Fkurt welch						
Fskew welch						
PT welch						
Pmax welch	1.67×10^{-3}			1.72×10^{-4}		
FMN welch	1.75×10^{-2}			1.23×10^{-2}		
FMD welch						
PT trapz welch	1.67×10^{-3}			1.72×10^{-4}		
P 0 100 welch	1.34×10^{-3}			3.88×10^{-4}		
P 100 200 welch	1.22×10^{-3}			3.88×10^{-4}		
AE	4.68×10^{-4}			6.69×10^{-5}		
ASM	6.78×10^{-4}			3.70×10^{-4}		
ASS	7.78×10^{-4}			2.41×10^{-4}		
CV						
DAMV	7.78×10^{-4}			3.06×10^{-4}		
DASDV	1.53×10^{-3}			2.19×10^{-4}		
DVARV	1.53×10^{-3}			2.19×10^{-4}		
EMAV	1.02×10^{-3}			2.53×10^{-4}		
EWL	1.07×10^{-3}			3.53×10^{-4}		
FZC						
KURT						
IEMG	4.47×10^{-4}			8.61×10^{-5}		
IQR	1.12×10^{-3}			2.19×10^{-4}		
LCV						
LD	9.76×10^{-4}			2.19×10^{-4}		
LDAMV	7.78×10^{-4}			3.06×10^{-4}		
LDASDV	1.53×10^{-3}			2.19×10^{-4}		
LTKEO	1.40×10^{-3}			2.09×10^{-4}		
MAD	2.07×10^{-3}			3.88×10^{-4}		3.54×10^{-2}
MAV	7.10×10^{-4}			2.65×10^{-4}		
MFL	1.53×10^{-3}			2.19×10^{-4}		
MN	4.07×10^{-4}			9.05×10^{-5}		
MD	8.14×10^{-4}			1.22×10^{-3}		
MMAV	4.47×10^{-4}			3.53×10^{-4}		
MMAV2	9.76×10^{-3}			1.07×10^{-3}		
MSR	3.37×10^{-4}			7.40×10^{-5}		
RMS	4.68×10^{-4}			6.69×10^{-5}		
SD	8.62×10^{-3}			7.10×10^{-4}		1.56×10^{-2}
SKEW						
SSI	1.67×10^{-3}			1.56×10^{-4}		
TM	6.76×10^{-3}			2.92×10^{-4}		
VAR	8.62×10^{-3}			7.10×10^{-4}		3.12×10^{-2}
VARE	1.67×10^{-3}			1.56×10^{-4}		
VO	1.67×10^{-3}			1.56×10^{-4}		
WL	3.88×10^{-4}			4.69×10^{-5}		
L-moments mean						
L-moments scale	3.59×10^{-2}			8.91×10^{-4}		
L-moments Skewness	3.21×10^{-2}			9.76×10^{-4}		
L-moments Kurtosis	2.98×10^{-2}			1.02×10^{-3}		

Chapter 8

Discussion

8.1 BioVRSea as a Multisystem Framework for Postural-Control Assessment

The studies included in this thesis investigated postural control through the BioVRSea paradigm, an experimental framework designed to expose participants to a realistic and progressively challenging visuomotor perturbation. Across the different papers, the same task was used to study how participants maintained balance when exposed to a virtual sea environment and, depending on the phase of the protocol, to corresponding moving-platform stimulation. This design allowed postural control to be assessed not only during quiet standing, but also during visual conflict, combined visual-motor perturbation, and post-perturbation recovery.

A central contribution of the BioVRSea paradigm is that it does not reduce balance assessment to a single outcome. Instead, it allows postural control to be investigated as a quantitative multisystem response involving biomechanical, neuromuscular, and cortical mechanisms. CoP analysis describes the observable outcome of postural regulation, providing information on sway amplitude, spatial dispersion, temporal organization, and complexity. EMG provides insight into the muscular strategies used to maintain stability, including muscle-specific activation patterns and neuromuscular variability. EEG, through spectral analysis and dynamic functional connectivity, extends the interpretation to cortical activity and large-scale brain-network organization. Together, these signals show that balance is not a passive mechanical process, but an active and adaptive control mechanism.

For this reason, the results of the individual studies should not be interpreted as isolated findings. Rather, they collectively demonstrate that postural control is context-dependent and that the physiological meaning of a given response depends on the population being studied. In Parkinson's disease, altered sway, modified lower-limb muscle activation, and changes in cortical activity suggest a constrained and compensatory postural-control strategy. In seafarers, increased sway variability and complexity, together with specific lower-limb

muscle activation patterns, appear to reflect functional adaptation to prolonged exposure to unstable environments. In healthy controls, the response to the task provides a reference model of physiological adaptation to visual and mechanical perturbation.
The value of the BioVRSea approach, therefore, lies in its ability to reveal how different populations solve the same balance challenge through different control strategies. The following discussion is organized around the main topics investigated across the thesis: CoP, EMG, and EEG. This structure allows the biomechanical, neuromuscular, and cortical components of the BioVRSea response to be discussed separately, while preserving their interpretation as complementary levels of the same multisystem postural-control process.

8.1.1 Center of Pressure as a Marker of Postural Strategy

CoP analysis was central across the studies because it provided a direct quantitative description of postural behavior. The extracted CoP features described sway excursion, velocity, variability, entropy, complexity, and spatial distribution. These parameters made it possible to move beyond a simple interpretation of balance as either stable or unstable. Instead, CoP features allowed the characterization of different postural strategies.
In the context of BioVRSea, CoP features were particularly informative because the protocol progressively challenged sensory integration. The PRE phase mainly reflected the response to visual stimulation, while the MOV and POST phases reflected combined visuomotor perturbation and subsequent recovery. Therefore, changes in CoP across phases provided information on how participants adapted to the task and how their postural-control system reorganized after perturbation.

Reduced and constrained sway in Parkinson's disease Across the Parkinson's disease studies included in this thesis, CoP analysis consistently indicated that participants with PD adopted a more constrained postural strategy than healthy controls. Taken together, these studies show that the BioVRSea paradigm can reveal disease-related differences in postural regulation, particularly after exposure to visual and mechanical perturbation.
In the first exploratory study, CoP analysis highlighted reduced sway in PD participants during the task. This finding was relevant because quantitative assessment of PD-related balance impairment has often focused on gait analysis, including accelerometers and force sensors placed inside the shoes, rather than on force-platform-based assessment during standing [230]. Within the BioVRSea paradigm, the standing postural response was assessed during phases of visual and motor stimulation, enabling the identification of altered balance strategies that standard gait-based approaches may miss.
The reduced sway observed in PD participants should not be interpreted as better stability. Rather, it may reflect a more rigid and less flexible postural-control strategy. Parkinson's disease can interfere with the ability to maintain and adjust balance through several mechanisms, including impaired coordination between agonist and antagonist muscles, altered automatic postural responses,

axial rigidity, and reduced mobility [231]. These factors may lead individuals with PD to limit their sway as a compensatory strategy, thereby reducing movement amplitude to maintain stability. In this sense, reduced CoP excursion may reflect pathological constraint rather than efficient balance control.

In the initial small-cohort study, the clearest differences between PD and healthy controls emerged in the POST phase, that is, after exposure to platform-induced movement. This phase is particularly informative because it reflects the ability of the postural-control system to reorganize after a sensory and mechanical perturbation. Among the extracted features, the mediolateral complexity index showed a large effect size, with higher values in the PD group. This result was noteworthy because it contrasted with previous studies suggesting that postural complexity often decreases with disease and aging [232, 233]. Therefore, while the first study supported the presence of altered postural dynamics in PD, it also highlighted the difficulty of interpreting nonlinear CoP measures in small cohorts. In particular, higher complexity in PD may indicate compensatory reorganization, altered variability structure, or instability of control, but the study could not determine the precise mechanism.

The larger matched study provided a more robust interpretation of these preliminary findings. In this analysis, the comparison between the PRE and POST phases was especially important because the two phases shared the same visual condition, while POST occurred after the platform movement. CoP analysis showed that only a limited subset of features differed between PD and controls in PRE, whereas a broader range of global, distance-based, variability, velocity, and spatial descriptors became significant in POST. This indicates that the perturbation phase amplified group differences and exposed a reduced capacity of PD participants to recover or reorganize their postural response after stimulation.

Across both PRE and POST, the most consistent differences were related to sway magnitude and velocity, particularly along the anteroposterior axis. Controls showed larger total excursions and higher sway velocities than PD participants, including higher TOTEX, TOTEX AP, MVELO, and MVELO AP values. They also exhibited larger anterior and posterior sway magnitudes. In POST, this separation became more evident, with controls showing larger sway ellipses and broader spatial dispersion. These findings reinforce the interpretation that PD participants did not display superior stability, but rather a restricted sway pattern and reduced postural flexibility.

This distinction is important because postural stability is not simply the absence of movement. In healthy balance control, a certain amount of sway variability is physiological and reflects the ability of the system to explore, adjust, and respond to changing sensory conditions. By contrast, an excessively constrained sway pattern may indicate reduced adaptability. In PD, this may result from impaired sensorimotor integration, abnormal automatic postural responses, rigidity, or difficulty adapting postural strategies to changing task demands [1, 11, 222]. The stronger group separation observed in POST suggests that the BioVRSea perturbation exposed persistent differences in how PD and control participants regulated balance after stimulation.

The progression from the first to the second PD study is therefore important. The initial study demonstrated that BioVRSea could detect altered CoP behavior in a small early-stage PD cohort, with POST-phase differences and an unexpected increase in mediolateral complexity. The larger matched analysis confirmed the general interpretation of constrained postural control but provided a clearer and more stable pattern: PD participants showed reduced sway magnitude, reduced velocity, and smaller spatial dispersion, especially after perturbation. Thus, the larger study refined the interpretation of the preliminary findings by showing that the dominant CoP signature of PD in this paradigm is not simply altered complexity but a broader reduction in postural flexibility and adaptive sway.
Overall, the CoP findings support the view that Parkinson's disease is associated with altered postural regulation and reduced adaptability during complex sensory-motor conditions [222, 223, 226]. The BioVRSea paradigm appears particularly sensitive to these alterations because it challenges the postural-control system through visual conflict and platform-induced movement. The POST phase, in particular, may represent a useful window for identifying PD-related impairments, as it captures the residual effects of perturbation and the capacity of the system to return to an adaptive balance strategy. Therefore, reduced and constrained sway in PD should be interpreted not as preserved stability, but as evidence of a less flexible postural-control strategy that becomes more evident after perturbation.

Increased sway complexity in seafarers The seafarer study provided a complementary perspective to the Parkinson's disease studies because it did not compare a pathological cohort with healthy controls, but rather two healthy cohorts with different sensorimotor histories. Specifically, the analysis compared 21 sailors recently exposed to prolonged maritime conditions with 21 healthy controls selected to be comparable in terms of anthropometric characteristics. Therefore, the differences observed in this study should not be interpreted as disease-related alterations, but as the expression of expertise-dependent adaptation to an unstable environment.
The CoP results showed that sailors adopted a more dynamic postural strategy than healthy controls during the BioVRSea task. During the adaptation phase, sailors exhibited significantly higher total excursion in the antero-posterior direction (TOTEX AP) and higher mean velocity in the same direction (MVELO AP). These features indicate that sailors allowed larger and faster CoP displacements while maintaining an upright stance. In a pathological population, increased sway amplitude and velocity could be interpreted as reduced stability. However, in the present study, no balance loss or inability to complete the task was observed in sailors. Therefore, these higher values are better interpreted as functional postural flexibility rather than impaired balance. The increased AP excursion and velocity likely reflect a more responsive control strategy developed through repeated exposure to moving support surfaces, where continuous forward-backward adjustments are required to maintain equilibrium [127, 234,

235].

This interpretation is further supported by the entropy- and complexity-based CoP features. During the adaptation phase (PRE and MOV), sailors showed significantly higher ML Sample Entropy, ML Complexity Index, Magnitude Entropy, Direction Entropy, and Multivariate Complexity Index compared with controls. These findings suggest that their postural sway was not simply larger, but also more irregular, variable, and dynamically organized. Higher magnitude entropy indicates greater variability in the amplitude of sway over time, suggesting continuous modulation of postural corrections. Higher direction entropy indicates a less predictable sway trajectory, compatible with the use of multidirectional adjustments. Higher multivariate complexity suggests a more integrated interaction between the antero-posterior and medio-lateral components of sway.

Together, these results indicate that sailors did not maintain balance by minimizing movement. Instead, they appeared to maintain balance by allowing a richer and more flexible sway pattern. This is an important distinction because effective postural control does not necessarily correspond to reduced sway. In expert or adapted individuals, increased variability may represent a functional resource that allows the system to respond efficiently to changing environmental demands. In this sense, the seafarers' increased sway complexity may reflect a more adaptable postural-control system rather than poorer stability.

The fact that several significant differences emerged during the adaptation phase (PRE and MOV) is particularly relevant. This phase exposed participants to the combined effect of visual and mechanical perturbation, resembling the type of sensory-motor challenge that sailors experience in maritime environments. The higher TOTEX AP and MVELO AP values suggest that sailors responded to the perturbation with larger and faster antero-posterior adjustments, while the entropy and complexity measures indicate that these adjustments were organized in a more variable and multidimensional way. This pattern is consistent with the hypothesis that repeated exposure to unstable surfaces promotes the development of flexible postural strategies.

The habituation phase (POST) also supported this interpretation. Sailors showed a significantly higher antero-posterior Complexity Index than controls, indicating that their sway dynamics remained more complex even after the main perturbation. This suggests that expertise-related adaptation was not limited to the immediate response to movement, but also influenced the way the postural-control system reorganized after exposure to the task. The higher AP complexity in sailors may reflect an enhanced ability to maintain adaptive variability during recovery or habituation.

Overall, the seafarer findings show that increased sway and increased complexity can have a positive functional meaning when observed in a healthy expert population. Unlike Parkinson's disease, where altered sway was interpreted as constrained and less adaptive postural control, the seafarer cohort showed a pattern of increased dynamic flexibility. This comparison is important for the thesis because it demonstrates that BioVRSea does not simply classify larger sway as pathological or smaller sway as stable. Rather, the paradigm reveals

how different populations use different postural strategies according to their physiological condition and previous sensorimotor experience.
Therefore, in sailors, increased CoP excursion, velocity, entropy, and complexity likely represent expertise-dependent adaptation to unstable environments. The findings suggest that prolonged maritime exposure may train the postural-control system to tolerate and exploit variability, allowing more flexible and responsive balance regulation under dynamic conditions.

8.1.2 Electromyography as a Marker of Neuromuscular Adaptation

EMG analysis provided complementary information to CoP by identifying the muscular strategies associated with postural behavior. While CoP describes the global outcome of balance control, EMG describes how the neuromuscular system contributes to that outcome. In the BioVRSea studies, lower-limb muscles were particularly relevant because ankle and leg musculature are essential for maintaining upright stance and generating corrective responses to perturbation. The analysis of tibialis anterior, gastrocnemius lateralis, and soleus activity allowed the investigation of both anterior and posterior lower-limb control mechanisms. These muscles contribute to ankle stabilization, anterior-posterior sway regulation, and compensatory postural adjustments. Differences in their activation patterns therefore, provide insight into how participants respond to the task at the motor-execution level.

Muscle activation patterns in Parkinson's disease The EMG findings in Parkinson's disease indicate that the neuromuscular component of postural control is altered in a muscle- and phase-specific manner. Lower-limb muscles are fundamental for postural and balance regulation, particularly during ankle-based corrective strategies [236]. Across the Parkinson's disease studies included in this thesis, EMG analysis showed that group differences were not uniformly distributed across all recorded muscles, but depended on the muscle considered, the phase of the BioVRSea protocol, and the size and composition of the cohort. In the first BioVRSea study on early-stage Parkinson's disease, based on a smaller cohort of 9 PD participants and 29 healthy controls, the most evident EMG differences were found in the right tibialis anterior, with additional significant activity observed in the right soleus and left tibialis anterior [190]. In that study, only features extracted from the right tibialis anterior statistically differentiated the two groups. This result was interpreted in relation to the functional role of the tibialis anterior as the primary dorsiflexor of the foot, which is involved in ankle control and is critical during gait, especially for lifting the foot during the swing phase. The predominance of right-sided findings was also discussed in relation to possible limb dominance, considering the high prevalence of right-handedness in the general population [237]. However, given the limited number of PD participants, these findings should be interpreted as exploratory and as an initial indication that Parkinson's disease may alter lower-limb recruitment during the BioVRSea task.

The subsequent analysis conducted on a larger matched cohort refined this interpretation. In this later study, the final sample included 39 PD participants and 39 controls after exclusions and control selection, allowing a more robust evaluation of muscle-specific EMG patterns. The results showed that neuromuscular differences were not concentrated only in the tibialis anterior. Instead, they appeared to involve selective reorganization across the lower limb. The soleus displayed the fewest significant differences, with no effects in PRE and only a limited set of variability-related measures in POST, mainly on the left side. The tibialis anterior showed a phase-specific profile, with several baseline differences, no significant effects in PRE, and only a small number of POST effects confined to the right side. In contrast, the gastrocnemius lateralis showed the most extensive pattern of differences, with several significant features at baseline and additional effects persisting in POST, including variability-, distribution-, and amplitude-related measures such as CV, LCV, VAR, kurtosis, IEMG, waveform length, and ASS.

Taken together, these two studies suggest that EMG alterations in Parkinson's disease should not be interpreted as a uniform increase or decrease in lower-limb activity. Rather, they point toward a selective reorganization of neuromuscular control. The initial study highlighted the possible sensitivity of the right tibialis anterior, whereas the larger cohort suggested that the gastrocnemius lateralis may be particularly informative within the BioVRSea paradigm. This progression is important because it shows how the interpretation changed with increased sample size: what appeared initially as a mainly tibialis-anterior-driven effect became, in the larger cohort, a broader but still muscle-specific pattern of altered postural muscle recruitment.

A relevant aspect of the larger study is that several EMG differences were already present at baseline, before the visually perturbed PRE phase and before the movement phase. This suggests that Parkinson's disease participants may present an underlying alteration in neuromuscular control even before exposure to the full sensory-motor challenge. In contrast, CoP differences became especially informative in POST, indicating that the BioVRSea paradigm captures both baseline neuromuscular alterations and altered recovery or adaptation after perturbation. This distinction is important because it suggests that EMG and CoP provide complementary information: EMG may reveal pre-existing abnormalities in muscle recruitment, whereas CoP may better reflect the global postural outcome after the system has been challenged.

Overall, the EMG findings support the view that postural impairment in Parkinson's disease is expressed through task-dependent and muscle-specific alterations in automatic balance regulation rather than through a homogeneous impairment of all lower-limb muscles. This interpretation is consistent with previous evidence that Parkinson's disease affects postural muscle recruitment and automatic postural responses in a context-dependent manner [69, 238]. However, these results do not directly demonstrate specific mechanisms such as rigidity, co-contraction, or sensory reweighting. Instead, they indicate that BioVRSea is sensitive to altered neuromuscular organization and may help identify muscle-specific biomarkers of impaired balance control in Parkinson's

disease [190, 219, 221, 223].

Soleus-driven adaptation in seafarers The EMG results in the seafarer study provided complementary evidence that the differences observed in CoP behavior were supported by a specific neuromuscular strategy. Although several EMG features showed trends toward significance across muscles and phases before correction, only skewness (SKEW) of the right soleus during the adaptation phase remained statistically significant after Bonferroni correction. This result indicates that the clearest neuromuscular difference between sailors and matched healthy controls was not a generalized alteration of lower-limb muscle activity, but a selective change in the temporal distribution of soleus activation during the phase of active visuomotor perturbation.

Skewness describes the asymmetry of the EMG amplitude distribution over time and can provide information about how muscle activation is organized in terms of intensity and frequency of recruitment [239]. A positive skewness value indicates that the signal is characterized by frequent low-intensity activity with occasional high-intensity bursts. Conversely, a negative skewness value suggests a distribution with more frequent high-intensity activity or a more sustained activation pattern. Values close to zero indicate a more symmetrical distribution between lower and higher activation levels [240]. In the present study, healthy controls showed a slightly negative mean SKEW value, whereas sailors showed a positive mean SKEW value during the adaptation phase. This suggests that the two healthy cohorts used different neuromuscular activation strategies when exposed to the BioVRSea perturbation.

The positive skewness observed in sailors may reflect a strategy based on low-level background activation interrupted by occasional corrective bursts. This pattern is consistent with an adaptive postural-control strategy in which the muscle remains ready to respond, but is not continuously recruited at high intensity. Such organization may be advantageous in unstable environments because it allows rapid corrective responses while avoiding unnecessary sustained muscular effort. In contrast, the slightly negative skewness observed in healthy controls may indicate a different distribution of activation, possibly reflecting a less specialized response to the moving-platform condition.

The involvement of the soleus is physiologically meaningful. The soleus is one of the main ankle muscles contributing to upright stance and antero-posterior balance regulation. It plays an important role in maintaining the body against gravity and in producing corrective responses during postural perturbations. Since the BioVRSea task challenges balance through visual and platform-induced motion, a selective difference in soleus activation during the adaptation phase suggests that sailors rely on an ankle-based neuromuscular strategy shaped by repeated exposure to unstable support surfaces. This interpretation is consistent with classical models of postural control, in which ankle musculature contributes substantially to quiet standing and to corrective postural responses [1, 175].

The fact that the significant EMG difference emerged during the adaptation phase is also important. This phase corresponds to the condition in which

participants were exposed to the most relevant dynamic challenge, combining visual stimulation and platform movement. For sailors, this condition may resemble the type of sensorimotor demand experienced during maritime activity, where the support surface is continuously moving and balance must be maintained through rapid but efficient adjustments. The right soleus SKEW difference therefore suggests that maritime exposure may have shaped not only the amount of sway, but also the temporal structure of muscle recruitment used to control that sway.

This result complements the CoP findings. Sailors showed greater antero-posterior sway excursion and velocity, together with higher entropy and complexity measures. The EMG result suggests that this more dynamic sway behavior was not uncontrolled, but was accompanied by a specific neuromuscular organization. In other words, sailors did not simply sway more; they appeared to regulate this increased sway through a burst-like soleus activation strategy. This supports the interpretation that their postural response was adaptive rather than unstable.

From a motor-control perspective, the pattern observed in sailors may reflect experience-dependent neuromuscular plasticity. Repeated exposure to balance-challenging environments can modify postural strategies and refine the timing of muscle activation. In maritime environments, maintaining balance requires continuous integration of visual, vestibular, and somatosensory information, together with fast anticipatory and compensatory adjustments. The observed right soleus skewness may therefore represent a learned strategy in which low-level tonic activity is combined with intermittent bursts to respond efficiently to unpredictable perturbations [241, 242].

However, the specificity of the result should also be considered. Since only one EMG feature in one muscle and one phase survived correction for multiple comparisons, the finding should not be overinterpreted as evidence of a global neuromuscular difference between sailors and controls. Rather, it indicates that the most robust EMG marker of maritime adaptation in this study was the temporal asymmetry of right soleus activation during the adaptation phase. This is coherent with the role of the soleus in ankle-based postural regulation and with the CoP evidence of increased antero-posterior sway dynamics.

Overall, the EMG findings suggest that seafarers' postural adaptation is not only expressed through greater sway complexity, but also through a selective reorganization of ankle-muscle activation. The positive SKEW of the right soleus supports the idea of an efficient burst-based strategy, in which the muscle remains active at low intensity and produces stronger corrective activations when needed. This pattern may represent a functional adaptation to unstable maritime environments and highlights the capacity of the neuromuscular system to adapt to repeated balance demands over time.

8.1.3 Electroencephalography as a Marker of Cortical Involvement

EEG analysis provided a further level of interpretation by investigating the cortical mechanisms associated with postural control. Balance regulation is often considered primarily biomechanical or spinal, but the studies included in this thesis support the role of cortical activity in responding to complex sensory and motor perturbations. This is especially relevant in Parkinson's disease, where postural instability may involve not only peripheral motor impairment but also altered central processing.
Two main EEG approaches were used across the studies: spectral analysis and dynamic functional connectivity. Spectral analysis examined frequency-specific power changes, while connectivity analysis investigated the organization and temporal evolution of large-scale brain networks. These approaches are complementary. Spectral analysis identifies where and in which frequency bands cortical activity differs between groups, whereas dynamic connectivity describes how brain regions interact over time during the task.

Spectral alterations in Parkinson's disease The EEG spectral analysis provided an additional level of interpretation by showing that the postural alterations observed in Parkinson's disease were accompanied by differences in cortical activity. The involvement of the cerebral cortex in postural responses to perturbation is well established, particularly when balance control requires sensory integration, attentional monitoring, and adaptation to changing environmental conditions [7, 243, 244]. However, the way in which cortical mechanisms are altered in neurological conditions affecting mobility, such as Parkinson's disease, is still not fully understood. For this reason, the analysis of EEG activity during the BioVRSea task was important to investigate whether the altered CoP and EMG responses observed in PD were associated with changes in cortical processing.
In the first BioVRSea study on early-stage Parkinson's disease, topographical maps of absolute power spectral density were computed across frequency bands and experimental phases. The clearest group differences between PD participants and healthy controls emerged in the theta and alpha bands, especially during the POST phase. This phase followed the combined visual and mechanical perturbation and therefore provided information on the cortical response after exposure to the most demanding part of the task. The presence of significant EEG differences in POST supports the idea that PD participants differed from controls not only in their biomechanical and neuromuscular responses, but also in the cortical processes involved in postural recovery and adaptation.
Theta-band differences were observed mainly in temporal electrodes, including T7, T8, C6, and FT7, with additional significant electrodes in frontal and occipital regions, such as AF3 and PO6. This distribution suggests that the theta response to the BioVRSea perturbation involved regions associated with sensory processing, attentional control, and integration of visual and postural information. Theta activity is known to be involved in attention, memory

processes, and cognitive-motor control [245]. In postural tasks, theta oscillations may reflect the increased cognitive demand required to monitor body orientation, process sensory conflict, and plan corrective responses. Although the role of alpha activity in balance control has been more extensively described, theta activity is increasingly recognized as relevant during postural tasks, especially when task difficulty increases or visual feedback is altered [246].

The theta findings are also consistent with previous BioVRSea work on healthy subjects, in which theta-band changes were observed during postural perturbation, particularly over parietal regions, suggesting a role in the processing of body orientation and sensory information [128]. In the PD study, theta responses showed different behavior depending on brain region and phase. In healthy subjects, parietal theta activity decreased from PRE to POST, in agreement with previous observations in healthy participants exposed to the BioVRSea paradigm [128]. In contrast, frontal theta activity was higher in healthy controls across task phases. Since theta rhythms are associated with cognitive and motor functions, and irregular theta activity has been reported in PD during lower-limb activation, these findings may reflect altered cortical regulation of postural responses in the PD group [247].

Alpha-band differences were also evident in the POST phase, with significant electrodes located mainly in temporal regions, including FC5, T7, T8, and FT8, together with parietal and occipital electrodes such as P4 and PO6. The alpha band is particularly relevant in this context because alpha oscillations are involved in sensory processing, attentional regulation, and the control of cortical excitability. Different studies have shown that balance tasks can modulate alpha activity, indicating that alpha oscillations participate in postural regulation rather than representing only an idling rhythm [248, 249]. Alpha activity has also been associated with cognitive events, motor planning, and action execution [250]. Therefore, alpha-band differences during BioVRSea suggest that maintaining balance under visual and mechanical perturbation requires active cortical engagement.

In the PD study, healthy controls generally showed greater alpha power than PD participants in both PRE and POST phases. This finding may indicate that PD participants experienced greater difficulty in coping with the balance task or were less able to recruit the cortical mechanisms normally involved in adaptive postural control. Previous studies have shown that alpha power can decrease with increasing postural task difficulty during upright stance [246, 251, 252]. Therefore, the lower alpha activity observed in the PD group may reflect increased postural demand, altered sensory integration, or reduced efficiency of cortical regulation during the task.

The involvement of temporal, parietal, frontal, and occipital electrodes is physiologically meaningful within the BioVRSea paradigm. The visual sea environment and moving platform require continuous integration of visual, vestibular, somatosensory, and motor information. Occipital regions may reflect visual processing, parietal regions may contribute to body orientation and spatial integration, frontal regions may be involved in attentional and executive control, and temporal regions may participate in multisensory processing. Therefore,

the distribution of theta and alpha differences supports the idea that postural control during BioVRSea relies on a distributed cortical network rather than on isolated motor areas.
Overall, the EEG spectral results indicate that theta and alpha activity can discriminate between early-stage PD participants and healthy controls during a complex postural-control task. These findings complement the CoP and EMG results by showing that the altered postural strategy observed in PD is associated with altered cortical processing. In particular, the POST-phase differences suggest that PD affects the cortical mechanisms involved in recovering from, and adapting to, sensory-motor perturbation. Thus, spectral EEG analysis supports the broader interpretation that postural control impairment in PD is a multisystem phenomenon involving biomechanical, neuromuscular, and cortical components.

Dynamic connectivity and brain-network reorganization The dynamic connectivity analyses extended the EEG investigation from regional spectral alterations to the temporal organization of large-scale brain networks. While spectral power analysis identified frequency-specific differences between Parkinson's disease and healthy controls, BNS analysis allowed the characterization of transient functional connectivity configurations occurring during the BioVRSea task. This approach was particularly relevant because postural control is not a static process, but requires continuous reconfiguration of visual, attentional, sensory, motor, and cognitive networks in response to changing task demands. Across the EEG connectivity studies included in this thesis, BNSs were extracted using a methodological framework adapted from Poulsen et al. [208]. This framework included the selection and optimization of clustering solutions, followed by back-fitting procedures to derive temporal metrics such as coverage, occurrence, and duration. These metrics provided complementary information: coverage described how much time a given state occupied, occurrence described how frequently the state was entered, and duration described how long the state persisted once activated. Therefore, BNS analysis made it possible to investigate not only whether a network configuration was present, but also how stable, recurrent, or persistent it was during the BioVRSea phases.
The first dynamic connectivity study focused on the alpha band and represented an initial application of BNS analysis to the BioVRSea paradigm in early-stage Parkinson's disease. This study showed that the main group differences were not expressed as completely distinct transition pathways, but rather as subtle alterations in the flexibility of state transitions. Across phases, both PD and control participants showed broadly similar transition structures, but controls tended to display more distributed transitions, whereas PD participants showed a tendency toward more repetitive exchanges within a narrower subset of states. In particular, transitions involving BNS1↔BNS4 and BNS3↔BNS4 appeared more pronounced in PD during task-related phases, although these differences were not stable enough to define a clear diagnostic transition pattern.
This finding is important because it suggests that early-stage PD may not

produce a complete reorganization of alpha-band network transitions, but rather a reduction in dynamic flexibility. In the context of BioVRSea, such reduced flexibility may indicate difficulty in shifting efficiently between network configurations required for visual processing, attentional control, and postural adjustment. This interpretation is consistent with the idea that postural impairment in PD involves not only motor dysfunction, but also altered cognitive-motor integration and reduced adaptability of brain network dynamics.

The alpha-band BNS-specific analysis further suggested that PD and control participants differed in the relative expression of states involving canonical resting-state networks, including the visual network (VIS), dorsal attention network (DAN), salience network (SAN), auditory network (AUD), and default mode network (DMN). Although resting-state networks are typically described during rest, their components also contributed to task-related BNSs, indicating that these large-scale systems remain functionally relevant during active postural control. Within the BioVRSea task, this is physiologically plausible because participants had to process visual motion, maintain attention, respond to salient stimuli, integrate multisensory information, and regulate posture simultaneously.

In the alpha study, BNS1 was characterized mainly by VIS and SAN components. This state was particularly relevant during the PRE phase, when visual stimulation began. The involvement of VIS is coherent with the visual demands of the virtual sea environment, which required motion perception, spatial awareness, and continuous processing of visual cues [253–255]. The involvement of SAN suggests that participants also needed to maintain alertness and respond to salient changes in the immersive environment. Previous studies have reported altered occipital function and visual-network connectivity in PD, including reduced activity in occipito-parietal regions and decreased occipital functional connectivity [256–258]. Therefore, differences in visually and salience-related BNSs may reflect altered processing of the visual cues required for postural orientation.

BNS2, which was more prevalent in controls, was mainly associated with DAN and SAN. These networks are essential for sustained attention, voluntary allocation of attention, cognitive control, and responsiveness to task-relevant stimuli [253, 259–261]. Within BioVRSea, DAN and SAN engagement likely supported the ability to focus on postural adjustments while monitoring continuous visual stimulation. The reduced expression of this state in PD is consistent with previous evidence of altered DAN and SAN connectivity in Parkinson's disease [262–265]. Functionally, this may indicate reduced attentional efficiency during the task, which could contribute to impaired postural regulation under dynamic visual conditions.

BNS3 was associated with DAN and AUD, suggesting involvement of attentional and sensory-integration mechanisms. The auditory network includes regions such as the primary auditory cortex, insula, and superior temporal gyrus, and contributes to processing sound stimuli and multisensory information [253, 266]. In the BioVRSea paradigm, visual and auditory inputs are part of the immersive environment, and their integration may be especially important when participants experience sensory conflict. The greater relevance of BNS3 in

PD may therefore reflect increased reliance on multisensory integration as a compensatory response to postural-control deficits [267, 268].
BNS4 showed greater expression in the PD cohort and was characterized by DAN and VIS components. This pattern may indicate increased reliance on visual-attentional processing in PD during the task. In the BioVRSea environment, where visual motion cues are central to the perturbation, increased DAN–VIS involvement may reflect an attempt to stabilize posture through continuous visual monitoring. This interpretation is coherent with the broader view that PD patients may rely more strongly on visual feedback when automatic postural control and sensory integration are compromised.
BNS5 and BNS6 were both associated with DAN and SAN, but showed different group prevalence. BNS5 was more represented in PD, whereas BNS6 was more prevalent in controls. These findings suggest that both groups recruited attention and salience-related systems, but possibly with different temporal organization or efficiency. Previous work has shown that SAN and DMN interactions are altered in PD, with disrupted anti-correlation between salience-related and default-mode systems [269–271]. In healthy individuals, SAN activation typically supports switching between internally oriented DMN activity and externally oriented task-positive networks. In PD, impaired SAN-DMN coupling may reduce the efficiency of this switching mechanism, leading to less flexible cognitive control during complex tasks. This is relevant for BioVRSea because the task requires sustained attention to external visual and motor demands rather than internally oriented processing [272, 273].
Overall, the alpha-band study suggested that PD was associated with altered BNS expression involving visual, attentional, salience, auditory, and default-mode systems. The most robust finding was reduced BNS2 coverage in PD during visual and visuomotor task phases, suggesting decreased engagement of an attention- and salience-related configuration during the phases requiring active processing of the BioVRSea environment. The transition analysis further suggested less flexible state switching in PD, although without a fully distinct transition signature. Together, these findings supported the interpretation that alpha-band network dynamics in PD reflect altered attentional control, sensory integration, and compensatory reliance on visual processing during postural regulation.
The subsequent cross-frequency BNS study expanded this interpretation by investigating delta-, theta-, and beta-band dynamic connectivity during the same BioVRSea framework. This analysis showed that PD was not characterized by a simple global increase or decrease in connectivity. Instead, PD was associated with a frequency-specific redistribution of brain-state dynamics. The most relevant alterations involved increased recurrence of a delta-band attention-dominant state, prolonged engagement of a theta-band DMN-centered state during visually induced self-motion, and reduced stability of a beta-band integrative state that was dominant in controls.
In the delta band, PD showed increased occurrence of BNS4, particularly during baseline. This state was primarily DAN-dominant, with strong VIS involvement and a posterior-centered organization including midline and occipital regions

such as the precuneus, posterior cingulate cortex, cuneus, lingual gyrus, fusiform gyrus, and lateral occipital cortex. Delta oscillations are involved in long-range cortical integration, attentional regulation, and large-scale coordination across distributed brain systems [274–276]. In motor and postural contexts, delta activity may contribute to global network organization and coordination of sensorimotor and cognitive systems [277, 278]. Increased delta activity and cortical slowing are also well-established features of PD, linked to thalamo-cortical dysfunction and large-scale network impairment [147, 279, 280]. Therefore, the increased recurrence of a DAN–VIS delta state in PD may reflect repeated recruitment of a slow visual-attentional monitoring configuration, even in the absence of explicit platform movement.

This delta finding extends previous spectral observations by showing that PD-related slowing is not only a matter of increased low-frequency power, but also of altered temporal organization of low-frequency network states. The increased occurrence of BNS4 suggests that PD participants repeatedly re-entered this attention-dominant posterior monitoring state. This pattern is consistent with reports of abnormal delta-band synchronization and disrupted network integration in PD [281–283]. From a dynamical systems perspective, frequent re-entry into the same state may indicate a less flexible attractor landscape, in which specific slow integrative configurations become more easily accessible and more repeatedly visited [284, 285].

In the theta band, PD showed prolonged duration of BNS4 during the PRE phase. This is particularly important because PRE involved visual sea-motion simulation without mechanical platform displacement. Therefore, the increased duration of this state should be interpreted as a visually driven postural-processing effect rather than as a response to actual mechanical perturbation. Theta BNS4 was a DMN-centered, globally integrated configuration involving medial DMN hubs such as the posterior cingulate cortex, precuneus, rostral anterior cingulate cortex, and orbitofrontal cortex, together with motor, attentional, and posterior visual regions. This suggests that PD participants remained for longer periods in a large-scale integrative state during visually induced self-motion.

Theta oscillations are associated with cognitive-motor integration, attentional control, sensory conflict processing, and adaptive sensorimotor regulation [275, 286, 287]. In balance paradigms, theta activity has been linked to increased cognitive monitoring and integration of visual, vestibular, and sensorimotor information under challenging conditions [153, 288]. Within this framework, prolonged theta BNS4 duration in PD may reflect abnormal stabilization of a DMN-centered integrative state during visual-motion processing. Rather than flexibly transitioning toward task-optimized configurations, PD participants may remain engaged in a broader compensatory network involving internally oriented, attentional, and motor systems. This interpretation is consistent with evidence of altered DMN dynamics and impaired segregation between DMN and task-positive networks in Parkinson's disease [283, 289]. It is also coherent with the role of medial frontal and cingulate theta activity in performance monitoring and control allocation [290].

In the beta band, the main findings were reduced coverage and duration of BNS1 in PD compared with controls, together with increased occurrence of BNS2 in PD. BNS1 represented a dominant beta-band configuration in controls, characterized by integration of DMN, DAN, posterior visual, sensorimotor, and associative regions. Its reduced coverage and duration in PD suggest that participants with PD were less able to maintain a stable beta-mediated integrative state supporting visual feedback, attentional allocation, and motor readiness. Beta oscillations are strongly associated with stabilization of the current sensorimotor and cognitive state [291, 292]. In Parkinson's disease, abnormal beta synchronization is linked to motor impairment, rigidity of neural processing, and reduced flexibility of motor networks [293, 294]. Therefore, the reduced stability of BNS1 may indicate impaired maintenance of an efficient sensorimotor-cognitive configuration during postural control.
Conversely, BNS2 in the beta band was a DMN-centered integrative configuration linking midline default-mode hubs with posterior visual, parietal, and temporal associative cortices. The increased occurrence of BNS2 in PD suggests more frequent transitions into an alternative midline-driven state. This may reflect temporal fragmentation of beta-band dynamics, with PD participants shifting away from the dominant control-like visuomotor stabilization state toward a more labile configuration emphasizing internally oriented and associative processing. The contrast between BNS1 and BNS2 is therefore informative: while BNS1 tightly coupled posterior visual and sensorimotor regions with midline hubs, BNS2 emphasized medial integrative structures with less direct motor dominance. This shift suggests that PD alters beta-band organization by reducing the stability of task-relevant visuomotor integration and increasing recurrence of alternative DMN-centered states.
Taken together, the alpha, delta, theta, and beta BNS findings converge on the interpretation that early-stage PD alters the temporal regulation of large-scale brain networks during postural control. In the alpha band, PD showed reduced engagement of attention- and salience-related configurations and a tendency toward less flexible transitions. In the delta band, PD showed repeated recruitment of a slow attention-dominant visual-monitoring state. In the theta band, PD showed prolonged engagement of a DMN-centered integrative state during visually induced self-motion. In the beta band, PD showed reduced stability of the dominant control-like integrative state and increased recurrence of an alternative DMN-centered configuration.
The common element across frequencies was not the alteration of one single network, but reduced dynamic flexibility of large-scale brain-state organization. PD participants appeared less able to maintain or flexibly transition between configurations involving visual, attentional, salience, default-mode, sensory, and motor systems. This cross-frequency pattern suggests that postural-control impairment in early-stage PD is associated with altered large-scale network reconfiguration, rather than with an isolated abnormality in a single frequency band or brain region.
These findings have important implications for the interpretation of BioVRSea results. CoP and EMG analyses showed that PD participants adopted a more

constrained and altered postural strategy, while EEG connectivity analysis suggests that this behavioral pattern is accompanied by reduced flexibility of neural network dynamics. Therefore, the BioVRSea paradigm appears capable of linking biomechanical, neuromuscular, and cortical features of postural control. In particular, BNS analysis may provide candidate neurophysiological markers of early PD by identifying how the brain organizes and reorganizes task-relevant networks during visual and visuomotor perturbation.

Clinically, this approach may be relevant because altered brain-state dynamics could appear before severe postural instability becomes clinically evident. By quantifying coverage, occurrence, and duration of BNSs during a controlled balance challenge, EEG connectivity analysis may help detect subtle abnormalities in attention, sensory integration, and motor-cognitive control. Although these findings require validation in larger cohorts and longitudinal studies, they support the potential of BioVRSea combined with dynamic brain-network analysis as a tool for characterizing early postural-control dysfunction in Parkinson's disease.

Chapter 9

Conclusions

The findings of this thesis lead to four main conclusions regarding the quantitative assessment of postural control using the BioVRSea paradigm.

Postural control is a multisystem and context-dependent process. The first major conclusion is that postural control cannot be fully characterized through a single physiological measure. Across the studies included in this thesis, CoP, EMG, and EEG provided complementary information on biomechanical behavior, neuromuscular organization, and cortical processing, respectively. This is consistent with current models describing balance as the result of continuous integration between sensory information, motor responses, and higher-level neural processes [1, 7, 11]. Within this framework, BioVRSea provided a common experimental perturbation through which these different levels of postural regulation could be investigated simultaneously or in combination.
Importantly, the physiological meaning of a postural response depended on the population being studied. The same BioVRSea challenge revealed a constrained strategy in Parkinson's disease and a more dynamic strategy in seafarers. Therefore, neither greater nor smaller sway should be interpreted independently as better or worse balance; instead, postural behavior should be interpreted according to the adaptive capacity and physiological context of the individual.

Early-stage Parkinson's disease is characterized by constrained and less adaptable postural control. Across the Parkinson's disease studies, the most consistent biomechanical finding was a reduction in postural flexibility. PD participants showed reduced CoP excursion, velocity, and spatial dispersion compared with healthy controls, particularly after exposure to the visuomotor perturbation. These findings support previous evidence that Parkinson's disease affects automatic postural regulation, sensorimotor integration, and the ability to adapt balance strategies to changing environmental conditions [1, 11, 222, 223].
The POST phase emerged as particularly informative, as group differences became more evident after the moving-platform stimulation. This suggests

that challenging the postural-control system may expose alterations that are less apparent during less demanding conditions. The reduced sway observed in PD should therefore not be interpreted as improved stability, but as a more restricted postural strategy with reduced capacity for adaptive reorganization. The EMG findings complemented this interpretation by demonstrating that neuromuscular alterations were muscle- and phase-specific rather than uniformly distributed across the lower limb. This is consistent with previous evidence showing context-dependent alterations in automatic postural muscle recruitment in Parkinson's disease [69, 238]. Together, the CoP and EMG results indicate that PD-related postural dysfunction involves both altered neuromuscular organization and reduced flexibility of the resulting postural response.

Altered postural control in Parkinson's disease is accompanied by reduced flexibility of cortical dynamics. The EEG findings demonstrate that the alterations observed at the biomechanical and neuromuscular levels were accompanied by changes in cortical activity. Spectral analysis identified differences particularly in theta and alpha activity, supporting the involvement of cortical mechanisms associated with attention, sensory integration, and cognitive-motor control during challenging postural conditions [7, 246, 248].
Dynamic functional-connectivity analysis extended these findings by showing that PD-related abnormalities were not restricted to individual brain regions or a single frequency band. Alpha-band analysis suggested altered recruitment of visual, attentional, salience, auditory, and default-mode systems, while the subsequent multiband analysis identified frequency-specific alterations in delta-, theta-, and beta-band Brain Network States.
Despite these frequency-specific differences, the common feature across the connectivity studies was a reduction in the flexibility of large-scale brain-state dynamics. PD participants showed altered maintenance, recurrence, and transition between cortical configurations involved in visual processing, attentional control, sensory integration, and motor regulation. This interpretation is consistent with evidence that Parkinson's disease involves disrupted large-scale network integration and reduced dynamical flexibility [281, 283–285, 289].
Thus, the findings of this thesis suggest that reduced adaptability in PD is expressed across multiple organizational levels: as constrained postural behavior, altered muscle recruitment, and reduced flexibility of cortical network dynamics.

Increased postural variability can represent functional adaptation rather than impairment. The seafarer study provided an important counterpoint to the Parkinson's disease findings. Sailors showed greater CoP excursion and velocity together with increased entropy and complexity during the BioVRSea task. Rather than indicating poorer stability, these changes were interpreted as an expertise-dependent strategy associated with prolonged exposure to unstable maritime environments. This interpretation is consistent with previous evidence that postural variability can represent adaptive flexibility and

that repeated exposure to unstable environments can modify postural-control strategies [127, 234, 235].
The EMG findings supported this interpretation by identifying a selective difference in right soleus activation during the adaptation phase. The observed activation distribution was compatible with low-level activity combined with intermittent corrective bursts, consistent with the role of the soleus in ankle-based postural regulation [175, 241, 242]. Therefore, the increased sway observed in sailors was accompanied by a specific neuromuscular organization rather than representing uncontrolled instability.
These findings demonstrate that postural variability cannot be interpreted independently of context. Whereas reduced movement in PD reflected a constrained strategy, increased movement and complexity in seafarers were compatible with functional adaptation. BioVRSea therefore appears particularly useful for distinguishing different strategies used to solve the same postural challenge rather than simply classifying participants according to the magnitude of their sway.

Overall conclusion Taken together, the five studies demonstrate that BioVRSea provides a quantitative framework for investigating how postural control is organized under controlled visual and mechanical perturbations. Its main contribution is not the identification of a single marker of balance impairment, but the ability to characterize different postural-control strategies across biomechanical, neuromuscular, and cortical levels.
In early-stage Parkinson's disease, the converging evidence indicates a more constrained and less dynamically flexible system, expressed through altered CoP behavior, selective neuromuscular changes, and reduced flexibility of cortical network organization. In contrast, seafarers demonstrated a more variable and complex postural strategy compatible with experience-dependent adaptation to unstable environments.
In this framework, the integration of complementary physiological signals, including EEG, EMG, and CoP, enables a quantitative characterization of postural control across neural, muscular, and biomechanical levels. Within BioVRSea, this multimodal approach revealed distinct postural-control patterns associated with physiological adaptation and pathological restriction, including subtle alterations emerging during the early stages of neurophysiological disorders.

Chapter 10

Limitations and Future Perspectives

10.1 Limitations Across Studies

The limitations of this thesis can be summarized into five main areas concerning cohort characteristics, disease classification, methodological choices, multimodal comparability, and the generalizability of the BioVRSea framework.

Sample size and cohort composition The first limitation concerns sample size and cohort composition. The initial BioVRSea study in early-stage Parkinson's disease included a relatively small PD cohort, reducing statistical power and limiting the generalizability of the CoP, EMG, and EEG findings [190]. Although this was partly addressed in the later CoP and EMG study with a larger matched cohort, the first study should still be considered exploratory. Similarly, the seafarer study included 21 sailors and 21 matched controls, all male, limiting the extension of the findings to larger maritime populations, female sailors, or mixed occupational groups.

Cohort heterogeneity and disease classification A second limitation concerns cohort heterogeneity and disease classification. Early-stage PD is not an absolute category and may vary according to clinical evaluation, disease duration, symptom profile, medication status, and individual compensatory strategies. Therefore, the findings should be interpreted as evidence of altered postural-control strategies in the studied cohorts rather than as a definitive characterization of all early-stage PD patients.
Moreover, although CoP and EMG findings suggest a more constrained and less adaptive postural strategy in PD, the underlying mechanisms were not directly measured. These patterns may reflect rigidity, impaired sensory reweighting, altered automatic postural responses, co-contraction, reduced confidence, or compensatory stabilization [1, 11, 222, 231].

EEG acquisition and analytical choices EEG acquisition during dynamic postural tasks presents specific methodological challenges. EEG is sensitive to movement, muscle activity, eye movements, and headset displacement, and results obtained during visual stimulation and mechanical platform movement must therefore be interpreted cautiously.
In addition, connectivity analyses depend on methodological choices related to source reconstruction, connectivity estimation, parcellation, and clustering. The wMNE–PLV pipeline was adopted for consistency with previous source-connectivity literature and earlier BioVRSea studies [191, 199, 219]; nevertheless, the resulting Brain Network States remain dependent on the analytical framework used.

Frequency coverage and multimodal comparability The EEG connectivity studies differed in frequency content and interpretation. The first alpha-band study provided an initial dynamic connectivity investigation of BioVRSea in a neurodegenerative cohort, whereas the subsequent multiband study extended the analysis to delta, theta, and beta bands. This extension was relevant because beta oscillations are related to motor control and pathological synchronization in PD [295, 296], theta activity is associated with cognitive control, error monitoring, and sensorimotor integration [297, 298], and delta activity may reflect large-scale coordination and compensatory processes under increased cortical demand [299]. However, gamma-band connectivity was not examined because of the computational burden associated with larger connectivity matrices.
Furthermore, not all studies used the same combination of CoP, EMG, and EEG signals. This limits direct comparison across modalities and cohorts and prevents a complete characterization of the relationships between biomechanical behavior, neuromuscular activation, and cortical dynamics across all populations investigated.

10.2 Future Perspectives

Based on these limitations and on the findings of this thesis, five main directions for future research can be identified.

Validation in larger, more diverse, and longitudinal cohorts Future work should expand and validate the BioVRSea framework in larger and more diverse cohorts. This is particularly important for confirming findings obtained in the smaller exploratory PD study and for determining whether the adaptations observed in the male seafarer cohort generalize to female sailors and broader maritime populations.
Longitudinal studies would provide an additional dimension that cannot be addressed through the current cross-sectional investigations. In seafarers and other occupational groups, repeated assessments could clarify whether postural

adaptations develop progressively with exposure to unstable environments, persist after return to land, or gradually disappear over time.

Clinical characterization and stratification of Parkinson's disease In Parkinson's disease, larger cohorts should allow subgroup analyses according to disease stage, motor phenotype, medication status, cognitive profile, and fall history. This would help determine how the postural-control patterns identified through BioVRSea vary across the heterogeneous clinical spectrum of PD and whether specific features are associated with disease progression or fall-risk stratification.
More detailed clinical and physiological characterization could also help clarify the mechanisms underlying the constrained postural strategy observed in this thesis, including the potential contribution of rigidity, altered sensory reweighting, abnormal automatic postural responses, or compensatory stabilization.

Methodological validation and extension of EEG analysis Future EEG studies should assess the robustness of the connectivity findings using alternative analytical approaches. This should include testing different source-reconstruction methods, connectivity measures, cortical parcellations, and clustering strategies to determine whether the identified Brain Network States and group differences remain stable across methodological choices.
Future work could also extend the connectivity analysis to additional frequency ranges. In particular, gamma-band connectivity was not investigated in the present studies because of the computational demands associated with the larger connectivity matrices and could therefore represent an additional direction for characterizing the cortical dynamics associated with postural control.

Direct multimodal integration Future analyses should integrate CoP, EMG, and EEG correlation more directly rather than interpreting the signals predominantly as separate levels of postural control. Temporal relationships between cortical network states, muscle activation bursts, and CoP corrections could help determine how neural activity is translated into neuromuscular control and observable postural behavior.
Such analyses could provide a more complete representation of the multisystem organization of balance and help identify combinations of features that distinguish pathological, adaptive, and physiological postural-control strategies. Machine-learning approaches may support the identification of compact multimodal feature sets, provided that resulting models are appropriately validated and remain physiologically interpretable.

Clinical translation, new applications, and rehabilitation For clinical translation, BioVRSea should be simplified into shorter and more accessible protocols. The findings of this thesis suggest that CoP and EMG may be sufficient for some clinical and rehabilitation applications, whereas EEG and Brain Network State analysis may be more suitable for advanced neurophysiological

characterization or research contexts. Future work should therefore identify a reduced set of robust features that can be acquired with simpler equipment and shorter protocols.

The framework could also be extended to other populations characterized by impaired balance control, including older adults and individuals with vestibular disorders, multiple sclerosis, stroke, traumatic brain injury, limb amputation, or other neurodegenerative and neuromuscular conditions.

In individuals with lower-limb amputation, BioVRSea may provide a controlled method for assessing how different prosthetic devices influence postural stability, muscular recruitment, and adaptation to sensory and mechanical perturbations. Ongoing work conducted in collaboration with Össur applies the BioVRSea protocol to individuals with lower-limb amputation while using three different prosthetic feet. This application may help determine whether distinct prosthetic designs promote different postural-control strategies and may support the objective comparison and functional validation of prosthetic components under challenging but reproducible conditions. More broadly, this application illustrates the potential of BioVRSea not only for characterizing patient populations but also for evaluating assistive technologies and supporting device selection and rehabilitation decisions.

Finally, the paradigm may have rehabilitative potential. Repeated exposure to controlled sensory and mechanical perturbations could potentially be used not only to assess postural control but also to train adaptive balance strategies. Future studies should therefore investigate whether repeated BioVRSea sessions improve balance confidence, reactive postural responses, and functional mobility, and whether these effects transfer to daily-life situations.

Chapter 11

Appendices

11.1 Shared Supplementary Methods for Brain Connectivity Analyses

11.1.1 ROI–Node–RSN Mapping

Table 11.1: Regions of Interest (ROIs) and their Functional Network Associations.

ROI	Label	Acronym	RSN	ROI	Label	Acronym	RSN
1	l.bankssts	l.BSTS	Other	29	l.middletemporal	l.MTG	DAN
2	r.bankssts	r.BSTS	Other	30	r.middletemporal	r.MTG	DAN
3	l.cACC	l.cACC	SAN	31	l.paracentral	l.paraC	MOT
4	r.cACC	r.cACC	SAN	32	r.paracentral	r.paraC	MOT
5	l.cMFG	l.cMFG	SAN	33	l.pericalcarine	l.periCAL	Other
6	r.cMFG	r.cMFG	SAN	34	r.pericalcarine	r.periCAL	Other
7	l.cuneus	l.CUN	VIS	35	l.postcentral	l.postC	MOT
8	r.cuneus	r.CUN	VIS	36	r.postcentral	r.postC	MOT
9	l.entorhinal	l.ENT	Other	37	l.posteriorcingulate	l.PCC	DMN
10	r.entorhinal	r.ENT	Other	38	r.posteriorcingulate	r.PCC	DMN
11	l.superiorfrontal	l.sFG	Other	39	l.precentral	l.preC	MOT
12	r.superiorfrontal	r.sFG	Other	40	r.precentral	r.preC	MOT
13	l.fusiform	l.FUS	VIS	41	l.precuneus	l.PCUN	DMN
14	r.fusiform	r.FUS	VIS	42	r.precuneus	r.PCUN	DMN
15	l.inferiorparietal	l.IPL	Other	43	l.rACC	l.rACC	DMN
16	r.inferiorparietal	r.IPL	Other	44	r.rACC	r.rACC	DMN
17	l.ITG	l.ITG	DAN	45	l.rMFG	l.rMFG	SAN
18	r.ITG	r.ITG	DAN	46	r.rMFG	r.rMFG	SAN
19	l.pOPER	l.pOPER	DAN	47	l.SPL	l.SPL	Other
20	r.pOPER	r.OPER	DAN	48	r.SPL	r.SPL	Other
21	l.isthmuscingulate	l.iCC	DMN	49	l.STG	l.STG	AUD
22	r.isthmuscingulate	r.iCC	DMN	50	r.STG	r.STG	AUD
23	l.lateraloccipital	l.LOG	VIS	51	l.SMAR	l.SMAR	SAN
24	r.lateraloccipital	r.LOG	VIS	52	r.SMAR	r.SMAR	SAN
25	l.LOF	l.LOF	DMN	53	l.TP	l.TP	Other
26	r.LOF	r.LOF	DMN	54	r.TP	r.TP	Other
27	l.LING	l.LING	VIS	55	l.TT	l.TT	Other
28	r.LING	r.LING	VIS	56	r.TT	r.TT	Other

11.1.2 Phase-Locking Value (PLV) Calculation

The dynamic Phase-Locking Value (PLV) dynamic connectivity matrices are computed using the function:

$$\boxed{N = \left\lfloor \frac{NumberofSamples - OverlapWindow}{TotalWindow - OverlapWindow} \right\rfloor}$$

where:

$$\begin{cases} \text{NumberOfSamples} &= \text{EpochDuration} \times \text{SamplingRate} \\ f_{\text{Interest}} &= f_{\min} + \dfrac{f_{\max} - f_{\min}}{2} \\ \text{TotalWindow} &= \left\lfloor \dfrac{6}{f_{\text{Interest}}} \times \text{SamplingRate} \right\rfloor \\ \text{OverlapWindow} &= \left\lfloor \dfrac{\text{OverlapPercentage}}{100} \times \dfrac{6}{f_{\text{Interest}}} \times \text{SamplingRate} \right\rfloor \end{cases}$$

This function takes as input:

- *EpochDuration*: EEG time series with dimensions $[n_{\text{channels}}, n_{\text{samples}}]$.
- *SamplingRate*: The EEG sampling frequency.
- *fmin*, *fmax*: The lower and upper-frequency limits of the band of interest.
- *OverlapPercentage*: The percentage of overlap between time windows.

The number of dynamic matrices (N) generated for each frequency band depends on the *length* of each analysis window and on the *overlap* between consecutive windows. Following [207], each window spans six cycles of the band's center frequency to ensure reliable phase estimation.
In our implementation, the *Epoch Duration* was 273s, the *Sampling Rate* was 1024Hz, and the *Overlap Percentage* between consecutive windows was set to 50%, providing a balance between temporal resolution and the stability of the phase-locking estimates.

Band	**Frequency parameters (Hz)**			**Window parameters (samples)**		
	$f_{\min}$	$f_{\max}$	f_{Interest}	TotalWindow (samples per segment)	OverlapWindow (samples shared)	N (PLV matrices)
Delta	1	4	2.50	2457	1228	226
Theta	4	8	6.00	1024	512	545
Alpha	**8**	**13**	**10.5**	**585**	**292**	**953**
Beta	13	30	21.5	285	142	1953
Gamma	30	45	37.5	163	81	3408

Example calculation for the alpha band:
Epoch Duration = 273 s; Sampling Rate = 1024 Hz; Overlap = 50%.

Number of Samples = $273 \times 1024 = 279552$ samples.

$f_{\min} = 8$ Hz; $f_{\max} = 13$ Hz $\Rightarrow f_{\text{Interest}} = 10.5$ Hz.

Total Window = $\lfloor 6/10.5 \times 1024 \rfloor = \lfloor 585.14 \rfloor = 585$ samples

Overlap Window = $\lfloor 0.5 \times 585.14 \rfloor = \lfloor 292.47 \rfloor = 292$ samples

$$N = \left\lfloor \frac{279552 - 292}{585 - 292} \right\rfloor = \left\lfloor \frac{279260}{293} \right\rfloor = \lfloor 953.10 \rfloor = \mathbf{953}.$$

11.1.3 Computational Methods for BNSs metrics

Table 11.2: Description of parameters used in the analysis of brain network states (BNSs), including their formulas and interpretations.

Parameter	Formula	Description
Coverage	$\text{Coverage}_i = \frac{T_i}{T_{\text{total}}}$ where T_i is the total time state i was active, and T_{total} is the total analysis time.	Coverage represents the proportion of time a BNS is active relative to the total time.
Duration	$\text{Duration}_i = \frac{T_i}{N_i}$ where T_i is the total time state i was active, and N_i is the number of times state i was activated.	Duration is the average time a BNS remains active before switching to another.
GEV	$\text{GEV}_i = \frac{\sum_{t \in i} \text{GFP}(t) \cdot \text{CC}(t)^2}{\sum_t \text{GFP}(t)}$ where $\text{GFP}(t)$ is the Global Field Power at time t, and $\text{CC}(t)$ is the spatial correlation between the map at time t and the template map of state i.	GEV represents the proportion of the Global Field Power explained by each BNS, indicating how well each state represents the data.
GFP	$\text{GFP}(t) = \sqrt{\frac{1}{N}\sum_{i=1}^{N}\left(V_i(t) - \overline{V(t)}\right)^2}$ where $V_i(t)$ is the voltage at sensor i at time t, $\overline{V(t)}$ is the mean voltage across all sensors, and N is the total number of sensors.	GFP quantifies the variance of the EEG signal at a given time point, providing a measure of the strength of brain activity.
GMD	$\text{GMD}(t) = \sqrt{\frac{1}{N}\sum_{i=1}^{N}\left(\frac{V_i(t)}{\sqrt{\sum_{i=1}^{N} V_i^2(t)}} - \frac{V_i(r)}{\sqrt{\sum_{i=1}^{N} V_i^2(r)}}\right)^2}$ where $V_i(t)$ and $V_i(r)$ are the voltages at sensor i at times t and r, respectively, and N is the total number of sensors.	GMD quantifies the dissimilarity between two topographical voltage distributions over time.
Occurrence	$\text{Occurrence}_i = \frac{N_i}{T_{\text{total}}}$ where N_i is the number of times state i was activated, and T_{total} is the total analysis time.	Occurrence measures how many times a specific BNS appears within a time window.
TP	$T_{ij} = \frac{N_{ij}}{\sum_j N_{ij}}$ where T_{ij} is the transition probability from state i to state j, N_{ij} is the observed transitions from i to j, and $\sum_j N_{ij}$ is the total transitions from i to any state.	TP describes the probabilities of transitioning between different BNSs over time.

11.2 Paper 2: Exploring dynamic alpha band connectivity in Parkinson's disease: A novel approach to postural control assessment using the BioVRSea paradigm

11.2.1 Linear Mixed Model: Statistical Results in Alpha Band

11.2.1.1 Statistical Result of Coverage.

Table 11.3: Coverage p-values and adjusted p-values after FDR correction for different BNSs across phases (BL, PRE, MOV, POST) in the CTR - PD contrast.

BL Phase			**PRE Phase**			**MOV Phase**			**POST Phase**		
BNS	p-value	adjusted p-value	BNS	p-value	adjusted p-value	BNS	p-value	adjusted p-value	BNS	p-value	adjusted p-value
4	0.024	0.143	2	0.003	**0.019***	2	0.006	**0.036***	4	0.018	0.109
1	0.178	0.337	3	0.077	0.231	5	0.100	0.300	2	0.086	0.259
6	0.201	0.337	1	0.271	0.541	3	0.159	0.319	1	0.459	0.854
3	0.229	0.337	5	0.504	0.673	6	0.723	0.904	3	0.570	0.854
5	0.281	0.337	6	0.561	0.673	1	0.769	0.904	5	0.859	0.944
2	0.671	0.671	4	0.815	0.815	4	0.904	0.904	6	0.944	0.944

11.2.1.2 Statistical Result of Occurrence.

Table 11.4: Occurrence p-values and adjusted p-values after FDR correction for different BNSs across phases (BL, PRE, MOV, POST) in the CTR - PD contrast.

BL Phase			**PRE Phase**			**MOV Phase**			**POST Phase**		
BNS	p-value	adjusted p-value	BNS	p-value	adjusted p-value	BNS	p-value	adjusted p-value	BNS	p-value	adjusted p-value
1	0.082	0.372	2	0.032	0.174	2	0.038	0.228	6	0.324	0.877
6	0.124	0.372	1	0.058	0.174	1	0.566	0.793	1	0.513	0.877
4	0.607	0.672	6	0.450	0.678	5	0.581	0.793	2	0.553	0.877
5	0.615	0.672	5	0.452	0.678	6	0.626	0.793	5	0.615	0.877
3	0.653	0.672	4	0.815	0.978	4	0.661	0.793	3	0.730	0.877
2	0.672	0.672	3	1.000	1.000	3	0.885	0.885	4	0.975	0.975

11.2.1.3 Statistical Result of Duration.

Table 11.5: Duration p-values and adjusted p-values after FDR correction for different BNSs across phases (BL, PRE, MOV, POST) in the CTR - PD contrast.

BL Phase			**PRE Phase**			**MOV Phase**			**POST Phase**		
BNS	p-value	adjusted p-value	BNS	p-value	adjusted p-value	BNS	p-value	adjusted p-value	BNS	p-value	adjusted p-value
5	0.042	0.253	1	0.312	0.727	5	0.096	0.231	4	0.035	0.210
3	0.111	0.261	6	0.327	0.727	6	0.134	0.231	6	0.244	0.724
4	0.130	0.261	3	0.440	0.727	4	0.165	0.231	1	0.362	0.724
6	0.400	0.601	4	0.485	0.727	3	0.168	0.231	3	0.548	0.768
1	0.750	0.893	2	0.682	0.757	1	0.192	0.231	2	0.702	0.768
2	0.893	0.893	5	0.757	0.757	2	0.366	0.366	5	0.768	0.768

11.3 Paper 3: Dynamic connectivity patterns in Parkinson's disease: A new framework for postural control assessment with BioVRSea

11.3.1 Time-resolved BNS occupancy: descriptive visualization

To provide a descriptive representation of how group differences evolved over time, we examined the time-resolved occupancy of each BNS across the experimental timeline (Figures 11.3–11.2). Occupancy was computed at each time point as the proportion of subjects assigned to a given BNS, based on the temporally smoothed state-label sequence. This visualization complements the phase-wise presence analysis by illustrating the continuous temporal evolution of group-level state prevalence, while quantitative comparisons are reported using phase-wise BNS metrics.
In the **Delta** band (Figure 11.1), CTR exhibited a relatively distributed occupancy across multiple states, with *BNS1*, *BNS2*, and *BNS5* contributing throughout the protocol. In contrast, PD showed a clear predominance of *BNS3*, *BNS4*, and *BNS6*, which remained the most prevalent state across all phases. This pattern was accompanied by consistently lower occupancy of lower-index states, particularly *BNS1* and *BNS2*, and appeared stable across the entire experimental timeline.

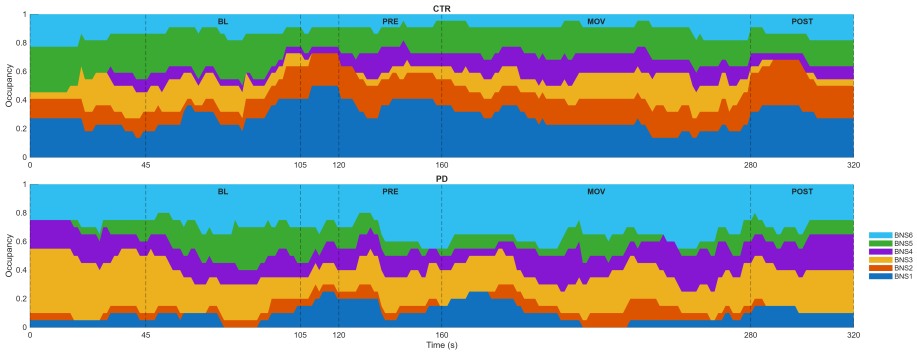


Figure 11.1: **Time-resolved occupancy of BNSs in CTR and PD in the Delta band.** Stacked area plots show the proportion of subjects assigned to each BNS at each time point. Vertical dashed lines indicate phase boundaries.

In the **Theta** band (Figure 11.2), occupancy patterns reflected a redistribution between the two dominant configurations. CTR was primarily characterized by higher occupancy of *BNS1*, whereas PD showed a reduced prevalence of this state and increased occupancy of *BNS2*. In addition, PD exhibited greater contributions from higher-index states, particularly *BNS4* and *BNS5*, across phases. These differences were evident throughout the experimental timeline and were consistent with the phase-wise presence patterns.

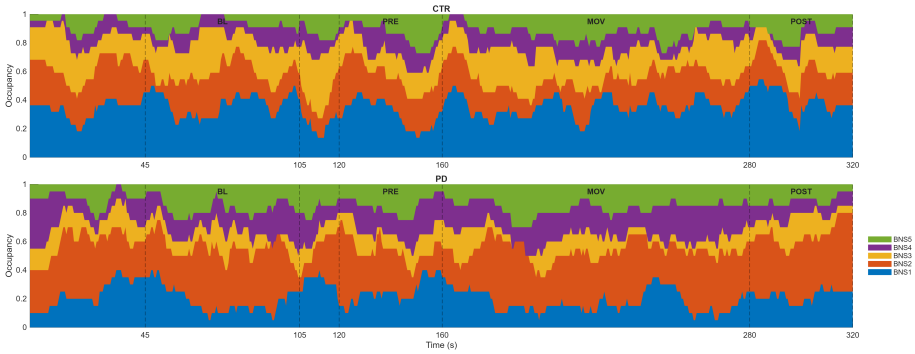


Figure 11.2: **Time-resolved occupancy of BNSs in CTR and PD in the Theta band.** Stacked area plots show the proportion of subjects assigned to each BNS at each time point. Vertical dashed lines indicate phase boundaries.

In the **Beta** band (Figure 11.3), CTR showed a consistent predominance of *BNS1* across the experimental timeline, with relatively stable occupancy and moderate temporal fluctuations. In contrast, PD exhibited a markedly reduced prevalence of *BNS1* and a corresponding increase in alternative configurations, particularly *BNS3–BNS5*. These differences were sustained across phases and were especially evident during the PRE and MOV phases, where PD showed more pronounced temporal variability and greater contributions from higher-index states.

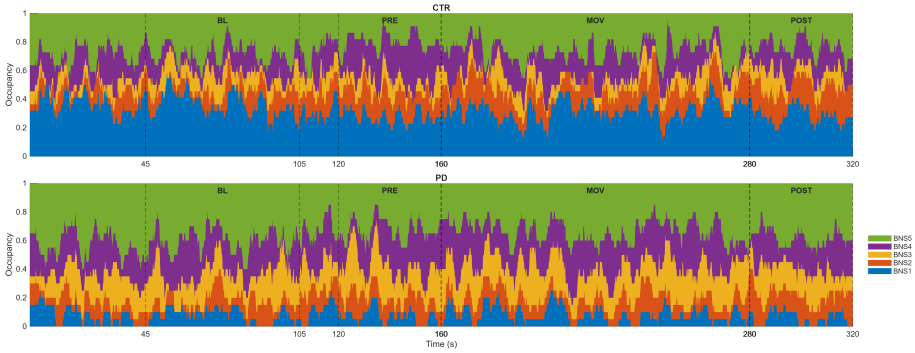


Figure 11.3: **Time-resolved occupancy of BNSs in CTR and PD in the Beta band.** Stacked area plots show the proportion of subjects assigned to each BNS at each time point. Vertical dashed lines indicate phase boundaries, and labels denote Baseline (BL), Preparation (PRE), Movement (MOV), and Post-movement (POST) phases.

11.3.2 Phase-wise BNS presence across frequency bands

Figure 11.4 reports the phase-wise BNS presence (percentage of samples assigned to each BNS) for CTR and PD across BL, PRE, MOV, and POST, separately for the Beta, Delta, and Theta bands.
Table 11.6 provides the corresponding numerical values, reporting the mean percentage presence of each BNS for each phase and group. Overall, CTR and PD exhibited distinct distributions of BNS presence, with group differences that were broadly consistent across phases within each frequency band.

Table 11.6: Mean phase-wise BNS presence for CTR and PD across frequency bands. Values are expressed as percentages and were derived from the temporally smoothed state-label matrix (subjects × time samples), where each time sample was assigned to a BNS. For each phase (BL, PRE, MOV, POST), BNS presence was computed at the subject level as the proportion of samples assigned to each state within the corresponding phase window, and then averaged across participants within each group (×100).

Delta

	CTR						PD					
Phase	**BNS1**	**BNS2**	**BNS3**	**BNS4**	**BNS5**	**BNS6**	**BNS1**	**BNS2**	**BNS3**	**BNS4**	**BNS5**	**BNS6**
BL	28.42	11.54	15.36	5.35	26.77	12.55	6.76	5.18	24.42	14.21	21.05	28.38
PRE	38.04	19.37	4.32	12.27	16.93	9.07	14.57	5.50	21.77	14.63	9.25	34.28
MOV	24.17	16.80	15.63	13.41	19.65	10.34	9.20	6.63	22.19	15.80	8.72	37.46
POST	31.93	26.54	2.52	7.12	15.89	16.01	12.61	0.64	28.92	20.90	10.21	26.73

Theta

	CTR					PD				
Phase	**BNS1**	**BNS2**	**BNS3**	**BNS4**	**BNS5**	**BNS1**	**BNS2**	**BNS3**	**BNS4**	**BNS5**
BL	33.51	30.23	18.18	10.36	7.72	28.14	35.58	13.84	10.81	11.63
PRE	32.45	20.85	24.45	8.93	13.32	24.14	32.76	10.17	13.28	19.66
MOV	33.98	21.48	25.32	11.80	7.41	18.45	34.76	11.49	18.10	17.20
POST	35.58	28.68	18.65	7.99	9.09	21.03	39.48	12.76	13.97	12.76

Beta

	CTR					PD				
Phase	**BNS1**	**BNS2**	**BNS3**	**BNS4**	**BNS5**	**BNS1**	**BNS2**	**BNS3**	**BNS4**	**BNS5**
BL	36.51	10.53	11.29	13.47	28.19	7.94	9.71	19.26	23.01	40.08
PRE	27.65	16.60	9.44	26.34	19.97	7.11	13.57	21.99	24.55	32.79
MOV	32.05	15.14	9.30	16.98	26.53	8.50	10.90	22.24	24.87	33.48
POST	28.63	19.65	10.07	17.77	23.88	5.92	16.10	17.86	21.90	38.22

In the Delta band, the two groups exhibited substantial differences in the distribution of BNS presence across all states (Fig. 11.4, Table 11.6). *BNS1* was consistently higher in CTR than PD in every phase (CTR: 24.17–38.04% vs PD: 6.76–14.57%), with the largest differences in PRE (38.04% vs 14.57%, Δ=23.47) and BL (28.42% vs 6.76%, Δ=21.66). *BNS2* was also markedly higher in CTR than PD throughout (CTR: 11.54–26.54% vs PD: 0.64–6.63%), with the strongest contrast in POST (26.54% vs 0.64%, Δ=25.90). *BNS3* showed the opposite pattern, being substantially higher in PD than CTR across all phases (PD: 21.77–28.92% vs CTR: 2.52–15.63), with the largest differences in POST (28.92% vs 2.52%, Δ=26.40) and PRE (21.77% vs 4.32%, Δ=17.45). *BNS4* was generally higher in PD than CTR in all phases (PD: 14.21–20.90% vs

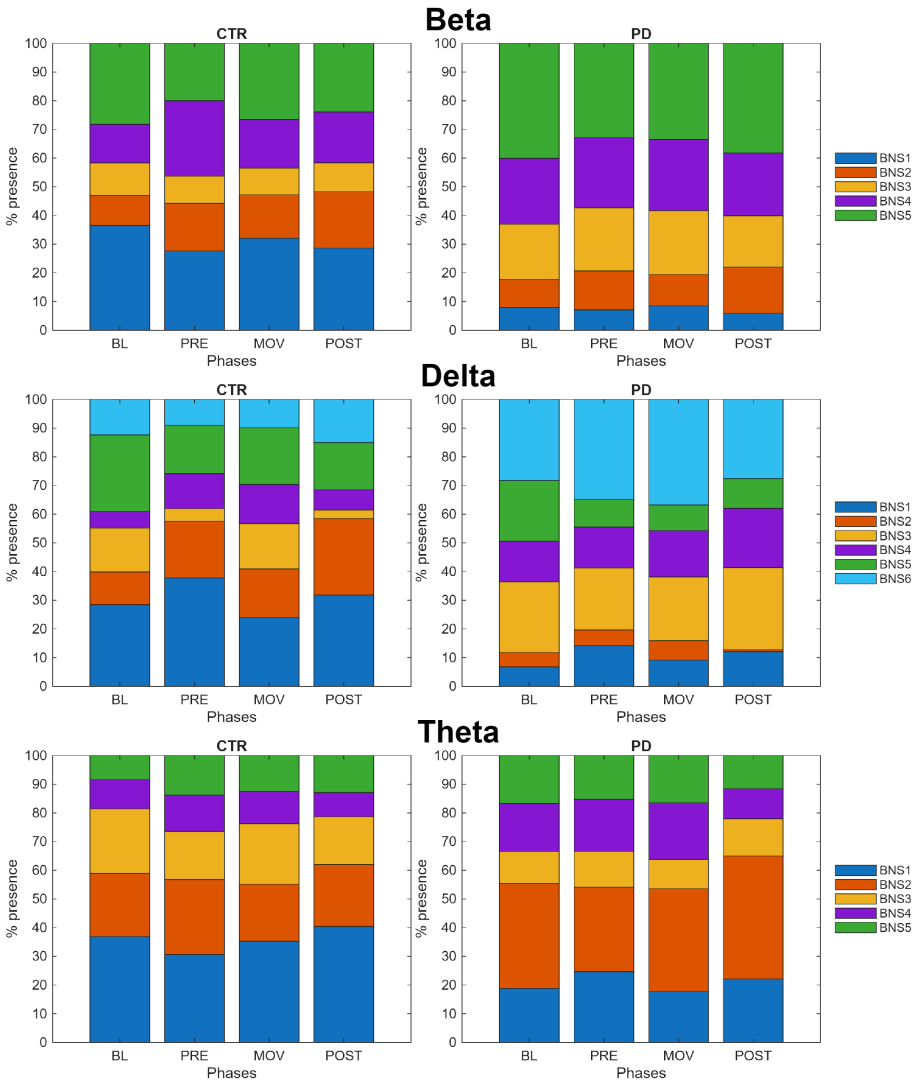


Figure 11.4: **Mean phase-wise BNS presence in CTR and PD across frequency bands.** Stacked bar plots show the mean percentage presence of each BNS within BL, PRE, MOV, and POST phases for CTR and PD. Presence was computed as the proportion of samples assigned to each BNS within each phase and averaged across subjects. Panels report results for Beta, Delta, and Theta bands.

CTR: 5.35–13.41), with the largest group difference at POST (20.90% vs 7.12%, Δ=13.78). *BNS5* was higher in CTR than PD throughout the protocol (CTR: 15.89–26.77% vs PD: 8.72–10.21%), with the largest contrast in BL (26.77% vs 21.05%, Δ=5.72). Finally, *BNS6* represented the dominant state in PD in all

phases (28.38–37.46%) and was consistently higher than in CTR (9.07–16.01), showing the strongest differences in MOV (37.46% vs 10.34%, Δ=27.12) and PRE (34.28% vs 9.07%, Δ=25.21). Overall, Delta-band dynamics in PD were characterized by reduced occupancy of lower-index states (BNS1–BNS2 and BNS5) and increased presence of higher-index states, particularly BNS3 and BNS6, relative to CTR. Specifically, CTR was primarily characterized by higher contributions of BNS1–BNS2 (and BNS5 at BL), whereas PD was dominated by BNS6 across all phases, with BNS3 representing the second most prominent component.

In the Theta band, group differences were mainly expressed as a redistribution between the two dominant states, BNS1 and BNS2 (Fig.11.4, Table 11.6). *BNS1* was consistently higher in CTR than PD across all phases (CTR: 32.45–35.58% vs PD: 18.45–28.14%), with the largest difference in POST (35.58% vs 21.03%, Δ=14.55) and MOV (33.98% vs 18.45%, Δ=15.53). Conversely, *BNS2* was consistently higher in PD than CTR throughout the protocol (PD: 32.76–39.48% vs CTR: 20.85–30.23%), with the strongest group difference in POST (39.48% vs 28.68%, Δ=10.80). *BNS3* contributed moderately in both groups and was generally higher in CTR (CTR: 18.18–25.32% vs PD: 10.17–13.84), with the largest difference in MOV (25.32% vs 11.49%, Δ=13.83) and PRE (24.45% vs 10.17%, Δ=14.28). In contrast, *BNS4* showed consistently higher presence in PD than CTR across phases (PD: 10.81–18.10% vs CTR: 7.99–11.80), with the largest difference in MOV (18.10% vs 11.80%, Δ=6.30). Finally, *BNS5* was also higher in PD than CTR in all phases (PD: 11.63–19.66% vs CTR: 7.41–13.32), with the largest contrast in PRE (19.66% vs 13.32%, Δ=6.34) and MOV (17.20% vs 7.41%, Δ=9.79). Overall, Theta-band dynamics in PD were characterized by reduced BNS1 and BNS3 and increased BNS2 together with higher contributions of BNS4–BNS5 compared to CTR.

In the Beta band, the two groups showed a marked redistribution of BNS presence across all states (Fig. 11.4, Table 11.6). *BNS1* was consistently higher in CTR than PD across all phases (CTR: 27.65–36.51% vs PD: 5.92–8.50%), yielding the largest group differences (e.g., BL: 36.51% vs 7.94%, Δ=28.57; MOV: 32.05% vs 8.50%, Δ=23.55). *BNS2* showed comparable contributions between groups, with slightly higher values in CTR. *BNS3* was consistently higher in PD than CTR across all phases (PD: 17.86–22.24% vs CTR: 9.30–11.29), with the largest differences in MOV (22.24% vs 9.30%, Δ=12.94) and PRE (21.99% vs 9.44%, Δ=12.55). *BNS4* was also higher in PD than CTR in every phase (PD: 21.90–24.87% vs CTR: 13.47–26.34), although CTR exhibited a pronounced increase in PRE (26.34%), resulting in a smaller or reversed group difference specifically in this phase (CTR: 26.34% vs PD: 24.55). Finally, *BNS5* represented the dominant state in PD throughout (32.79–40.08%) and was consistently higher than in CTR (19.97–28.19), with the largest differences at POST (38.22% vs 23.88%, Δ=14.34) and PRE (32.79% vs 19.97%, Δ=12.82). Overall, Beta-band dynamics in PD were characterized by reduced BNS1 and increased occupancy of higher-index states, primarily BNS3–BNS5, relative to CTR.

11.3.3 Detailed discussion of individual BNSs

This study investigated dynamic brain network organization during a complex postural control task in patients with early-stage PD using the BioVRSea paradigm. The main methodological contribution of this work is the use of a visuomotor stimulation protocol combining virtual reality and EEG recordings, allowing the investigation of motor-cognitive processes involved in postural control under ecologically relevant conditions. This approach provided a detailed framework for assessing postural control alterations in PD.
To characterize time-varying brain network activity, we employed a methodological pipeline adapted from Poulsen et al. for the extraction of BNSs from functional connectivity data [208, 219]. The procedure involved selecting the most appropriate clustering approach, optimizing the number and structure of BNSs, and applying back-fitting to quantify temporal properties of each state, including coverage, occurrence, and duration [219]. By applying this framework to EEG connectivity data acquired during the BioVRSea paradigm, we aimed to identify dynamic neurophysiological signatures of PD that may contribute to earlier disease characterization.
BNSs describe transient patterns of functional connectivity among distributed brain regions. In contrast to RSNs, which represent relatively stable patterns of connectivity commonly observed during rest, BNSs capture short-lived network configurations that fluctuate over time and may vary according to task demands or experimental conditions. Several regions contributing to the identified BNSs overlapped with established RSNs, including default mode, motor, visual, and attention-related networks. This indicates that canonical large-scale systems continue to shape brain organization during task execution, while their temporal expression changes dynamically across the paradigm.
Differences in BNS expression between PD patients and CTR suggest disease-related alterations in the dynamic organization of large-scale functional connectivity. Specifically, altered BNS patterns may reflect a reduced capacity to flexibly reconfigure brain networks in response to changing sensory, cognitive, and postural demands. Such reduced network flexibility may represent a neurophysiological mechanism contributing to the motor and cognitive disturbances observed in PD.

11.3.3.1 Delta band

BNS1: In the delta band, BNS1 showed a clear phase-dependent modulation in CTR, peaking during PRE (38.04%), decreasing during MOV (24.17%), and partially recovering during POST (31.93%), relative to baseline (28.42%). In contrast, PD exhibited markedly reduced occupancy across all phases (BL: 6.76%, PRE: 14.57%, MOV: 9.20%, POST: 12.61%) (Supplementary Material 11.3.2). BNS1 was primarily characterized by strong contributions from the DAN and SAN networks, with additional involvement of sensorimotor and occipital regions. This configuration suggests a role in slow attentional control and salience-mediated coordination of distributed cortical systems. Delta

oscillations have been associated with sustained attentional regulation and long-range coordination [274, 276]. The increased expression during PRE in CTR likely reflects recruitment of attentional and salience-control mechanisms during sustained visual stimulation, while the reduction during MOV suggests reconfiguration toward states supporting motor execution. The strongly attenuated presence of BNS1 in PD indicates impaired engagement of slow attentional control mechanisms and reduced salience-guided switching. Dysfunction of attentional and salience networks has been widely reported in PD and linked to impaired motor preparation and reduced adaptability [300, 301]. The reduced availability of this state may therefore contribute to impaired preparation and adaptive control during postural regulation.

BNS2: BNS2 exhibited progressive modulation in CTR, culminating in a marked increase during POST, suggesting engagement during recovery and reintegration phases. In contrast, PD showed consistently reduced occupancy across all phases, with near suppression during the POST phase. This state showed a broadly distributed integrative profile involving attentional, motor, visual, salience, auditory, and default-mode networks, indicating a large-scale coordination state. Slow delta oscillations have been associated with large-scale integration and recovery-related processes [276, 277]. The increase in BNS2 during POST in CTR suggests its involvement in restoring coordinated network organization after movement. The absence of this increase in PD indicates impaired recovery-related network reorganization. This finding aligns with previous reports of disrupted low-frequency connectivity and reduced network flexibility in PD [279, 281] and suggests a specific deficit in restoring functional balance after motor activity.

BNS3: In CTR, BNS3 showed strong modulation across phases, with suppression during PRE and POST and transient recruitment during MOV, indicating flexible engagement depending on task demands. In contrast, PD showed persistently elevated BNS3 occupancy across all phases, particularly during BL and POST, where CTR showed minimal expression. BNS3 displayed balanced contributions from multiple RSNs, indicating a globally synchronized integrative configuration (Supplementary Material 11.3.2). The abnormal persistence of this state in PD suggests impaired disengagement from globally synchronized delta configurations. Rather than flexibly transitioning between states, the PD brain appears to remain trapped in a low-frequency coherent state. This interpretation is consistent with previous findings of excessive low-frequency synchronization and reduced dynamical flexibility in PD [147, 282, 302].

BNS4: BNS4 showed significantly higher *occurrence* in PD compared to CTR during BL after FDR correction, and increased percentage presence across all phases, with particularly pronounced differences during POST. Together with the time-resolved occupancy pattern showing stable expression of higher-index delta states in PD, these results indicate that BNS4 is not merely elevated in average prevalence, but is also *recurrently re-entered* more often in PD, consistent with the fragmented temporal organization of slow network states. Beyond its global integrative signature, the spatial topology of BNS4 provides a more specific interpretation. In the delta band, BNS4 was dominated by DAN and

VIS (highest mean strength in DAN, closely followed by VIS), and displayed a *posterior-dominant* organization anchored on a midline backbone. Medially, prominent hubs included the precuneus (PCUN), posterior cingulate cortex (PCC), and isthmus cingulate (iCC), which were densely interconnected with bilateral occipital associative regions such as cuneus (CUN), lingual gyrus (LING), fusiform gyrus (FUS), and lateral occipital cortex (LOG). Laterally, strong nodes were evident in temporo-parietal DAN regions (MTG, ITG, pOPER) and parietal associative cortices (IPL, SPL), forming extensive links with occipital and midline hubs (Fig. 11.5).

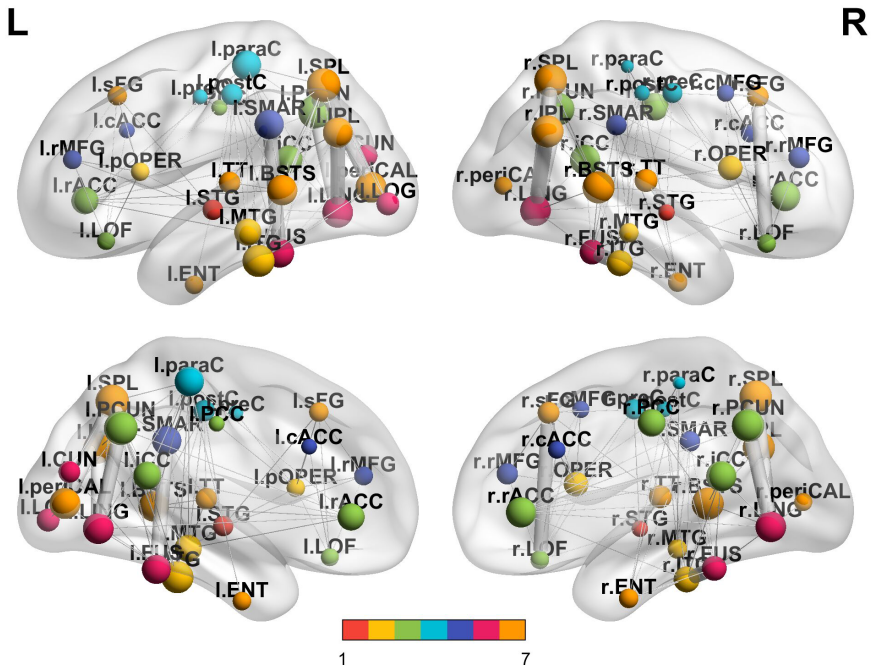


Figure 11.5: **BNS4 in the delta band.** Spatial representation of BNS1 connectivity pattern in the delta frequency band. Lateral and medial views of both hemispheres are shown: the top row displays the lateral views of the left (L) and right (R) hemispheres, while the bottom row displays the corresponding medial views. Nodes represent cortical regions and are colored according to their assigned resting-state network, while edges represent functional connections between regions. For visualization purposes, only connections with an edge weight greater than 0.04 are shown. This representation highlights the large-scale network organization and dominant inter-regional interactions characterizing BNS1 in the delta band.

In contrast, anterior frontal and salience-related regions (rACC, cACC; rMFG, cMFG) were present but comparatively less central, suggesting that the functional core of this state is a slow, posterior attentional-visual integration mode

rather than an anterior executive configuration (Fig. 11.5). Functionally, this anatomy is consistent with a delta-mediated state supporting externally oriented visuo-spatial integration and sustained attentional monitoring at slow timescales [274–276]. The strong coupling of occipital associative cortices with PCUN/PCC midline hubs suggests a configuration linking visual processing with medial integrative structures, while temporo-parietal DAN nodes indicate top-down attentional allocation over sensory representations. In the context of PC, such a state plausibly reflects reliance on visual-attentional monitoring to stabilize posture and maintain task set during prolonged standing or recovery. The increased *occurrence* of this posterior DAN-VIS state during baseline in PD suggests that patients repeatedly transition into an externally oriented monitoring configuration even in the absence of movement demands. This pattern is consistent with the broader notion that PD is associated with cortical slowing and abnormal low-frequency synchronization [147, 279, 280], and with reports of altered large-scale integration/segregation and reduced dynamical flexibility [281–283]. From a dynamical systems perspective, the frequent re-entry into BNS4 is compatible with an altered attractor landscape in which specific slow integrative states become easier to access and more repeatedly visited [284, 285]. Critically, the posterior-centric nature of BNS4 suggests that this stabilization is not generic global slowing, but is expressed as preferential engagement of a visuospatial attention–integration mode, potentially reflecting compensatory reliance on sensory-attentional resources when automatic postural control mechanisms are degraded. Finally, the elevated presence of BNS4 during POST in PD may indicate impaired recovery dynamics: rather than reinstating a broader repertoire of delta configurations after movement, PD patients may remain biased toward a posterior monitoring state, consistent with reduced ability to restore flexible large-scale coordination following motor perturbation [279, 281, 283].

BNS5: BNS5 showed a consistently higher presence in CTR compared to PD in all phases. This state displayed a balanced integrative profile involving attention, motor, visual, salience, and default-mode networks. Its higher expression in CTR suggests a role in flexible integration of distributed functional systems. The reduced engagement of this state in PD indicates that not all delta configurations are uniformly increased. Instead, PD is characterized by selective redistribution, with reduced engagement of potentially adaptive integrative states. This pattern is consistent with previous evidence of disrupted integration–segregation balance in PD [147, 281, 283].

BNS6: BNS6 showed the most pronounced group difference, with consistently higher presence in PD across all phases. This state was characterized by strong involvement of DAN, SAL, and VIS, along with motor system contributions. Its predominance in PD indicates a pathological shift toward a delta-mediated attentional configuration. While recruitment of attentional networks is necessary for postural control, excessive persistence of this state likely reflects inefficient network regulation. Dysfunction of dorsal attention and salience networks has been linked to motor and cognitive impairments in PD [300, 301]. These findings extend previous evidence of cortical slowing in PD [279, 282] by demonstrating

that disease-related abnormalities are expressed as altered temporal distribution of specific large-scale network states.

11.3.3.2 Theta band

BNS1: In CTR, BNS1 represented one of the dominant theta configurations across phases, whereas PD showed consistently reduced occupancy. Spatially, BNS1 was dominated by DAN contributions, with strong involvement of SAN and VIS, and widespread anterior–posterior connectivity linking frontal control regions, central sensorimotor cortices, and posterior occipital areas. This topology suggests that BNS1 reflects a theta-mediated attentional–sensorimotor coordination state, integrating frontal control systems with motor and visual processing. Fronto-parietal theta synchronization has been repeatedly linked to adaptive cognitive control and task-set maintenance [290, 303]. The reduced engagement of this configuration in PD, therefore, suggests diminished recruitment of coordinated attentional control mechanisms during postural regulation. Importantly, the attenuation of BNS1 in PD parallels the reduction of stabilization-related configurations observed in the beta band, suggesting that both fast (beta) and slower (theta) control-related dynamics are compromised, albeit via distinct network topologies.
BNS2: In contrast, BNS2 was consistently higher in PD across phases and represented the dominant theta configuration in patients. Spatially, BNS2 displayed relatively uniform strength across networks, with slightly higher DAN involvement, and widespread bilateral connectivity linking anterior frontal regions, lateral temporal cortices, central motor areas, and posterior visual regions. This configuration appears less specialized and more diffusely integrative than BNS1. The increased reliance on BNS2 in PD may reflect compensatory recruitment of distributed integrative processes when more efficient attentional–sensorimotor coordination states are under-expressed. Theta-band increases in PD have previously been associated with compensatory cognitive engagement and increased control demands [279]. The shift toward BNS2 may therefore indicate greater dependence on globally coordinated theta activity to sustain task performance.
BNS3: BNS3 showed higher strength in the DAN and displayed marked hemispheric asymmetry, with larger nodes predominantly located in the left inferior–posterior and lateral temporal regions. Although this state contributed moderately in both groups, it was generally higher in CTR. The asymmetric organization and strong attentional contributions suggest that BNS3 may reflect lateralized attentional modulation of sensorimotor integration. Its relative reduction in PD may indicate impaired hemispheric specialization or reduced flexibility in recruiting lateralized attentional processes, consistent with altered functional lateralization reported in PD.
BNS4: BNS4 showed a particularly important alteration: LMM analysis revealed significantly longer *duration* in PD during the PRE phase. Unlike the DAN-dominant states, BNS4 was centered on DMN hubs, with the highest mean nodal strength in DMN, followed by strong MOT and DAN contributions. Medially, large hubs were observed in the PCC, precuneus, rostral ACC, and

orbitofrontal cortex, forming a midline core extensively connected with bilateral motor cortices (precentral, postcentral, paracentral lobule). DAN regions in lateral temporal areas and posterior visual cortices were integrated into this network, creating a globally distributed configuration linking self-referential, motor, and attentional systems (Fig. 11.6). The prolonged duration of this DMN-centered theta state in PD during PRE suggests impaired disengagement from internally oriented integrative configurations during movement preparation. Theta activity within medial frontal and cingulate regions has been associated with performance monitoring and control allocation [290]. However, excessive persistence of such states may reflect reduced flexibility in switching toward task-optimized configurations. In the context of PD, altered DMN dynamics and impaired segregation between DMN and task-positive networks have been widely reported [283, 289]. The increased stability of BNS4 may therefore represent pathological over-integration between DMN and motor systems, limiting efficient preparatory reconfiguration.

BNS5: BNS5, characterized by strong VIS and DAN contributions, was consistently higher in PD than CTR across phases. Spatially, this state displayed prominent frontal and posterior occipital nodes with continuous anterior–posterior connectivity, particularly in the right hemisphere. This pattern suggests increased theta-mediated coupling between frontal control regions and visual associative cortices. Given the reliance of PD patients on visual cues for postural and motor control [304, 305], the enhanced presence of BNS5 likely reflects compensatory visual-attentional engagement. However, its persistent elevation across phases indicates that this configuration may become chronically engaged rather than flexibly recruited.

11.3.3.3 Beta band

BNS1: BNS1 represented the dominant beta configuration in CTR across all experimental phases, whereas PD showed markedly reduced expression. This imbalance was confirmed both in phase-wise presence and time-resolved occupancy, indicating a persistent reduction of this state in PD. Importantly, the spatial topology of BNS1 was not generic: it was characterized by dense bilateral connectivity linking posterior occipital cortices (CUN, LOG, LING, FUS), central sensorimotor regions (preC, postC, paraC), and core DMN hubs (PCC, PCUN, rACC, LOF), with additional DAN contributions (MTG, ITG, pOPER). The configuration therefore, combined visual integration, sensorimotor execution areas, and midline integrative regions within a largely symmetric large-scale network backbone (Fig. 11.7). This posterior–midline–sensorimotor architecture strongly supports the interpretation of BNS1 as a stabilization state: it integrates visual feedback, attentional allocation, and motor readiness within a coherent beta-mediated configuration. Beta oscillations are widely associated with maintenance of the current sensorimotor set and resistance to state change [291, 292]. The strong engagement of PCC–precuneus midline hubs together with bilateral visual–motor coupling suggests that in healthy individuals, this state supports stable visuomotor integration during PC. The

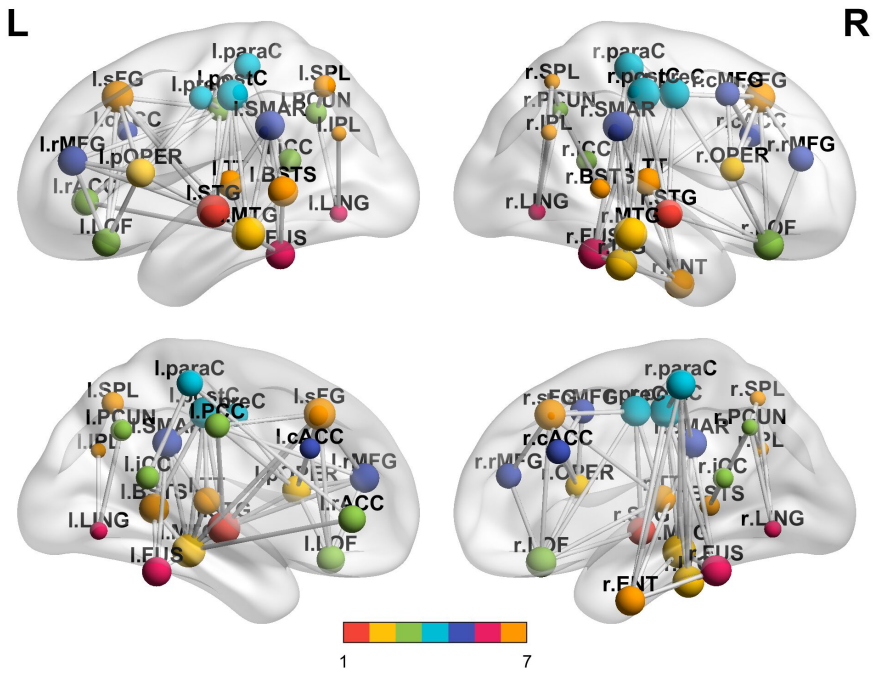


Figure 11.6: **BNS4 in the theta band.** Spatial representation of BNS1 connectivity pattern in the theta frequency band. Lateral and medial views of both hemispheres are shown: the top row displays the lateral views of the left (L) and right (R) hemispheres, while the bottom row displays the corresponding medial views. Nodes represent cortical regions and are colored according to their assigned resting-state network, while edges represent functional connections between regions. For visualization purposes, only connections with an edge weight greater than 0.04 are shown. This representation highlights the large-scale network organization and dominant inter-regional interactions characterizing BNS1 in the theta band.

significant reduction of both coverage and duration of BNS1 in PD indicates that this integrative posterior–sensorimotor configuration is not only less prevalent but also less temporally stable. Given that beta synchronization in PD is abnormally regulated and excessively rigid at the local level [293, 294], our findings suggest a complementary large-scale phenomenon: instead of maintaining a coherent distributed stabilization state, PD patients fail to sustain this balanced integrative configuration.

BNS2: Although overall presence of BNS2 was broadly comparable between groups, PD patients showed significantly higher occurrence during baseline, indicating more frequent transitions into BNS2. Spatially, BNS2 displayed a distinct topology centered on midline DMN hubs (PCC, PCUN, ACC), forming a dense medial backbone that extended bilaterally toward lateral parietal re-

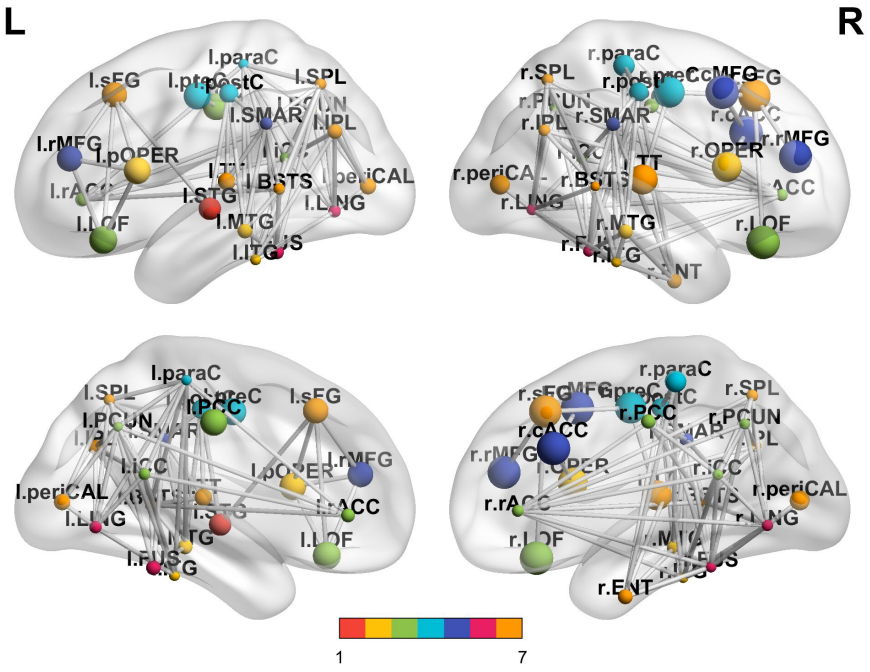


Figure 11.7: **BNS1 in the beta band.** Spatial representation of BNS1 connectivity pattern in the beta frequency band. Lateral and medial views of both hemispheres are shown: the top row displays the lateral views of the left (L) and right (R) hemispheres, while the bottom row displays the corresponding medial views. Nodes represent cortical regions and are colored according to their assigned resting-state network, while edges represent functional connections between regions. For visualization purposes, only connections with an edge weight greater than 0.04 are shown. This representation highlights the large-scale network organization and dominant inter-regional interactions characterizing BNS1 in the beta band.

gions (IPL, SPL), temporal cortices (MTG, STG), and posterior visual–ventral temporal areas (FUS, LOG, LING). Compared with BNS1, sensorimotor regions were less dominant, and the configuration appeared more centered on midline integrative and associative visual–temporal systems. This pattern suggests that BNS2 represents a large-scale integrative state linking internally oriented DMN processing with associative visual and parietal cortices, potentially reflecting monitoring, integration of environmental information, or transitional cognitive–perceptual processing rather than direct motor stabilization. The increased occurrence but unchanged coverage in PD indicates instability of this midline-driven configuration. Rather than sustaining coherent DMN–posterior integration, PD patients appear to enter and exit this state more frequently, reflecting temporal fragmentation. Such instability is consistent with altered

beta-band regulation and impaired large-scale coordination described in PD [293, 294]. Importantly, the spatial contrast between BNS1 and BNS2 is revealing: whereas BNS1 tightly couples posterior visual and central sensorimotor cortices with midline hubs, BNS2 emphasizes medial integrative structures with broader associative posterior connectivity and reduced motor dominance. The reduced stability of BNS1, together with increased fragmentation in BNS2, suggests that PD shifts beta-band dynamics away from sustained visuomotor stabilization toward more labile midline-integrative states.

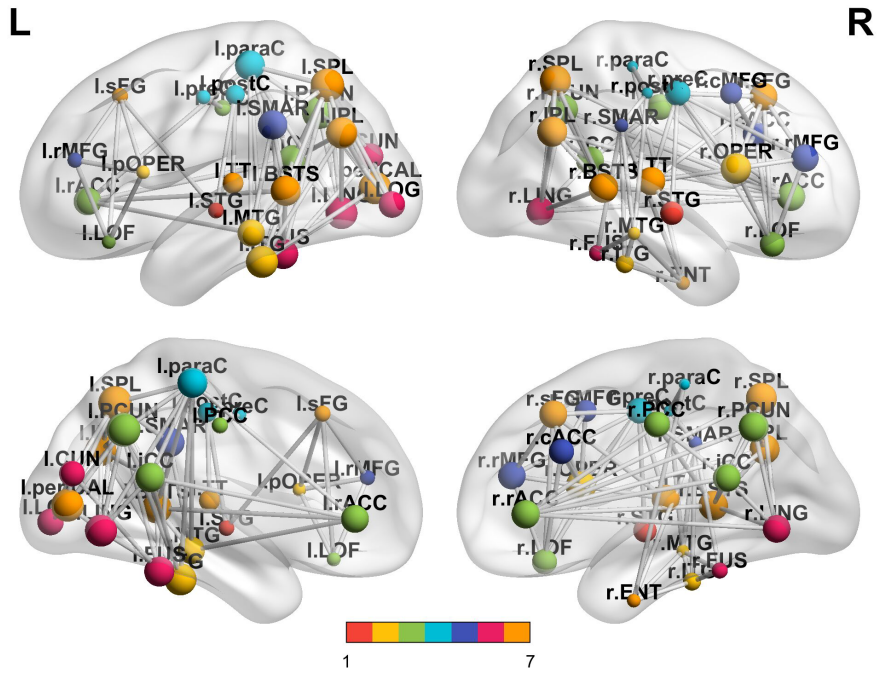


Figure 11.8: **BNS2 in the beta band.** Spatial representation of BNS1 connectivity pattern in the beta frequency band. Lateral and medial views of both hemispheres are shown: the top row displays the lateral views of the left (L) and right (R) hemispheres, while the bottom row displays the corresponding medial views. Nodes represent cortical regions and are colored according to their assigned resting-state network, while edges represent functional connections between regions. For visualization purposes, only connections with an edge weight greater than 0.04 are shown. This representation highlights the large-scale network organization and dominant inter-regional interactions characterizing BNS1 in the beta band.

BNS3: BNS3 was consistently more expressed in PD than in CTR across all phases, with PD values approximately double those of CTR. This difference was stable across the experimental timeline, as confirmed by occupancy analysis. Spatially, BNS3 showed broadly distributed strength with slightly

higher contributions from the DAN and VIS, suggesting an externally oriented attentional–visuomotor configuration. The increased presence of this state in PD is coherent with extensive evidence showing that PD patients rely more heavily on attentional control to maintain posture and gait when automatic motor control is impaired [304, 306]. This increased recruitment of attentional networks likely reflects compensatory mechanisms supporting postural regulation. Importantly, the presence of this difference at baseline suggests that it reflects intrinsic alterations in beta-band network organization rather than purely task-induced modulation, consistent with broader connectivity findings in PD [307].

BNS4: BNS4 also showed consistently higher presence in PD across most phases, whereas CTR exhibited a marked transient increase during PRE. Spatially, BNS4 combined DMN and DAN contributions, suggesting an integrative configuration supporting preparation and attentional monitoring. The transient recruitment observed in CTR suggests flexible, phase-dependent modulation of network states. In contrast, the persistent elevation observed in PD indicates reduced modulation and impaired flexibility of large-scale beta-band coordination. This finding aligns with previous work demonstrating that pathological beta activity in PD is associated with reduced adaptability and impaired updating of motor-network states [293, 294].

BNS5: BNS5 was the dominant configuration in PD across all phases and consistently exceeded CTR values. Spatially, BNS5 showed strong involvement of the DAN, suggesting externally oriented attentional and sensory processing. This increased dominance indicates greater reliance on attentional control and sensory monitoring in PD, consistent with evidence showing increased attentional demands during postural and motor control in PD [304, 305]. The persistence of this configuration during BL further suggests that this reorganization reflects intrinsic beta-band alterations rather than purely task-driven effects, consistent with previous studies demonstrating altered beta dynamics in PD [294].

11.3.4 Linear Mixed Model: Statistical Result in Bands

Table 11.7: Beta: Coverage

BL Phase			**PRE Phase**			**MOV Phase**			**POST Phase**		
BNS	p-value	Adjusted p-value	BNS	p-value	Adjusted p-value	BNS	p-value	Adjusted p-value	BNS	p-value	Adjusted p-value
1	0.001	**0.004**	5	0.185	0.698	1	0.010	0.051	1	0.131	0.436
2	0.114	0.197	1	0.370	0.698	4	0.114	0.284	5	0.175	0.436
3	0.118	0.197	3	0.419	0.698	2	0.346	0.577	2	0.662	0.837
5	0.187	0.234	4	0.991	0.992	5	0.609	0.761	3	0.785	0.837
4	0.300	0.300	2	0.992	0.992	3	0.949	0.949	4	0.837	0.837

Table 11.8: Beta: Duration

BL Phase			**PRE Phase**			**MOV Phase**			**POST Phase**		
BNS	p-value	Adjusted p-value	BNS	p-value	Adjusted p-value	BNS	p-value	Adjusted p-value	BNS	p-value	Adjusted p-value
1	0.002	**0.012**	5	0.326	0.766	1	0.591	0.840	5	0.223	0.999
3	0.260	0.650	3	0.378	0.766	3	0.740	0.840	1	0.851	0.999
5	0.391	0.652	1	0.538	0.766	4	0.751	0.840	2	0.897	0.999
4	0.609	0.758	4	0.613	0.766	5	0.758	0.840	4	0.986	0.999
2	0.758	0.758	2	0.916	0.916	2	0.840	0.840	3	0.999	0.999

Table 11.9: Beta: Occurrence

BL Phase			PRE Phase			MOV Phase			POST Phase		
BNS	p-value	Adjusted p-value	BNS	p-value	Adjusted p-value	BNS	p-value	Adjusted p-value	BNS	p-value	Adjusted p-value
2	0.006	**0.032**	1	0.489	0.772	1	0.030	0.150	1	0.141	0.705
1	0.092	0.229	5	0.508	0.772	4	0.140	0.349	2	0.371	0.735
5	0.373	0.622	4	0.602	0.772	2	0.477	0.660	5	0.554	0.735
3	0.517	0.646	2	0.654	0.772	3	0.645	0.660	3	0.693	0.735
4	0.663	0.663	3	0.772	0.772	5	0.660	0.660	4	0.735	0.735

Table 11.10: Delta: Coverage

BL Phase			PRE Phase			MOV Phase			POST Phase		
BNS	p-value	Adjusted p-value	BNS	p-value	Adjusted p-value	BNS	p-value	Adjusted p-value	BNS	p-value	Adjusted p-value
1	0.184	0.897	4	0.098	0.559	6	0.092	0.353	2	0.021	0.128
4	0.410	0.897	3	0.259	0.559	2	0.135	0.353	3	0.114	0.342
2	0.686	0.897	1	0.473	0.559	1	0.185	0.353	4	0.290	0.580
3	0.815	0.897	6	0.503	0.559	5	0.235	0.353	6	0.872	0.959
5	0.878	0.897	2	0.541	0.559	3	0.383	0.460	1	0.944	0.959
6	0.897	0.897	5	0.559	0.559	4	0.576	0.576	5	0.959	0.959

Table 11.11: Delta: Duration

BL Phase			PRE Phase			MOV Phase			POST Phase		
BNS	p-value	Adjusted p-value	BNS	p-value	Adjusted p-value	BNS	p-value	Adjusted p-value	BNS	p-value	Adjusted p-value
1	0.106	0.634	4	0.097	0.580	6	0.170	0.386	2	0.021	0.128
3	0.816	0.898	3	0.225	0.651	1	0.248	0.386	3	0.129	0.334
2	0.827	0.898	1	0.461	0.651	5	0.266	0.386	4	0.167	0.334
5	0.879	0.898	6	0.479	0.651	3	0.290	0.386	1	0.793	0.978
4	0.881	0.898	5	0.548	0.651	2	0.322	0.386	5	0.943	0.978
6	0.898	0.898	2	0.651	0.651	4	0.709	0.709	6	0.978	0.978

Table 11.12: Delta: Occurrence

BL Phase			PRE Phase			MOV Phase			POST Phase		
BNS	p-value	Adjusted p-value	BNS	p-value	Adjusted p-value	BNS	p-value	Adjusted p-value	BNS	p-value	Adjusted p-value
4	0.003	**0.016**	2	0.291	0.999	2	0.189	0.686	4	0.021	0.125
1	0.044	0.132	5	0.546	0.999	6	0.229	0.686	6	0.255	0.764
2	0.339	0.678	6	0.940	0.999	4	0.574	0.768	1	1.000	1.000
5	0.927	0.991	4	0.968	0.999	1	0.587	0.768	3	1.000	1.000
3	0.970	0.991	3	0.982	0.999	3	0.640	0.768	5	1.000	1.000
6	0.991	0.991	1	0.999	0.999	5	1.000	1.000	2	1.000	1.000

Table 11.13: Theta: Coverage

BL Phase			PRE Phase			MOV Phase			POST Phase		
BNS	p-value	Adjusted p-value	BNS	p-value	Adjusted p-value	BNS	p-value	Adjusted p-value	BNS	p-value	Adjusted p-value
2	0.042	0.117	4	0.023	0.113	1	0.011	0.055	2	0.029	0.145
1	0.047	0.117	1	0.469	0.879	2	0.069	0.161	1	0.606	0.941
4	0.263	0.438	2	0.583	0.879	4	0.097	0.161	4	0.755	0.941
3	0.446	0.558	5	0.704	0.879	5	0.189	0.236	3	0.762	0.941
5	0.583	0.583	3	0.952	0.952	3	0.286	0.286	5	0.941	0.941

Table 11.14: Theta: Duration

BL Phase			PRE Phase			MOV Phase			POST Phase		
BNS	p-value	Adjusted p-value	BNS	p-value	Adjusted p-value	BNS	p-value	Adjusted p-value	BNS	p-value	Adjusted p-value
1	0.037	0.116	4	0.010	**0.048**	1	0.102	0.460	2	0.246	0.796
2	0.046	0.116	1	0.363	0.696	5	0.184	0.460	4	0.656	0.796
3	0.390	0.650	5	0.533	0.696	2	0.515	0.858	5	0.693	0.796
4	0.556	0.655	2	0.557	0.696	4	0.831	0.993	3	0.795	0.796
5	0.655	0.655	3	0.891	0.891	3	0.993	0.993	1	0.796	0.796

Table 11.15: Theta: Occurrence

BL Phase			PRE Phase			MOV Phase			POST Phase		
BNS	p-value	Adjusted p-value	BNS	p-value	Adjusted p-value	BNS	p-value	Adjusted p-value	BNS	p-value	Adjusted p-value
2	0.156	0.778	2	0.156	0.778	2	0.156	0.778	2	0.156	0.778
5	0.555	1.000	5	0.555	1.000	5	0.555	1.000	5	0.555	1.000
1	0.625	1.000	1	0.625	1.000	1	0.625	1.000	1	0.625	1.000
3	0.862	1.000	3	0.862	1.000	3	0.862	1.000	3	0.862	1.000
4	1.000	1.000	4	1.000	1.000	4	1.000	1.000	4	1.000	1.000

List of Figures

1.1 **Physiological mechanisms underlying postural control.** Visual, vestibular, and proprioceptive/somatosensory information is integrated at multiple levels of the central nervous system, including the cerebral cortex, basal ganglia, cerebellum, brainstem, and spinal cord. The resulting motor commands generate coordinated musculoskeletal responses that maintain the centre of mass within the base of support. Continuous sensory feedback, sensory reweighting, and reactive and anticipatory postural adjustments enable postural responses to adapt to environmental and task-related demands [1, 3, 4]. 2

3.1 **Schematic representation of the BioVRSea experimental setup and protocol.** Participants stood on the instrumented moving platform while wearing a virtual-reality headset and multimodal acquisition equipment. The protocol included a 105-s baseline with a static mountain scene, a 15-s white-screen transition, and a 40-s pre-motion phase with sea visualization and no platform movement. This was followed by three 40-s motion phases at 25%, 50%, and 75% intensity and a final 40-s post-motion phase with the platform stationary. EEG, heart-rate, and EMG recordings began at baseline, while force-platform acquisition started during the pre-motion phase. 24

3.2 **BioVRSea multimodal acquisition system and sensor placement.** Anterior and posterior views illustrate the 64-channel EEG cap worn together with the virtual-reality headset, the bilateral placement of six wireless surface EMG sensors over the tibialis anterior, lateral gastrocnemius, and soleus muscles, and the force-platform measurement of centre-of-pressure (CoP) displacement. The EEG amplifier and wireless EMG acquisition unit are also shown. 26

3.3 **Schematic representation of the BioVRSea experimental protocol.** The protocol consists of baseline (BL), pre-phase (PRE), three moving-platform phases corresponding to 25%, 50%, and 75% of the maximal wave amplitude, and post-phase (POST). The three moving-platform stimulation phases are collectively referred to as the MOV phase. 27

3.4 **Center-of-pressure ellipses in the initial seafarer application of BioVRSea.** Mean CoP ellipses are shown for healthy controls and sailors during the adaptation and habituation phases. The major axis represents anteroposterior sway, whereas the minor axis represents mediolateral sway. 29
3.5 **Right soleus skewness during the adaptation phase.** Boxplots show the distribution of right soleus EMG skewness in healthy controls and sailors. Sailors showed higher skewness values, suggesting a pattern of low-intensity background activity combined with intermittent high-intensity corrective bursts during BioVRSea stimulation. 30
3.6 **EEG acquisition system and electrode montage.** (a) EEG recording setup including the electrode cap, acquisition unit, and computer interface used for real-time monitoring of the recorded signals. (b) Spatial distribution of the EEG electrodes according to the extended 10–10 system, showing the left and right hemispheric positions and the mastoid electrodes M1 and M2. 31
3.7 **EMG acquisition system and sensors placement.** (a) The image shows the Kine wireless EMG device and sensor units used for recording lower-limb muscle activity during the experimental protocol. (b) The tibialis anterior, gastrocnemius lateralis, and soleus are highlighted, with white markers indicating approximate electrode placement sites. 34
3.8 **Force-platform configuration and representative center-of-pressure trajectory.** (a) Top view of the two independent foot platforms integrated into the BioVRSea moving platform, with the force-sensor locations highlighted in red. The anteroposterior (AP) and mediolateral (ML) directions are indicated. Vertical force measurements were acquired at a sampling frequency of $F_s = 90$ Hz and used to estimate the center of pressure (CoP). (b) Representative CoP trajectory in the AP–ML plane, illustrating postural sway during the experimental conditions. The platform was synchronized with the virtual sea scenario displayed through the VR headset, enabling the assessment of postural responses under controlled sensory-conflict conditions. 36

4.1 **Comparison of center of pressure ellipse areas between Parkinson's disease and healthy control groups.** Ellipse areas are shown for the PRE and POST phases of the experiment 44
4.2 **Theta and alpha absolute power spectral density comparison.** Absolute PSD values are compared between participants with Parkinson's disease and healthy controls. 45

5.1 **Workflow description.** EEGs were recorded using 64 electrodes during the BioVRSea experiment. The cortical sources were reconstructed by solving the inverse problem using the wMNE method. After source reconstruction, the signals were divided into 56 brain Regions of Interest (ROIs) derived from the Desikan–Killiany atlas, originally composed of 68 ROIs. The reduction to 56 ROIs was performed to address the spatial resolution limitations of EEG source estimation by aggregating anatomically related regions, and to ensure methodological consistency with the network analysis by selecting ROIs according to their assignment to the seven canonical Resting-State Networks (RSNs). Functional connectivity matrices were computed between the 56 regional time series using the PLV method across five frequency bands (Delta, Theta, Alpha, Beta, Gamma). Connectivity matrices were first obtained separately for the PD and CTR groups, then concatenated before being input into the k-means++ clustering algorithm. This clustering process identified distinct Brain Network States (BNSs), followed by network analysis at the subject level to compute metrics for group comparisons. 50

5.2 **Percentage representation of Brain Network States.** Distribution of Brain Network States (BNSs) across different experimental time phases for (a) PD patients and (b) the CTR group. Each bar represents the frequency of a specific BNS during the respective phase, illustrating how often each state was engaged throughout the experiment. (c) Lists the identified BNSs. 54

5.3 **Linear Mixed Model analysis.** Coverage for each Brain Network States (BNSs) across all experimental phases in PD patients and CTR. Coverage refers to the proportion of total activity distributed across the six identified BNSs, indicating how dominant each BNS was relative to the others during each phase. Significant differences between groups, corrected using the False Discovery Rate (FDR) method, are highlighted: * $p < 0.05$. 56

5.4 **Transition Probability matrices.** PD and CTR subjects across baseline (BL), pre-motor stimulus (PRE), movement-stimulus (MOV), and post-motor stimulus (POST) phases. Each heatmap represents the likelihood of transitioning between different Brain Network States (BNSs) within each phase, with lighter colors indicating higher transition probabilities. These matrices highlight the patterns of state transitions and the differences between groups in terms of network dynamics. 57

5.5 **Prevalence of Resting Network States in each Brain Network State.** Calculated as the sum of the node strength values for each Region of interest (ROI) associated with the specific Resting Network State (RSNs). Each Brain Network State (BNS) is visualized with nodes sized proportionally to their strength (the sum of connections at each node), and edges are shown based on their connectivity, with a sparsity threshold of 0.01 applied to filter weak connections. Different colors represent distinct RSNs, facilitating clear visual differentiation of the dominant networks in each BNS. This visualization highlights the key RSNs contributing to the overall network dynamics across experimental phases. 58

6.1 **BioVRSea EEG-processing workflow.** EEG was recorded using 64 electrodes, and cortical sources were reconstructed with wMNE and mapped to 68 Desikan–Killiany regions, subsequently aggregated into 56 ROIs. PLV-based functional connectivity matrices were computed across the delta, theta, and beta bands for PD and CTR groups, concatenated, and clustered using k-means++ to identify BNSs. Subject-level network metrics were then extracted for between-group comparisons. 62

6.2 **Delta: Prevalence of RSNs in each BNS.** Calculated as the sum of the node strength values for each ROI associated with each RSN. Each BNS is displayed with nodes sized proportionally to their strength, while edges are shown using a sparsity threshold of 0.04. Colors represent distinct RSNs: AUD (red), DAN (yellow), DMN (green), MOT (cyan), SAN (blue), VIS (magenta), and Other (orange). 66

6.3 **LMM analysis.** Linear mixed-model analysis revealed significant between-group differences in BNS dynamics. In the *delta* band, the PD group showed a higher *occurrence* of BNS4 during BL. 66

6.4 **Theta: Prevalence of RSNs in each BNS.** Prevalence was calculated as the sum of the node-strength values of the ROIs associated with each RSN. Node size is proportional to strength, while edges are displayed using a sparsity threshold of 0.04. Colors represent AUD (red), DAN (yellow), DMN (green), MOT (cyan), SAN (blue), VIS (magenta), and Other (orange). 67

6.5 **LMM analysis.** Linear mixed-model analysis revealed significant between-group differences in BNS dynamics. In the *theta* band, PD showed a longer *duration* of BNS4 during PRE. The reported effect survived FDR correction ($*p < 0.05$). 67

6.6 **Beta: Prevalence of RSNs in each BNS.** Prevalence was calculated as the sum of the node-strength values of the ROIs associated with each RSN. Node size is proportional to strength, while edges are displayed using a sparsity threshold of 0.01. Colors represent AUD (red), DAN (yellow), DMN (green), MOT (cyan), SAN (blue), VIS (magenta), and Other (orange). 68

6.7 **LMM analysis.** During BL in the *beta* band, CTR showed greater *coverage* and *duration* of BNS1, whereas PD showed greater *occurrence* of BNS2. All effects remained significant after FDR correction ($*p < 0.05$). 68

7.1 **CoP Total Excursion and Mean Velocity *a)*** Total CoP Excursion (TOTEX) for the control group (CTR, blue) positioned to the left and Parkinson's disease group (PD, orange) positioned to the right within each assessment phase, namely PRE and POST phases. Black horizontal lines represent the median values. Across the two phases, the control group showed a broader distribution and higher median values than the Parkinson group. ***b)*** Mean CoP Velocity (MVELO) for the control group (CTR, blue) positioned to the left and the Parkinson's disease group (PD, orange) positioned to the right within each assessment phase, namely PRE and POST. Black horizontal lines represent the median values. Across the two phases, the control group showed a broader distribution and higher median values than the Parkinson group. 72

7.2 **Mean center-of-pressure (CoP) ellipses for the control group (CTR) and Parkinson's disease group (PD) across the PRE, MOV, and POST phases.** Ellipses are shown in the mediolateral (ML, minor axis) and anteroposterior (AP, main axis) directions. Across all phases, the CTR group exhibited larger sway ellipses than the PD group, with the greatest ellipse area observed during the POST phase 73

7.3 **EMG coefficient of variation and standard deviation *a)*** EMG coefficient of variation (CV) for Soleus Left (SL) and Soleus Right (SR) in the PRE and POST phases. CTR (blue) is shown on the left and PD (orange) on the right within each phase. Black horizontal lines indicate the median. A significant inter-group difference was found for SL in the POST phase. ***b)*** EMG standard deviation (SD) for SL and SR in the PRE and POST phases. CTR (blue) is shown on the left and PD (orange) on the right within each phase. Black horizontal lines indicate the median. A significant inter-group difference was found for SL in the POST phase, with higher variability in CTR than in PD. 75

7.4 **EMG coefficient of variation, integrated EMG, and variance.** CTR (blue, left) and PD (orange, right) are compared in PRE and POST, with black horizontal lines indicating medians. ***a)*** CV for GLL and GLR, showing higher POST medians and dispersion in CTR. ***b)*** IEMG for GLL and GLR, showing higher medians and a broader upper distribution in PD. ***c)*** VAR for GLL and GLR, with higher POST median and dispersion for GLL in CTR. 76

7.5 **EMG Standard Deviation (SD) for the Tibialis Anterior Left (TAL) and Right (TAR).** The control group (CTR, blue) is positioned to the left and the Parkinson's disease group (PD, orange) to the right within each phase, namely PRE and POST. Black horizontal lines represent the median values. In the POST phase, the CTR group exhibited significantly higher median SD and broader dispersion in both muscles compared to the more constrained PD profile. 77

11.1 **Time-resolved occupancy of BNSs in CTR and PD in the Delta band.** Stacked area plots show the proportion of subjects assigned to each BNS at each time point. Vertical dashed lines indicate phase boundaries. 111

11.2 **Time-resolved occupancy of BNSs in CTR and PD in the Theta band.** Stacked area plots show the proportion of subjects assigned to each BNS at each time point. Vertical dashed lines indicate phase boundaries. 112

11.3 **Time-resolved occupancy of BNSs in CTR and PD in the Beta band.** Stacked area plots show the proportion of subjects assigned to each BNS at each time point. Vertical dashed lines indicate phase boundaries, and labels denote Baseline (BL), Preparation (PRE), Movement (MOV), and Post-movement (POST) phases. . . 112

11.4 **Mean phase-wise BNS presence in CTR and PD across frequency bands.** Stacked bar plots show the mean percentage presence of each BNS within BL, PRE, MOV, and POST phases for CTR and PD. Presence was computed as the proportion of samples assigned to each BNS within each phase and averaged across subjects. Panels report results for Beta, Delta, and Theta bands. 114

11.5 **BNS4 in the delta band.** Spatial representation of BNS1 connectivity pattern in the delta frequency band. Lateral and medial views of both hemispheres are shown: the top row displays the lateral views of the left (L) and right (R) hemispheres, while the bottom row displays the corresponding medial views. Nodes represent cortical regions and are colored according to their assigned resting-state network, while edges represent functional connections between regions. For visualization purposes, only connections with an edge weight greater than 0.04 are shown. This representation highlights the large-scale network organization and dominant inter-regional interactions characterizing BNS1 in the delta band. 118

11.6 **BNS4 in the theta band.** Spatial representation of BNS1 connectivity pattern in the theta frequency band. Lateral and medial views of both hemispheres are shown: the top row displays the lateral views of the left (L) and right (R) hemispheres, while the bottom row displays the corresponding medial views. Nodes represent cortical regions and are colored according to their assigned resting-state network, while edges represent functional connections between regions. For visualization purposes, only connections with an edge weight greater than 0.04 are shown. This representation highlights the large-scale network organization and dominant inter-regional interactions characterizing BNS1 in the theta band. 122

11.7 **BNS1 in the beta band.** Spatial representation of BNS1 connectivity pattern in the beta frequency band. Lateral and medial views of both hemispheres are shown: the top row displays the lateral views of the left (L) and right (R) hemispheres, while the bottom row displays the corresponding medial views. Nodes represent cortical regions and are colored according to their assigned resting-state network, while edges represent functional connections between regions. For visualization purposes, only connections with an edge weight greater than 0.04 are shown. This representation highlights the large-scale network organization and dominant inter-regional interactions characterizing BNS1 in the beta band. 123

11.8 **BNS2 in the beta band.** Spatial representation of BNS1 connectivity pattern in the beta frequency band. Lateral and medial views of both hemispheres are shown: the top row displays the lateral views of the left (L) and right (R) hemispheres, while the bottom row displays the corresponding medial views. Nodes represent cortical regions and are colored according to their assigned resting-state network, while edges represent functional connections between regions. For visualization purposes, only connections with an edge weight greater than 0.04 are shown. This representation highlights the large-scale network organization and dominant inter-regional interactions characterizing BNS1 in the beta band. 124

List of Tables

2.1 **Clinical and instrumental assessments across Parkinson's disease progression.** The table summarizes the clinical manifestations and the main assessments used throughout the progression of Parkinson's disease. Hoehn–Yahr stages are approximate indicators of motor disability and do not represent rigid boundaries between disease phases. 17

3.1 **EEG frequency bands and cortical regions.** Summary of the functional relevance of the EEG frequency bands and cortical regions considered in the analyses. 33
3.2 **EMG features extracted from the preprocessed signals.** The table summarizes the time-domain and frequency-domain parameters used to characterize lower-limb muscle activity across the experimental phases. 35
3.3 **CoP features extracted from the preprocessed signals.** The table summarizes the time-domain, entropy-based, geometric, fractal, and spectral parameters used to characterize postural sway across the experimental phases. 37

5.1 **Age and gender distribution in PD and CTR groups.** No significant differences were found (t-test for age, chi-squared test for gender) 49
5.2 **Dynamic Connectivity Variables.** A list of the number of matrices (N) calculated for each frequency band. The dimension (n) of each matrix is based on the number of ROIs, with each element ($A_{i,j}$) representing the connectivity between the respective regions 52

5.3 **Pearson correlation of the six Brain Network States across different clustering runs.** The optimal number of clusters ($K = 6$) was determined using the meta-criterion based on multiple internal Cluster Validity Indices (CVIs). Modified k-means clustering was then repeated four times with different parameter configurations. Cluster #1, defined by the parameters $K_{\text{range}} = 2{:}10$, rep = 100, ite = 1000, was used as the reference for comparison. We therefore computed the Pearson correlation between the corresponding cluster maps obtained in different runs to evaluate the similarity and stability of the clustering results 53
5.4 **Summary of main statistical outcomes for each Brain Network States metric and experimental phase.** Linear Mixed Model (LMM) analysis with False Discovery Rate (FDR) correction ($\alpha < 0.05$). Significant results are highlighted in bold, while non-significant trends are also indicated for clarity 57

6.1 **Delta mean strength values for each BNS across networks.** The highest value per BNS is highlighted in bold. 66
6.2 **Theta mean strength values for each BNS across networks.** The highest value for each BNS is highlighted in bold. 67
6.3 **Beta mean strength values for each BNS across networks.** The highest value for each BNS is highlighted in bold. 68

7.1 Statistical significance across phases (Bonferroni-corrected, $p < 0.05$) for S muscle. 78
7.2 Statistical significance across phases (Bonferroni-corrected, $p < 0.05$) for GL muscle. 79
7.3 Statistical significance across phases (Bonferroni-corrected, $p < 0.05$) for TA muscle. 80

11.1 Regions of Interest (ROIs) and their Functional Network Associations. 107
11.2 Description of parameters used in the analysis of brain network states (BNSs), including their formulas and interpretations. 109
11.3 Coverage p-values and adjusted p-values after FDR correction for different BNSs across phases (BL, PRE, MOV, POST) in the CTR - PD contrast. 110
11.4 Occurrence p-values and adjusted p-values after FDR correction for different BNSs across phases (BL, PRE, MOV, POST) in the CTR - PD contrast. 110
11.5 Duration p-values and adjusted p-values after FDR correction for different BNSs across phases (BL, PRE, MOV, POST) in the CTR - PD contrast. 110

11.6 Mean phase-wise BNS presence for CTR and PD across frequency bands. Values are expressed as percentages and were derived from the temporally smoothed state-label matrix (subjects × time samples), where each time sample was assigned to a BNS. For each phase (BL, PRE, MOV, POST), BNS presence was computed at the subject level as the proportion of samples assigned to each state within the corresponding phase window, and then averaged across participants within each group (×100). 113
11.7 Beta: Coverage 125
11.8 Beta: Duration 125
11.9 Beta: Occurrence 126
11.10Delta: Coverage 126
11.11Delta: Duration 126
11.12Delta: Occurrence 126
11.13Theta: Coverage 126
11.14Theta: Duration 126
11.15Theta: Occurrence 126

Bibliography

[1] F. B. Horak, "Postural orientation and equilibrium: What do we need to know about neural control of balance to prevent falls?" *Age and ageing*, vol. 35(no. suppl_2, pp. ii7–ii11, 2006.

[2] Y. Ivanenko and V. S. Gurfinkel, "Human postural control," *Frontiers in neuroscience*, vol. 12, p. 171, 2018.

[3] R. J. Peterka, "Sensory integration for human balance control," *Handbook of clinical neurology*, vol. 159, pp. 27–42, 2018.

[4] K. Takakusaki, "Functional neuroanatomy for posture and gait control," *Journal of movement disorders*, vol. 10(no. 1, p. 1, 2017.

[5] D. E. Angelaki and K. E. Cullen, "Vestibular system: The many facets of a multimodal sense," *Annu. Rev. Neurosci.*, vol. 31(no. 1, pp. 125–150, 2008.

[6] U. Proske and S. C. Gandevia, "The proprioceptive senses: Their roles in signaling body shape, body position and movement, and muscle force," *Physiological reviews*, vol. 92(no. 4, pp. 1651–1697, 2012.

[7] J. Jacobs and F. Horak, "Cortical control of postural responses," *Journal of neural transmission*, vol. 114(no. 10, pp. 1339–1348, 2007.

[8] J. Massion, "Movement, posture and equilibrium: Interaction and coordination," *Progress in neurobiology*, vol. 38(no. 1, pp. 35–56, 1992.

[9] C. J. Dakin and D. A. Bolton, "Forecast or fall: Prediction's importance to postural control," *Frontiers in neurology*, vol. 9, p. 924, 2018.

[10] F. B. Horak and L. M. Nashner, "Central programming of postural movements: Adaptation to altered support-surface configurations," *Journal of neurophysiology*, vol. 55(no. 6, pp. 1369–1381, 1986.

[11] R. J. Peterka, "Sensorimotor integration in human postural control," *Journal of neurophysiology*, 2002.

[12] L. Assländer and R. J. Peterka, "Sensory reweighting dynamics in human postural control," *Journal of neurophysiology*, vol. 111(no. 9, pp. 1852–1864, 2014.

[13] R. B. Parreira, L. A. C. Grecco, and C. S. Oliveira, "Postural control in blind individuals: A systematic review," *Gait & Posture*, vol. 57, pp. 161–167, 2017.

[14] J. F. Golding, "Motion sickness," *Handbook of clinical neurology*, vol. 137, pp. 371–390, 2016.

[15] J. R. Lackner, "Motion sickness: More than nausea and vomiting," *Experimental brain research*, vol. 232(no. 8, pp. 2493–2510, 2014.

[16] G. E. Riccio and T. A. Stoffregen, "An ecological theory of motion sickness and postural instability," *Ecological psychology*, vol. 3(no. 3, pp. 195–240, 1991.

[17] S. J. Villard, M. B. Flanagan, G. M. Albanese, and T. A. Stoffregen, "Postural instability and motion sickness in a virtual moving room," *Human factors*, vol. 50(no. 2, pp. 332–345, 2008.

[18] M. Bakker et al., "Postural responses to multidirectional stance perturbations in cerebellar ataxia," *Experimental neurology*, vol. 202(no. 1, pp. 21–35, 2006.

[19] A. Marquer, G. Barbieri, and D. Pérennou, "The assessment and treatment of postural disorders in cerebellar ataxia: A systematic review," *Annals of physical and rehabilitation medicine*, vol. 57(no. 2, pp. 67–78, 2014.

[20] G. Allali, M. Van Der Meulen, and F. Assal, "Gait and cognition: The impact of executive function.," *Swiss Archives of Neurology and Psychiatry*, vol. 161(no. 6, 2010.

[21] J. Verghese, C. Wang, R. B. Lipton, and R. Holtzer, "Motoric cognitive risk syndrome and the risk of dementia," *Journals of Gerontology Series A: Biomedical Sciences and Medical Sciences*, vol. 68(no. 4, pp. 412–418, 2013.

[22] F. Porciuncula, P. Wasserman, K. S. Marder, and A. K. Rao, "Quantifying postural control in premanifest and manifest huntington disease using wearable sensors," *Neurorehabilitation and neural repair*, vol. 34(no. 9, pp. 771–783, 2020.

[23] L. S. Talman and A. L. Hiller, "Approach to posture and gait in huntington's disease," *Frontiers in bioengineering and biotechnology*, vol. 9, p. 668 699, 2021.

[24] J. Konczak et al., "Proprioception and motor control in parkinson's disease," *Journal of motor behavior*, vol. 41(no. 6, pp. 543–552, 2009.

[25] B. Palakurthi and S. P. Burugupally, "Postural instability in parkinson's disease: A review," *Brain sciences*, vol. 9(no. 9, p. 239, 2019.

[26] K. Takakusaki, M. Takahashi, T. Noguchi, and R. Chiba, "Neurophysiological mechanisms of gait disturbance in advanced parkinson's disease patients," *Neurology and Clinical Neuroscience*, vol. 11(no. 4, pp. 201–217, 2023.

[27] K. J. Feller, R. J. Peterka, and F. B. Horak, "Sensory re-weighting for postural control in parkinson's disease," *Frontiers in human neuroscience*, vol. 13, p. 126, 2019.

[28] M. Duarte and S. M. Freitas, "Revision of posturography based on force plate for balance evaluation," *Brazilian Journal of physical therapy*, vol. 14, pp. 183–192, 2010.

[29] J. W. Błaszczyk, "The use of force-plate posturography in the assessment of postural instability," *Gait & posture*, vol. 44, pp. 1–6, 2016.

[30] F. Quijoux et al., "A review of center of pressure (cop) variables to quantify standing balance in elderly people: Algorithms and open-access code," *Physiological reports*, vol. 9(no. 22, e15067, 2021.

[31] F. Scoppa, R. Capra, M. Gallamini, and R. Shiffer, "Clinical stabilometry standardization: Basic definitions–acquisition interval–sampling frequency," *Gait & posture*, vol. 37(no. 2, pp. 290–292, 2013.

[32] T. E. Prieto, J. B. Myklebust, R. G. Hoffmann, E. G. Lovett, and B. M. Myklebust, "Measures of postural steadiness: Differences between healthy young and elderly adults," *IEEE Transactions on biomedical engineering*, vol. 43(no. 9, pp. 956–966, 1996.

[33] P. Schubert and M. Kirchner, "Ellipse area calculations and their applicability in posturography," *Gait & Posture*, vol. 39(no. 1, pp. 518–522, 2014.

[34] E. Tolosa, G. Wenning, and W. Poewe, "The diagnosis of parkinson's disease," *The Lancet Neurology*, vol. 5(no. 1, pp. 75–86, 2006.

[35] "Parkinson disease. "[Online]. Available: `https://www.who.int/news-room/fact-sheets/detail/parkinson-disease`.

[36] R. Geevarghese, D. E. Lumsden, N. Hulse, M. Samuel, and K. Ashkan, "Subcortical structure volumes and correlation to clinical variables in parkinson's disease," *Journal of Neuroimaging*, vol. 25(no. 2, pp. 275–280, 2015.

[37] F. R. Buttarelli et al., "Central and peripheral dopamine transporter reduction in parkinson's disease," *Neurological Research*, vol. 31(no. 7, pp. 687–691, 2009.

[38] R. G. Perez and T. G. Hastings, "Could a loss of α-synuclein function put dopaminergic neurons at risk?" *Journal of neurochemistry*, vol. 89(no. 6, pp. 1318–1324, 2004.

[39] M. J. Benskey, R. G. Perez, and F. P. Manfredsson, "The contribution of alpha synuclein to neuronal survival and function–implications for parkinson's disease," *Journal of neurochemistry*, vol. 137(no. 3, pp. 331–359, 2016.

[40] J. P. Anderson et al., "Phosphorylation of ser-129 is the dominant pathological modification of α-synuclein in familial and sporadic lewy body disease," *Journal of Biological Chemistry*, vol. 281(no. 40, pp. 29 739–29 752, 2006.

[41] M. H. Polymeropoulos et al., "Mutation in the α-synuclein gene identified in families with parkinson's disease," *science*, vol. 276(no. 5321, pp. 2045–2047, 1997.

[42] T. Kitada et al., "Mutations in the parkin gene cause autosomal recessive juvenile parkinsonism," *nature*, vol. 392(no. 6676, pp. 605–608, 1998.

[43] E. M. Valente et al., "Localization of a novel locus for autosomal recessive early-onset parkinsonism, park6, on human chromosome 1p35-p36," *The American Journal of Human Genetics*, vol. 68(no. 4, pp. 895–900, 2001.

[44] V. Bonifati et al., "Dj-1 (park7), a novel gene for autosomal recessive, early onset parkinsonism," *Neurological sciences*, vol. 24(no. 3, pp. 159–160, 2003.

[45] N. Ball, W.-P. Teo, S. Chandra, and J. Chapman, "Parkinson's disease and the environment," *Frontiers in neurology*, p. 218, 2019.

[46] E. R. Dorsey et al., "Global, regional, and national burden of parkinson's disease, 1990–2016: A systematic analysis for the global burden of disease study 2016," *The Lancet Neurology*, vol. 17(no. 11, pp. 939–953, 2018.

[47] M. Baldereschi et al., "Parkinson's disease and parkinsonism in a longitudinal study: Two-fold higher incidence in men," *Neurology*, vol. 55(no. 9, pp. 1358–1363, 2000.

[48] P. Solla et al., "Gender differences in motor and non-motor symptoms among sardinian patients with parkinson's disease," *Journal of the neurological sciences*, vol. 323(no. 1-2, pp. 33–39, 2012.

[49] S. A. Schneider and J. A. Obeso, "Clinical and pathological features of parkinson's disease," *Behavioral Neurobiology of Huntington's disease and Parkinson's disease*, pp. 205–220, 2015.

[50] N. Dahodwala et al., "Sex disparities in access to caregiving in parkinson disease," *Neurology*, vol. 90(no. 1, e48–e54, 2018.

[51] S. Cerri, L. Mus, and F. Blandini, "Parkinson's disease in women and men: What's the difference?" *Journal of Parkinson's disease*, vol. 9(no. 3, pp. 501–515, 2019.

[52] G. Alves et al., "Incidence of parkinson's disease in norway: The norwegian parkwest study," *Journal of Neurology, Neurosurgery & Psychiatry*, vol. 80(no. 8, pp. 851–857, 2009.

[53] A. Ascherio and M. A. Schwarzschild, "The epidemiology of parkinson's disease: Risk factors and prevention," *The Lancet Neurology*, vol. 15(no. 12, pp. 1257–1272, 2016.

[54] X. Ren and J.-F. Chen, "Caffeine and parkinson's disease: Multiple benefits and emerging mechanisms," *Frontiers in Neuroscience*, vol. 14, p. 602 697, 2020.

[55] K. C. Simon, X. Gao, H. Chen, M. A. Schwarzschild, and A. Ascherio, "Calcium channel blocker use and risk of parkinson's disease," *Movement disorders*, vol. 25(no. 12, pp. 1818–1822, 2010.

[56] G. DeMaagd and A. Philip, "Parkinson's disease and its management: Part 1: Disease entity, risk factors, pathophysiology, clinical presentation, and diagnosis," *Pharmacy and therapeutics*, vol. 40(no. 8, p. 504, 2015.

[57] K. A. Jellinger, "Neuropathobiology of non-motor symptoms in parkinson disease," *Journal of Neural Transmission*, vol. 122, pp. 1429–1440, 2015.

[58] R. Djaldetti, I. Ziv, and E. Melamed, "The mystery of motor asymmetry in parkinson's disease," *The Lancet Neurology*, vol. 5(no. 9, pp. 796–802, 2006.

[59] A. Berardelli, J. C. Rothwell, P. D. Thompson, and M. Hallett, "Pathophysiology of bradykinesia in parkinson's disease," *Brain*, vol. 124(no. 11, pp. 2131–2146, 2001.

[60] M. Bologna et al., "Neurophysiological correlates of bradykinesia in parkinson's disease," *Brain*, vol. 141(no. 8, pp. 2432–2444, 2018.

[61] M. Onofrj and A. Thomas, "Acute akinesia in parkinson disease," *Neurology*, vol. 64(no. 7, pp. 1162–1169, 2005.

[62] R. G. Lee, "Pathophysiology of rigidity and akinesia in parkinson's disease," *European neurology*, vol. 29(no. Suppl. 1, pp. 13–18, 1989.

[63] S. Sveinbjornsdottir, "The clinical symptoms of parkinson's disease," *Journal of neurochemistry*, vol. 139, pp. 318–324, 2016.

[64] P. J. G. Ruiz, M. Catalan, and J. F. Carril, "Initial motor symptoms of parkinson disease," *The neurologist*, vol. 17, S18–S20, 2011.

[65] R. Xia and Z.-H. Mao, "Progression of motor symptoms in parkinson's disease," *Neuroscience bulletin*, vol. 28, pp. 39–48, 2012.

[66] R. B. Dewey Jr et al., "Motor symptoms at onset of parkinson disease and risk for cognitive impairment and depression," *Cognitive and behavioral neurology: official journal of the Society for Behavioral and Cognitive Neurology*, vol. 25(no. 3, p. 115, 2012.

[67] N. Chastan et al., "Gait and balance disorders in parkinson's disease: Impaired active braking of the fall of centre of gravity," *Movement disorders: official journal of the Movement Disorder Society*, vol. 24(no. 2, pp. 188–195, 2009.

[68] A. Santamato et al., "Postural and balance disorders in patients with parkinson's disease: A prospective open-label feasibility study with two months of action observation treatment," *Parkinson's Disease*, vol. 2015, 2015.

[69] T. A. Boonstra, H. Van Der Kooij, M. Munneke, and B. R. Bloem, "Gait disorders and balance disturbances in parkinson's disease: Clinical update and pathophysiology," *Current opinion in neurology*, vol. 21(no. 4, pp. 461–471, 2008.

[70] P.-H. Chen, R.-L. Wang, D.-J. Liou, and J.-S. Shaw, "Gait disorders in parkinson's disease: Assessment and management," *International Journal of Gerontology*, vol. 7(no. 4, pp. 189–193, 2013.

[71] P. Lamberti et al., "Freezing gait in parkinson's disease," *European neurology*, vol. 38(no. 4, pp. 297–301, 1997.

[72] Y. Okuma, "Freezing of gait and falls in parkinson's disease," *Journal of Parkinson's disease*, vol. 4(no. 2, pp. 255–260, 2014.

[73] M. Mouradian, J. Junecos, G. Fabbrini, J. Schlegel, J. Bartko, and T. Chase, "Motor fluctuations in parkinson's disease: Central pathophysiological mechanisms, part ii," *Annals of Neurology: Official Journal of the American Neurological Association and the Child Neurology Society*, vol. 24(no. 3, pp. 372–378, 1988.

[74] R. Cano-de-la-Cuerda, M. Pérez-de-Heredia, J. C. Miangolarra-Page, E. Muñoz-Hellín, and C. Fernández-de-Las-Peñas, "Is there muscular weakness in parkinson's disease?" *American Journal of Physical Medicine & Rehabilitation*, vol. 89(no. 1, pp. 70–76, 2010.

[75] J. A. Obeso, M. C. Rodriguez-Oroz, M. Rodriguez, M. R. DeLong, and C. W. Olanow, "Pathophysiology of levodopa-induced dyskinesias in parkinson's disease: Problems with the current model.," *Annals of neurology*, vol. 47(no. 4 Suppl 1, S22–32, 2000.

[76] W. Poewe, "Non-motor symptoms in parkinson's disease," *European journal of neurology*, vol. 15, pp. 14–20, 2008.

[77] R. F. Pfeiffer, "Non-motor symptoms in parkinson's disease," *Parkinsonism & related disorders*, vol. 22, S119–S122, 2016.

[78] P. J. Garcia-Ruiz, K. R. Chaudhuri, and P. Martinez-Martin, "Non-motor symptoms of parkinson's disease a review… from the past," *Journal of the neurological sciences*, vol. 338(no. 1-2, pp. 30–33, 2014.

[79] P. Martinez-Martin, C. Rodriguez-Blazquez, M. M. Kurtis, K. R. Chaudhuri, and N. V. Group, "The impact of non-motor symptoms on health-related quality of life of patients with parkinson's disease," *Movement Disorders*, vol. 26(no. 3, pp. 399–406, 2011.

[80] I. Suttrup and T. Warnecke, "Dysphagia in parkinson's disease," *Dysphagia*, vol. 31(no. 1, pp. 24–32, 2016.

[81] D. Tulbă, L. Cozma, P. Bălănescu, A. Buzea, C. Băicuș, and B. O. Popescu, "Blood pressure patterns in patients with parkinson's disease: A systematic review," *Journal of Personalized Medicine*, vol. 11(no. 2, p. 129, 2021.

[82] D. C. Velseboer, R. J. de Haan, W. Wieling, D. S. Goldstein, and R. M. de Bie, "Prevalence of orthostatic hypotension in parkinson's disease: A systematic review and meta-analysis," *Parkinsonism & related disorders*, vol. 17(no. 10, pp. 724–729, 2011.

[83] M. Gjerstad, T. Wentzel-Larsen, D. Aarsland, and J. Larsen, "Insomnia in parkinson's disease: Frequency and progression over time," *Journal of Neurology, Neurosurgery & Psychiatry*, vol. 78(no. 5, pp. 476–479, 2007.

[84] B. Knie, M. T. Mitra, K. Logishetty, and K. R. Chaudhuri, "Excessive daytime sleepiness in patients with parkinson's disease," *CNS drugs*, vol. 25, pp. 203–212, 2011.

[85] J. L. Cummings, "Depression and parkinson's disease: A review.," *The American journal of psychiatry*, 1992.

[86] S. E. Starkstein and M. Merello, *Psychiatric and cognitive disorders in Parkinson's disease*. Cambridge University Press, 2002.

[87] B. Dubois and B. Pillon, "Cognitive deficits in parkinson's disease," *Journal of neurology*, vol. 244, pp. 2–8, 1996.

[88] I. G. McKeith and D. Burn, "Spectrum of parkinson's disease, parkinson's dementia, and lewy body dementia," *Neurologic clinics*, vol. 18(no. 4, pp. 865–883, 2000.

[89] K. K. Gnanalingham, E. J. Byrne, A. Thornton, M. A. Sambrook, and P. Bannister, "Motor and cognitive function in lewy body dementia: Comparison with alzheimer's and parkinson's diseases.," *Journal of Neurology, Neurosurgery & Psychiatry*, vol. 62(no. 3, pp. 243–252, 1997.

[90] M. Goedert and A. Compston, "Parkinson's disease—the story of an eponym," *Nature Reviews Neurology*, vol. 14(no. 1, pp. 57–62, 2018.

[91] C. Goetz, "Charcot: Past and present," *Revue Neurologique*, vol. 173(no. 10, pp. 628–636, 2017.

[92] K. A. Jellinger et al., "Accuracy of clinical diagnosis of parkinson disease: A systematic review and meta-analysisauthor response," *Neurology*, vol. 87(no. 2, pp. 237–238, 2016.

[93] A. J. Hughes, S. E. Daniel, L. Kilford, and A. J. Lees, "Accuracy of clinical diagnosis of idiopathic parkinson's disease: A clinico-pathological study of 100 cases.," *Journal of neurology, neurosurgery & psychiatry*, vol. 55(no. 3, pp. 181–184, 1992.

[94] D. J. Gelb, E. Oliver, and S. Gilman, "Diagnostic criteria for parkinson disease," *Archives of neurology*, vol. 56(no. 1, pp. 33–39, 1999.

[95] R. B. Postuma et al., "Mds clinical diagnostic criteria for parkinson's disease," *Movement disorders*, vol. 30(no. 12, pp. 1591–1601, 2015.

[96] H. Watanabe, K. Hara, M. Ito, M. Katsuno, and G. Sobue, "New diagnostic criteria for parkinson's disease: Mds-pd criteria," *Brain and nerve= Shinkei kenkyu no shinpo*, vol. 70(no. 2, pp. 139–146, 2018.

[97] C. G. Goetz et al., "Movement disorder society task force report on the hoehn and yahr staging scale: Status and recommendations the movement disorder society task force on rating scales for parkinson's disease," *Movement disorders*, vol. 19(no. 9, pp. 1020–1028, 2004.

[98] C. G. Goetz et al., "Movement disorder society-sponsored revision of the unified parkinson's disease rating scale (mds-updrs): Process, format, and clinimetric testing plan," *Movement disorders*, vol. 22(no. 1, pp. 41–47, 2007.

[99] C. Martignon et al., "Guidelines on exercise testing and prescription for patients at different stages of parkinson's disease," *Aging clinical and experimental research*, vol. 33(no. 2, pp. 221–246, 2021.

[100] N. Fox and J. H. Growdon, "Biomarkers and surrogates," *NeuroRx*, vol. 1(no. 2, p. 181, 2004.

[101] L. M. Chahine, M. B. Stern, and A. Chen-Plotkin, "Blood-based biomarkers for parkinson's disease," *Parkinsonism & related disorders*, vol. 20, S99–S103, 2014.

[102] B. D. W. Group et al., "Biomarkers and surrogate endpoints: Preferred definitions and conceptual framework," *Clinical pharmacology & therapeutics*, vol. 69(no. 3, pp. 89–95, 2001.

[103] B. Mollenhauer et al., "Total csf α-synuclein is lower in de novo parkinson patients than in healthy subjects," *Neuroscience letters*, vol. 532, pp. 44–48, 2013.

[104] P. G. Foulds et al., "A longitudinal study on α-synuclein in blood plasma as a biomarker for parkinson's disease," *Scientific reports*, vol. 3(no. 1, pp. 1–6, 2013.

[105] A. Lees and E. Smith, "Cognitive deficits in the early stages of parkinson's disease," *Brain*, vol. 106(no. 2, pp. 257–270, 1983.

[106] F.-M. Lu and Z. Yuan, "Pet/spect molecular imaging in clinical neuroscience: Recent advances in the investigation of cns diseases," *Quantitative imaging in medicine and surgery*, vol. 5(no. 3, p. 433, 2015.

[107] "Datscan tool used to confirm the diagnosis of parkinson's disease. "[Online]. Available: `https://parkinsonsnewstoday.com/parkinsons-disease-tests-diagnosis/datscan/`.

[108] S. Waninger et al., "Neurophysiological biomarkers of parkinson's disease," *Journal of Parkinson's disease*, vol. 10(no. 2, pp. 471–480, 2020.

[109] S. Heinzel et al., "Update of the mds research criteria for prodromal parkinson's disease," *Movement Disorders*, vol. 34(no. 10, pp. 1464–1470, 2019.

[110] T. Simuni et al., "A biological definition of neuronal α-synuclein disease: Towards an integrated staging system for research," *The Lancet Neurology*, vol. 23(no. 2, pp. 178–190, 2024.

[111] B. Orso, S. Brosse, J. Frasnelli, and D. Arnaldi, "Opportunities and pitfalls of rem sleep behavior disorder and olfactory dysfunction as early markers in parkinson's disease," *Journal of Parkinson's Disease*, vol. 14(no. s2, S275–S285, 2024.

[112] H. Li, M. Zecca, and J. Huang, "Evaluating the utility of wearable sensors for the early diagnosis of parkinson disease: Systematic review," *Journal of Medical Internet Research*, vol. 27, e69422, 2025.

[113] C. G. Goetz et al., "Movement disorder society-sponsored revision of the unified parkinson's disease rating scale (mds-updrs): Scale presentation and clinimetric testing results," *Movement disorders: official journal of the Movement Disorder Society*, vol. 23(no. 15, pp. 2129–2170, 2008.

[114] F. Hopfner, G. Höglinger, and C. Trenkwalder, "Definition and diagnosis of parkinson's disease: Guideline "parkinson's disease" of the german society of neurology," *Journal of neurology*, vol. 271(no. 11, pp. 7102–7119, 2024.

[115] A. Merlo et al., "Instrumental balance assessment in parkinson's disease and parkinsonism. a systematic review with critical appraisal of clinical applications and quality of reporting," *Frontiers in neurology*, vol. 16, p. 1 528 191, 2025.

[116] G. Cosentino et al., "A multinational consensus on dysphagia in parkinson's disease: Screening, diagnosis and prognostic value," *Journal of Neurology*, vol. 269(no. 3, pp. 1335–1352, 2022.

[117] D. Santos-García, T. de Deus Fonticoba, E. Suárez Castro, A. Aneiros Diaz, and D. McAfee, "5-2-1 criteria: A simple screening tool for identifying advanced pd patients who need an optimization of parkinson's treatment," *Parkinson's Disease*, vol. 2020(no. 1, p. 7 537 924, 2020.

[118] O. Rascol, P. Payoux, F. Ory, J. J. Ferreira, C. Brefel-Courbon, and J.-L. Montastruc, "Limitations of current parkinson's disease therapy," *Annals of Neurology: Official Journal of the American Neurological Association and the Child Neurology Society*, vol. 53(no. S3, S3–S15, 2003.

[119] C. Marsden and J. Parkes, "Success and problems of long-term levodopa therapy in parkinson's disease," *The Lancet*, vol. 309(no. 8007, pp. 345–349, 1977.

[120] A. Contreras and F. Grandas, "Risk of falls in parkinson's disease: A cross-sectional study of 160 patients," *Parkinson's Disease*, vol. 2012, 2012.

[121] F. Tjernström, O. Zur, and K. Jahn, "Current concepts and future approaches to vestibular rehabilitation," *Journal of neurology*, vol. 263, pp. 65–70, 2016.

[122] F. Barollo et al., "Postural control adaptation and habituation during vibratory proprioceptive stimulation: An hd-eeg investigation of cortical recruitment and kinematics," *IEEE Transactions on Neural Systems and Rehabilitation Engineering*, vol. 28(no. 6, pp. 1381–1388, 2020.

[123] F. Barollo et al., "Cortical pathways during postural control: New insights from functional EEG source connectivity," *IEEE Transactions on Neural Systems and Rehabilitation Engineering*, vol. 30, pp. 72–84, 2022.

[124] J. Reason, "Motion sickness: Some theoretical and practical considerations," *Applied ergonomics*, vol. 9(no. 3, pp. 163–167, 1978.

[125] B. Cohen, M. Dai, S. B. Yakushin, and C. Cho, "The neural basis of motion sickness," *Journal of neurophysiology*, vol. 121(no. 3, pp. 973–982, 2019.

[126] A. Koohestani et al., "A knowledge discovery in motion sickness: A comprehensive literature review," *IEEE access*, vol. 7, pp. 85 755–85 770, 2019.

[127] D. Jacob et al., "Towards defining biomarkers to evaluate concussions using virtual reality and a moving platform (biovrsea)," *Scientific Reports*, vol. 12(no. 1, p. 8996, 2022.

[128] R. Aubonnet, A. Shoykhet, D. Jacob, G. Di Lorenzo, H. Petersen, and P. Gargiulo, "Postural control paradigm (biovrsea): Towards a neurophysiological signature," *Physiological Measurement*, vol. 43(no. 11, p. 115 002, 2022.

[129] M. Recenti et al., "Toward predicting motion sickness using virtual reality and a moving platform assessing brain, muscles, and heart signals," *Frontiers in Bioengineering and Biotechnology*, vol. 9, p. 635 661, 2021.

[130] J. F. Golding, "Predicting individual differences in motion sickness susceptibility by questionnaire," *Personality and Individual differences*, vol. 41(no. 2, pp. 237–248, 2006.

[131] ANT Neuro, *ANT Neuro Academy FAQ*, `https://academy.ant-neuro.com/faq`, Accessed: 2026-05-11, 2023.

[132] C. A. E. Kothe and T.-P. Jung, "Artifact removal techniques with signal reconstruction," *6th International BCI Meeting*, 2016, US Patent App. 14/895,440.

[133] P. Ablin, J.-F. Cardoso, and A. Gramfort, "Faster ica under orthogonal constraint," in *2018 IEEE International Conference on Acoustics, Speech and Signal Processing (ICASSP)*, IEEE, 2018, pp. 4464–4468.

[134] "Parkinson disease. "[Online]. Available: `https://www.who.int/news-room/fact-sheets/detail/parkinson-disease`.

[135] A. M. Maitín, A. J. García-Tejedor, and J. P. R. Muñoz, "Machine learning approaches for detecting parkinson's disease from eeg analysis: A systematic review," *Applied Sciences*, vol. 10(no. 23, p. 8662, 2020.

[136] M. Maffoni, A. Giardini, A. Pierobon, D. Ferrazzoli, and G. Frazzitta, "Stigma experienced by parkinson's disease patients: A descriptive review of qualitative studies," *Parkinson's Disease*, vol. 2017, 2017.

[137] R. B. Postuma et al., "Mds clinical diagnostic criteria for parkinson's disease," *Movement Disorders*, vol. 30(no. 12, pp. 1591–1601, 2015. DOI: `https://doi.org/10.1002/mds.26424`. eprint: `https://movementdisorders.onlinelibrary.wiley.com/doi/pdf/10.1002/mds.26424`. [Online]. Available: `https://movementdisorders.onlinelibrary.wiley.com/doi/abs/10.1002/mds.26424`.

[138] C. Agliardi et al., "Oligomeric α-syn and snare complex proteins in peripheral extracellular vesicles of neural origin are biomarkers for parkinson's disease," *Neurobiology of Disease*, vol. 148, p. 105 185, 2021.

[139] M. Politis, "Neuroimaging in parkinson disease: From research setting to clinical practice," *Nature Reviews Neurology*, vol. 10(no. 12, pp. 708–722, 2014.

[140] D. Berg, J. Godau, and U. Walter, "Transcranial sonography in movement disorders," *The Lancet Neurology*, vol. 7(no. 11, pp. 1044–1055, 2008.

[141] M. J. Gandal, J. C. Edgar, K. Klook, and S. J. Siegel, "Gamma synchrony: Towards a translational biomarker for the treatment-resistant symptoms of schizophrenia," *Neuropharmacology*, vol. 62(no. 3, pp. 1504–1518, 2012.

[142] H. Hampel et al., "Biomarkers for alzheimer's disease: Academic, industry and regulatory perspectives," *Nature reviews Drug discovery*, vol. 9(no. 7, pp. 560–574, 2010.

[143] F. Kheiri, A. Bragin, J. Almajano, E. Winden, et al., "Non-linear classification of heart rate parameters as a biomarker for epileptogenesis," *Epilepsy research*, vol. 100(no. 1-2, pp. 59–66, 2012.

[144] C.-X. Han, J. Wang, G.-S. Yi, and Y.-Q. Che, "Investigation of eeg abnormalities in the early stage of parkinson's disease," *Cognitive neurodynamics*, vol. 7, pp. 351–359, 2013.

[145] K. Serizawa et al., "Comparison of quantitative eegs between parkinson disease and age-adjusted normal controls," *Journal of Clinical Neurophysiology*, vol. 25(no. 6, pp. 361–366, 2008.

[146] M. Moazami-Goudarzi, J. Sarnthein, L. Michels, R. Moukhtieva, and D. Jeanmonod, "Enhanced frontal low and high frequency power and synchronization in the resting eeg of parkinsonian patients," *Neuroimage*, vol. 41(no. 3, pp. 985–997, 2008.

[147] J. Bosboom et al., "Resting state oscillatory brain dynamics in parkinson's disease: An meg study," *Clinical Neurophysiology*, vol. 117(no. 11, pp. 2521–2531, 2006.

[148] C. Chu et al., "Deep learning reveals personalized spatial spectral abnormalities of high delta and low alpha bands in eeg of patients with early parkinson's disease," *Journal of Neural Engineering*, vol. 18(no. 6, p. 066 036, 2021.

[149] M. Neufeld, R. Inzelberg, and A. Korczyn, "Eeg in demented and non-demented parkinsonian patients," *Acta neurologica scandinavica*, vol. 78(no. 1, pp. 1–5, 1988.

[150] O. Sinanović, A. Kapidzić, L. Kovacević, J. Hudić, and D. Smajlović, "Eeg frequency and cognitive dysfunction in patients with parkinson's disease.," *Medicinski arhiv*, vol. 59(no. 5, pp. 286–287, 2005.

[151] G. Mochizuki, S. Boe, A. Marlin, and W. McIlRoy, "Perturbation-evoked cortical activity reflects both the context and consequence of postural instability," *Neuroscience*, vol. 170(no. 2, pp. 599–609, 2010.

[152] D. R. Curtis and P. Andersen, "Sir john carew eccles, ac 27 january 1903-2 may 1997," *Biographical Memoirs of Fellows of the Royal Society*, vol. 47, pp. 161–187, 2001.

[153] T. Hülsdünker, A. Mierau, C. Neeb, H. Kleinöder, and H. Strüder, "Cortical processes associated with continuous balance control as revealed by eeg spectral power," *Neuroscience letters*, vol. 592, pp. 1–5, 2015.

[154] A. R. Sipp, J. T. Gwin, S. Makeig, and D. P. Ferris, "Loss of balance during balance beam walking elicits a multifocal theta band electrocortical response," *Journal of neurophysiology*, vol. 110(no. 9, pp. 2050–2060, 2013.

[155] M. Torchiano, *Effsize: Efficient effect size computation*, 2020. [Online]. Available: `https://CRAN.R-project.org/package=effsize`.

[156] N. Cliff, "Dominance statistics: Ordinal analyses to answer ordinal questions," *Psychological Bulletin*, vol. 114, 1993.

[157] A. Shumway-Cook and M. H. Woollacott, *Motor control: translating research into clinical practice*. Lippincott Williams & Wilkins, 2007.

[158] M. Woollacott and A. Shumway-Cook, "Attention and the control of posture and gait: A review of an emerging area of research," *Gait & posture*, vol. 16(no. 1, pp. 1–14, 2002.

[159] A. Kilzheimer, T. Hentrich, S. Burkhardt, and J. M. Schulze-Hentrich, "The challenge and opportunity to diagnose parkinson's disease in midlife," *Frontiers in Neurology*, vol. 10, p. 1328, 2019.

[160] J. M. Hausdorff, "Gait dynamics in parkinson's disease: Common and distinct behavior among stride length, gait variability, and fractal-like scaling," *Chaos: An Interdisciplinary Journal of Nonlinear Science*, vol. 19(no. 2, 2009.

[161] S. Del Din, A. Godfrey, C. Mazzà, S. Lord, and L. Rochester, "Free-living monitoring of parkinson's disease: Lessons from the field," *Movement Disorders*, vol. 31(no. 9, pp. 1293–1313, 2016.

[162] M. Morris, R. Iansek, J. McGinley, T. Matyas, and F. Huxham, "Three-dimensional gait biomechanics in parkinson's disease: Evidence for a centrally mediated amplitude regulation disorder," *Movement disorders: official journal of the Movement Disorder Society*, vol. 20(no. 1, pp. 40–50, 2005.

[163] D. J. Brooks, "Imaging approaches to parkinson disease," *Journal of Nuclear Medicine*, vol. 51(no. 4, pp. 596–609, 2010.

[164] H. T. Benamer et al., "Accurate differentiation of parkinsonism and essential tremor using visual assessment of [123i]-fp-cit spect imaging: The [123i]-fp-cit study group," *Movement disorders: official journal of the Movement Disorder Society*, vol. 15(no. 3, pp. 503–510, 2000.

[165] S. T. Schwarz, M. Afzal, P. S. Morgan, N. Bajaj, P. A. Gowland, and D. P. Auer, "The 'swallow tail'appearance of the healthy nigrosome–a new accurate test of parkinson's disease: A case-control and retrospective cross-sectional mri study at 3t," *PloS one*, vol. 9(no. 4, e93814, 2014.

[166] C. Mulert, "Simultaneous eeg and fmri: Towards the characterization of structure and dynamics of brain networks," *Dialogues in clinical neuroscience*, vol. 15(no. 3, pp. 381–386, 2013.

[167] M. Hassan and F. Wendling, "Electroencephalography source connectivity: Aiming for high resolution of brain networks in time and space," *IEEE Signal Processing Magazine*, vol. 35(no. 3, pp. 81–96, 2018. DOI: 10.1109/MSP.2017.2777518.

[168] V. Sakkalis, "Review of advanced techniques for the estimation of brain connectivity measured with EEG/MEG," *Computers in biology and medicine*, vol. 41(no. 12, pp. 1110–1117, 2011.

[169] L. Molcho, N. B. Maimon, N. Hezi, T. Zeimer, N. Intrator, and T. Gurevich, "Evaluation of parkinson's disease early diagnosis using single-channel eeg features and auditory cognitive assessment," *Frontiers in Neurology*, vol. 14, p. 1 273 458, 2023.

[170] M. Aljalal, S. A. Aldosari, K. AlSharabi, A. M. Abdurraqeeb, and F. A. Alturki, "Parkinson's disease detection from resting-state eeg signals using common spatial pattern, entropy, and machine learning techniques," *Diagnostics*, vol. 12(no. 5, p. 1033, 2022.

[171] W. Zhang et al., "Analysis of brain functional network based on eeg signals for early-stage parkinson's disease detection," *IEEE Access*, vol. 10, pp. 21 347–21 358, 2022.

[172] A. A. Priplata, J. B. Niemi, J. D. Harry, L. A. Lipsitz, and J. J. Collins, "Vibrating insoles and balance control in elderly people," *The lancet*, vol. 362(no. 9390, pp. 1123–1124, 2003.

[173] E. Niedermeyer and F. L. da Silva, *Electroencephalography: basic principles, clinical applications, and related fields*. Lippincott Williams & Wilkins, 2005.

[174] M. Mancini and F. B. Horak, "The relevance of clinical balance assessment tools to differentiate balance deficits," *European journal of physical and rehabilitation medicine*, vol. 46(no. 2, p. 239, 2010.

[175] D. A. Winter, "Human balance and posture control during standing and walking," *Gait & posture*, vol. 3(no. 4, pp. 193–214, 1995.

[176] V. Kelly et al., "Association of cognitive domains with postural instability/gait disturbance in Parkinson's disease," *Parkinsonism & related disorders*, vol. 21(no. 7, pp. 692–697, 2015.

[177] D. Xu et al., "Executive function and postural instability in people with Parkinson's disease," *Parkinson's disease*, vol. 2014(no. 1, p. 684 758, 2014.

[178] L. Ma, P. J. Marshall, and W. G. Wright, "The impact of external and internal focus of attention on visual dependence and eeg alpha oscillations during postural control," *Journal of NeuroEngineering and Rehabilitation*, vol. 19(no. 1, p. 81, 2022.

[179] J. Lanthier, M. Simoneau, I. S. Knoth, S. Lippe, C. Bluteau, and C. Fortin, "Increased EEG alpha peak frequency in adolescents with idiopathic scoliosis during balance control in normal upright standing," *Neuroscience letters*, vol. 722, p. 134 836, 2020.

[180] H. Woo and K. Lee, "The influence of postural control training on alpha band power during balance tasks," *Journal of Neurophysiology*, vol. 122(no. 5, pp. 1934–1942, 2019.

[181] R. Balasubramaniam and A. M. Wing, "The dynamics of standing balance," *Trends in cognitive sciences*, vol. 6(no. 12, pp. 531–536, 2002.

[182] S. Doblhoff and W. Friedl, "Neuromuscular and cortical adaptations to postural control training," *Neuroscience Letters*, vol. 671, pp. 64–70, 2018.

[183] C. Del Percio et al., "Cortical alpha rhythms are correlated with body sway during quiet open-eyes standing in athletes: A high-resolution EEG study," *Neuroimage*, vol. 36(no. 3, pp. 822–829, 2007.

[184] T. Hülsdünker and H. Strüder, "Influence of visual and vestibular perturbations on cortical activity during postural control," *Experimental Brain Research*, vol. 239(no. 2, pp. 519–530, 2021.

[185] S. Dos and H. Santos, "Cortical alpha oscillations predict postural sway modifications induced by transcranial direct current stimulation," *Neuroscience Letters*, vol. 553, pp. 45–49, 2013.

[186] F. Araújo-Silva et al., "Temporal dynamics of cortical activity and postural control in response to the first levodopa dose of the day in people with parkinson's disease," *Brain Research*, vol. 1775, p. 147 727, 2022.

[187] S. A. Stehle et al., "Predicting postural control adaptation measuring eeg, emg, and center of pressure changes: Biovrsea paradigm," *Frontiers in Human Neuroscience*, vol. 16, p. 1 038 976, 2022.

[188] M. Recenti et al., "Predicting lifestyle using biovrsea multi-biometric paradigms," in *2022 IEEE International Conference on Metrology for Extended Reality, Artificial Intelligence and Neural Engineering (MetroXRAINE)*, IEEE, 2022, pp. 329–334.

[189] M. Recenti et al., "Heart rate variability during a complex postural control task with the BioVRSea paradigm," in *2023 IEEE International Conference on Metrology for eXtended Reality, Artificial Intelligence and Neural Engineering (MetroXRAINE)*, IEEE, 2023, pp. 876–881.

[190] D. Jacob et al., "Adaptation strategies and neurophysiological response in early-stage parkinson's disease: Biovrsea approach," *Frontiers in Human Neuroscience*, vol. 17, p. 1 197 142, 2023.

[191] R. Aubonnet, M. Hassan, A. Mheich, G. Di Lorenzo, H. Petersen, and P. Gargiulo, "Brain network dynamics in the alpha band during a complex postural control task," *Journal of Neural Engineering*, vol. 20(no. 2, p. 026 030, 2023.

[192] S. E. Petersen and O. Sporns, "Brain networks and cognitive architectures," *Neuron*, vol. 88(no. 1, pp. 207–219, 2015.

[193] M. X. Cohen, "Effects of time lag and frequency matching on phase-based connectivity," *Journal of neuroscience methods*, vol. 250, pp. 137–146, 2015.

[194] A. Tessitore, A. Giordano, R. De Micco, A. Russo, and G. Tedeschi, "Sensorimotor connectivity in parkinson's disease: The role of functional neuroimaging," *Frontiers in neurology*, vol. 5, p. 180, 2014.

[195] H. Lv et al., "Resting-state functional mri: Everything that nonexperts have always wanted to know," *American Journal of Neuroradiology*, vol. 39(no. 8, pp. 1390–1399, 2018.

[196] W. Shirer, S. Ryali, E. Rykhlevskaia, V. Menon, and M. Greicius, "Decoding subject-driven cognitive states with whole-brain connectivity patterns," *Cerebral Cortex*, vol. 22(no. 1, pp. 158–165, 2012.

[197] M. E. Raichle, "The brain's default mode network," *Annual review of neuroscience*, vol. 38, pp. 433–447, 2015.

[198] M. D. Fox and M. E. Raichle, "Spontaneous fluctuations in brain activity observed with functional magnetic resonance imaging," *Nature reviews neuroscience*, vol. 8(no. 9, pp. 700–711, 2007.

[199] M. Hassan, O. Dufor, I. Merlet, C. Berrou, and F. Wendling, "EEG source connectivity analysis: From dense array recordings to brain networks," *PloS one*, vol. 9(no. 8, e105041, 2014.

[200] R. Bhidayasiri, D. Tarsy, R. Bhidayasiri, and D. Tarsy, "Parkinson's disease: Hoehn and yahr scale," *Movement disorders: a video atlas: a video atlas*, pp. 4–5, 2012.

[201] K. J. Edmunds et al., "Cortical recruitment and functional dynamics in postural control adaptation and habituation during vibratory proprioceptive stimulation," *Journal of neural engineering*, vol. 16(no. 2, p. 026 037, 2019.

[202] A. Kabbara, V. Paban, and M. Hassan, "The dynamic modular fingerprints of the human brain at rest," *NeuroImage*, vol. 227, p. 117 674, 2021.

[203] R. S. Desikan et al., "An automated labeling system for subdividing the human cerebral cortex on mri scans into gyral based regions of interest," *Neuroimage*, vol. 31(no. 3, pp. 968–980, 2006.

[204] E. Guttmann-Flury, Y. Wei, S. Zhao, J. Zhao, and M. Sawan, "The cost of simplicity: How reducing eeg electrodes affects source localization and bci accuracy," *arXiv preprint arXiv:2510.10770*, 2025.

[205] S.-R. Farahibozorg, R. N. Henson, and O. Hauk, "Adaptive cortical parcellations for source reconstructed eeg/meg connectomes," *NeuroImage*, vol. 169, pp. 23–45, 2018.

[206] M. A. Lopes et al., "Computational modelling in source space from scalp eeg to inform presurgical evaluation of epilepsy," *Clinical Neurophysiology*, vol. 131(no. 1, pp. 225–234, 2020.

[207] J.-P. Lachaux, E. Rodriguez, M. Le Van Quyen, A. Lutz, J. Martinerie, and F. J. Varela, "Studying single-trials of phase synchronous activity in the brain," *International Journal of Bifurcation and Chaos*, vol. 10(no. 10, pp. 2429–2439, 2000.

[208] A. T. Poulsen, A. Pedroni, N. Langer, and L. K. Hansen, "Microstate EEGlab toolbox: An introductory guide," *BioRxiv*, p. 289 850, 2018.

[209] M. M. Murray, D. Brunet, and C. M. Michel, "Topographic erp analyses: A step-by-step tutorial review," *Brain topography*, vol. 20(no. 4, pp. 249–264, 2008.

[210] R. D. Pascual-Marqui, C. M. Michel, and D. Lehmann, "Segmentation of brain electrical activity into microstates: Model estimation and validation," *IEEE Transactions on Biomedical Engineering*, vol. 42(no. 7, pp. 658–665, 1995.

[211] R. Aubonnet, M. Hassan, P. Gargiulo, S. Seri, and G. Di Lorenzo, "Dynamic resting-state eeg alpha connectivity: Quantifying brain network state evolution in individuals with psychosis," *bioRxiv*, pp. 2024–06, 2024.

[212] Z. Zhu et al., "Dynamic functional connectivity changes of resting-state brain network in attention-deficit/hyperactivity disorder," *Behavioural Brain Research*, vol. 437, p. 114 121, 2023.

[213] A. Custo, D. Van De Ville, W. M. Wells, M. I. Tomescu, D. Brunet, and C. M. Michel, "Electroencephalographic resting-state networks: Source localization of microstates," *Brain connectivity*, vol. 7(no. 10, pp. 671–682, 2017.

[214] R. Mahini et al., "Optimal number of clusters by measuring similarity among topographies for spatio-temporal erp analysis," *Brain topography*, vol. 35(no. 5, pp. 537–557, 2022.

[215] A. José-García and W. Gómez-Flores, "Cvik: A matlab-based cluster validity index toolbox for automatic data clustering," *SoftwareX*, vol. 22, p. 101 359, 2023.

[216] A. Kabbara, W. El Falou, M. Khalil, F. Wendling, and M. Hassan, "The dynamic functional core network of the human brain at rest," *Scientific reports*, vol. 7(no. 1, p. 2936, 2017.

[217] M. Rubinov and O. Sporns, "Complex network measures of brain connectivity: Uses and interpretations," *Neuroimage*, vol. 52(no. 3, pp. 1059–1069, 2010.

[218] M. Xia, J. Wang, and Y. He, "Brainnet viewer: A network visualization tool for human brain connectomics," *PloS one*, vol. 8(no. 7, e68910, 2013.

[219] F. Pescaglia et al., "Exploring dynamic alpha band connectivity in parkinson's disease: A novel approach to postural control assessment using the biovrsea paradigm," *Brain Topography*, vol. 39(no. 2, p. 20, 2026.

[220] L. V. Kalia and A. E. Lang, "Parkinson's disease," *The lancet*, vol. 386(no. 9996, pp. 896–912, 2015.

[221] C. H. F. Camargo, S. A. Ferreira-Peruzzo, D. I. R. Ribas, G. L. Franklin, and H. A. Teive, "Imbalance and gait impairment in parkinson's disease: Discussing postural instability and ataxia," *Neurological Sciences*, vol. 45(no. 4, pp. 1377–1388, 2024.

[222] J. V. Jacobs and F. Horak, "Abnormal proprioceptive-motor integration contributes to hypometric postural responses of subjects with parkinson's disease," *Neuroscience*, vol. 141(no. 2, pp. 999–1009, 2006.

[223] M. Mancini et al., "Isway: A sensitive, valid and reliable measure of postural control," *Journal of neuroengineering and rehabilitation*, vol. 9(no. 1, p. 59, 2012.

[224] K. Berg, "Measuring balance in the elderly: Development and validation of an instrument," 1992.

[225] D. Podsiadlo and S. Richardson, "The timed "up & go": A test of basic functional mobility for frail elderly persons," *Journal of the American geriatrics Society*, vol. 39(no. 2, pp. 142–148, 1991.

[226] A. Kamieniarz et al., "Detection of postural control in early parkinson's disease: Clinical testing vs. modulation of center of pressure," *PLoS One*, vol. 16(no. 1, e0245353, 2021.

[227] A. Mirelman, I. Maidan, T. Herman, J. E. Deutsch, N. Giladi, and J. M. Hausdorff, "Virtual reality for gait training: Can it induce motor learning to enhance complex walking and reduce fall risk in patients with parkinson's disease?" *Journals of Gerontology Series A: Biomedical Sciences and Medical Sciences*, vol. 66(no. 2, pp. 234–240, 2011.

[228] K. Dockx et al., "Virtual reality for rehabilitation in parkinson's disease," *Cochrane Database of Systematic Reviews*, no. 12, 2016.

[229] M. Recenti et al., "New frontiers in postural control and motion sickness assessment: The biovrsea paradigm," in *2024 IEEE International Conference on Metrology for eXtended Reality, Artificial Intelligence and Neural Engineering (MetroXRAINE)*, IEEE, 2024, pp. 1034–1039.

[230] Y.-L. Hsieh and M. F. Abbod, "Gait analyses of parkinson's disease patients using multiscale entropy," *Electronics*, vol. 10(no. 21, p. 2604, 2021.

[231] M. Gandolfi et al., "Postural control in individuals with parkinson's disease," in *Different Areas of Physiotherapy*, IntechOpen, 2018.

[232] C. O'Keeffe, L. P. Taboada, N. Feerick, L. Gallagher, T. Lynch, and R. B. Reilly, "Complexity based measures of postural stability provide novel evidence of functional decline in fragile x premutation carriers," *Journal of neuroengineering and rehabilitation*, vol. 16(no. 1, p. 87, 2019.

[233] J. Zhou, D. Habtemariam, I. Iloputaife, L. A. Lipsitz, and B. Manor, "The complexity of standing postural sway associates with future falls in community-dwelling older adults: The mobilize boston study," *Scientific reports*, vol. 7(no. 1, p. 2924, 2017.

[234] C.-H. Lee and T.-L. Sun, "Evaluation of postural stability based on a force plate and inertial sensor during static balance measurements," *Journal of physiological anthropology*, vol. 37, pp. 1–16, 2018.

[235] M. Sarvari, S. Shanbehzadeh, Y. Shavehei, and S. ShahAli, "Postural control among older adults with fear of falling and chronic low back pain," *BMC geriatrics*, vol. 24(no. 1, p. 862, 2024.

[236] I. D. Loram, C. N. Maganaris, and M. Lakie, "Human postural sway results from frequent, ballistic bias impulses by soleus and gastrocnemius," *The Journal of Physiology*, vol. 564(no. 1, pp. 295–311, 2005. DOI: https://doi.org/10.1113/jphysiol.2004.076307. eprint: https://physoc.onlinelibrary.wiley.com/doi/pdf/10.1113/jphysiol.2004.076307. [Online]. Available: https://physoc.onlinelibrary.wiley.com/doi/abs/10.1113/jphysiol.2004.076307.

[237] M. Papadatou-Pastou et al., "Human handedness: A meta-analysis.," *Psychological bulletin*, vol. 146(no. 6, p. 481, 2020.

[238] F. B. Horak and M. Mancini, "Objective biomarkers of balance and gait for parkinson's disease using body-worn sensors," *Movement Disorders*, vol. 28(no. 11, pp. 1544–1551, 2013.

[239] Y. Wang, Z. Hu, K. Chen, and Y. Yang, "Automatic characterization of stroke patients' posturography based on probability density analysis," *BioMedical Engineering OnLine*, vol. 22(no. 1, p. 8, 2023.

[240] S. Thongpanja, A. Phinyomark, F. Quaine, Y. Laurillau, C. Limsakul, and P. Phukpattaranont, "Probability density functions of stationary surface emg signals in noisy environments," *IEEE Transactions on Instrumentation and Measurement*, vol. 65(no. 7, pp. 1547–1557, 2016.

[241] J. Massion, "Postural control system," *Current opinion in neurobiology*, vol. 4(no. 6, pp. 877–887, 1994.

[242] A. Gollhofer and H. Kyröläinen, "Neuromuscular control of the human leg extensor muscles in jump exercises under various stretch-load conditions," *International journal of sports medicine*, vol. 12(no. 01, pp. 34–40, 1991.

[243] B. E. Maki and W. E. McIlroy, "Cognitive demands and cortical control of human balance-recovery reactions," *Journal of neural transmission*, vol. 114(no. 10, pp. 1279–1296, 2007.

[244] S. Papegaaij, W. Taube, S. Baudry, E. Otten, and T. Hortobágyi, "Aging causes a reorganization of cortical and spinal control of posture," *Frontiers in aging neuroscience*, vol. 6, p. 28, 2014.

[245] B. J. Baars and N. M. Gage, *Cognition, brain, and consciousness: Introduction to cognitive neuroscience*. Academic Press, 2010.

[246] M. Kahya, K. Liao, K. M. Gustafson, A. E. Akinwuntan, B. Manor, and H. Devos, "Cortical correlates of increased postural task difficulty in young adults: A combined pupillometry and eeg study," *Sensors*, vol. 22(no. 15, p. 5594, 2022.

[247] A. Singh, R. C. Cole, A. I. Espinoza, D. Brown, J. F. Cavanagh, and N. S. Narayanan, "Frontal theta and beta oscillations during lower-limb movement in parkinson's disease," *Clinical Neurophysiology*, vol. 131(no. 3, pp. 694–702, 2020.

[248] S. M. Slobounov, E. Teel, and K. M. Newell, "Modulation of cortical activity in response to visually induced postural perturbation: Combined vr and eeg study," *Neuroscience letters*, vol. 547, pp. 6–9, 2013.

[249] D. Malisova, T. Petrenko, A. Kondratenko, and O. Bazanova, "Alpha eeg and emg indices of optimal music-performing movement and postural control," in *XXIII* . , 2017, pp. 967–968.

[250] G. Pfurtscheller, "Induced oscillations in the alpha band: Functional meaning," *Epilepsia*, vol. 44, pp. 2–8, 2003.

[251] C. Del Percio et al., "Cortical alpha rhythms are correlated with body sway during quiet open-eyes standing in athletes: A high-resolution eeg study," *NeuroImage*, vol. 36(no. 3, pp. 822–829, 2007, ISSN: 1053-8119. DOI: `https://doi.org/10.1016/j.neuroimage.2007.02.054`. [Online]. Available: `https://www.sciencedirect.com/science/article/pii/S1053811907001668`.

[252] T. Hülsdünker, A. Mierau, and H. K. Strüder, "Higher balance task demands are associated with an increase in individual alpha peak frequency," *Frontiers in Human Neuroscience*, vol. 9, 2016, ISSN: 1662-5161. DOI: `10.3389/fnhum.2015.00695`. [Online]. Available: `https://www.frontiersin.org/articles/10.3389/fnhum.2015.00695`.

[253] B. A. Seitzman, A. Z. Snyder, E. C. Leuthardt, and J. S. Shimony, "The state of resting state networks," *Topics in Magnetic Resonance Imaging*, vol. 28(no. 4, pp. 189–196, 2019.

[254] M. D. Fox, A. Z. Snyder, J. L. Vincent, M. Corbetta, D. C. Van Essen, and M. E. Raichle, "The human brain is intrinsically organized into dynamic, anticorrelated functional networks," *Proceedings of the National Academy of Sciences*, vol. 102(no. 27, pp. 9673–9678, 2005.

[255] C. F. Beckmann, M. DeLuca, J. T. Devlin, and S. M. Smith, "Investigations into resting-state connectivity using independent component analysis," *Philosophical Transactions of the Royal Society B: Biological Sciences*, vol. 360(no. 1457, pp. 1001–1013, 2005.

[256] N. Yao et al., "Resting activity in visual and corticostriatal pathways in Parkinson's disease with hallucinations," *Parkinsonism & related disorders*, vol. 21(no. 2, pp. 131–137, 2015.

[257] J. Hsu, C. Ouyang, P. Chen, K. Lai, C. Chiu, and P. Chen, "Brain network alterations in patients with visual hallucinations in Parkinson's disease," *Journal of Neurology*, vol. 264(no. 7, pp. 1479–1489, 2017.

[258] X. Hu, Y. Zhang, X. Hu, K. Li, Q. Yu, and K. Li, "Altered interhemispheric synchrony in Parkinson's disease patients with visual hallucinations: A resting-state fmri study," *Cortex*, vol. 124, pp. 201–210, 2020.

[259] M. Corbetta and G. L. Shulman, "The reorienting system of the human brain: From environment to theory of mind," *Neuron*, vol. 58(no. 3, pp. 306–324, 2008.

[260] V. Menon and L. Uddin, "Saliency, switching, attention and control: A network model of insula function," *Brain Structure and Function*, vol. 214(no. 5-6, pp. 655–667, 2015.

[261] D. Sridharan, D. Levitin, and V. Menon, "A critical role for the right fronto-insular cortex in switching between central-executive and default-mode networks," *Proceedings of the National Academy of Sciences*, vol. 105(no. 34, pp. 12 569–12 574, 2008.

[262] S. Vossel, J. J. Geng, and G. R. Fink, "Dorsal and ventral attention systems: Distinct neural circuits but collaborative roles," *The Neuroscientist*, vol. 20(no. 2, pp. 150–159, 2014.

[263] W. Hsu, T. Zanto, A. Gazzaley, and J. Anguera, "Functional connectivity of the dorsal attention network predicts post-stroke motor recovery," *Journal of Neuroscience*, vol. 32(no. 21, pp. 7338–7343, 2012.

[264] I. Maidan, Y. Jacob, N. Giladi, J. M. Hausdorff, and A. Mirelman, "Altered organization of the dorsal attention network is associated with freezing of gait in Parkinson's disease," *Parkinsonism & related disorders*, vol. 63, pp. 77–82, 2019.

[265] M. Fox, M. Corbetta, A. Snyder, J. Vincent, and M. Raichle, "Spontaneous neuronal activity distinguishes human dorsal and ventral attention systems," *Proceedings of the National Academy of Sciences*, vol. 103(no. 26, pp. 10 046–10 051, 2006.

[266] T. A. Hackett, T. M. Preuss, and J. H. Kaas, "Organization of the auditory cortex in humans and nonhuman primates: Functional anatomy of the lateral auditory belt and parabelt," *Progress in Brain Research*, vol. 130, pp. 273–288, 2001.

[267] T. T. Raij, L. McEvoy, J. P. Mäkelä, and R. Hari, "Human auditory cortex is activated by omissions of auditory stimuli," *Brain Research*, vol. 868(no. 2, pp. 163–165, 2000.

[268] P. E. Gander, H. R. Bosker, W. A. Teder-Sälejärvi, and M. Sams, "Multimodal integration of visual and auditory information during speech perception," *Human Brain Mapping*, vol. 40(no. 13, pp. 3796–3809, 2019.

[269] D. Putcha, R. S. Ross, A. Cronin-Golomb, A. C. Janes, and C. E. Stern, "Salience and default mode network coupling predicts cognition in aging and Parkinson's disease," *Journal of the International Neuropsychological Society*, vol. 22(no. 2, pp. 205–215, 2016.

[270] V. Menon, "The triple network model of psychopathology: Evidence from intrinsic functional connectivity and task effects," *Biological Psychiatry*, vol. 69(no. 12, pp. 1178–1185, 2011.

[271] D. Putcha, R. S. Ross, A. Cronin-Golomb, and C. E. Stern, "Default network connectivity and cognition in Parkinson's disease," *Human Brain Mapping*, vol. 35(no. 9, pp. 4018–4031, 2014.

[272] R. L. Buckner, J. R. Andrews-Hanna, and D. L. Schacter, "The brain's default network: Anatomy, function, and relevance to disease," *Annals of the New York Academy of Sciences*, vol. 1124(no. 1, pp. 1–38, 2008.

[273] J. R. Andrews-Hanna, J. Smallwood, and R. N. Spreng, "The default network and self-generated thought: Component processes, dynamic control, and clinical relevance," *Annals of the New York Academy of Sciences*, vol. 1316(no. 1, pp. 29–52, 2010.

[274] G. Buzsaki and A. Draguhn, "Neuronal oscillations in cortical networks," *science*, vol. 304(no. 5679, pp. 1926–1929, 2004.

[275] G. Buzsáki, *Rhythms of the Brain*. Oxford university press, 2006.

[276] G. G. Knyazev, "Eeg delta oscillations as a correlate of basic homeostatic and motivational processes," *Neuroscience & Biobehavioral Reviews*, vol. 36(no. 1, pp. 677–695, 2012.

[277] G. Deco, V. K. Jirsa, and A. R. McIntosh, "Emerging concepts for the dynamical organization of resting-state activity in the brain," *Nature reviews neuroscience*, vol. 12(no. 1, pp. 43–56, 2011.

[278] J. E. Bath and D. D. Wang, "Unraveling the threads of stability: A review of the neurophysiology of postural control in parkinson's disease," *Neurotherapeutics*, vol. 21(no. 3, e00354, 2024.

[279] D. Stoffers, J. Bosboom, J. Deijen, E. C. Wolters, H. Berendse, and C. Stam, "Slowing of oscillatory brain activity is a stable characteristic of parkinson's disease without dementia," *Brain*, vol. 130(no. 7, pp. 1847–1860, 2007.

[280] C. Babiloni et al., "Cortical sources of resting state electroencephalographic rhythms in parkinson's disease related dementia and alzheimer's disease," *Clinical Neurophysiology*, vol. 122(no. 12, pp. 2355–2364, 2011.

[281] K. T. Olde Dubbelink et al., "Disrupted brain network topology in parkinson's disease: A longitudinal magnetoencephalography study," *Brain*, vol. 137(no. 1, pp. 197–207, 2014.

[282] B. Voytek and R. T. Knight, "Dynamic network communication as a unifying neural basis for cognition, development, aging, and disease," *Biological psychiatry*, vol. 77(no. 12, pp. 1089–1097, 2015.

[283] J. Kim et al., "Abnormal intrinsic brain functional network dynamics in parkinson's disease," *Brain*, vol. 140(no. 11, pp. 2955–2967, 2017.

[284] G. Deco and M. L. Kringelbach, "Great expectations: Using whole-brain computational connectomics for understanding neuropsychiatric disorders," *Neuron*, vol. 84(no. 5, pp. 892–905, 2014.

[285] J. M. Shine and R. A. Poldrack, "Principles of dynamic network reconfiguration across diverse brain states," *NeuroImage*, vol. 180, pp. 396–405, 2018.

[286] W. Klimesch, "Eeg alpha and theta oscillations reflect cognitive and memory performance: A review and analysis," *Brain research reviews*, vol. 29(no. 2-3, pp. 169–195, 1999.

[287] P. Sauseng, B. Griesmayr, R. Freunberger, and W. Klimesch, "Control mechanisms in working memory: A possible function of eeg theta oscillations," *Neuroscience & Biobehavioral Reviews*, vol. 34(no. 7, pp. 1015–1022, 2010.

[288] S. Slobounov, C. Cao, N. Jaiswal, and K. M. Newell, "Neural basis of postural instability identified by vtc and eeg," *Experimental brain research*, vol. 199, pp. 1–16, 2009.

[289] M. Göttlich, T. F. Münte, M. Heldmann, M. Kasten, J. Hagenah, and U. M. Krämer, "Altered resting state brain networks in parkinson's disease," *PloS one*, vol. 8(no. 10, e77336, 2013.

[290] J. F. Cavanagh and M. J. Frank, "Frontal theta as a mechanism for cognitive control," *Trends in cognitive sciences*, vol. 18(no. 8, pp. 414–421, 2014.

[291] A. K. Engel and P. Fries, "Beta-band oscillations—signalling the status quo?" *Current opinion in neurobiology*, vol. 20(no. 2, pp. 156–165, 2010.

[292] B. E. Kilavik, M. Zaepffel, A. Brovelli, W. A. MacKay, and A. Riehle, "The ups and downs of beta oscillations in sensorimotor cortex," *Experimental neurology*, vol. 245, pp. 15–26, 2013.

[293] C. Hammond, H. Bergman, and P. Brown, "Pathological synchronization in parkinson's disease: Networks, models and treatments," *Trends in neurosciences*, vol. 30(no. 7, pp. 357–364, 2007.

[294] S. Little and P. Brown, "The functional role of beta oscillations in parkinson's disease," *Parkinsonism & related disorders*, vol. 20, S44–S48, 2014.

[295] E. Heinrichs-Graham and T. W. Wilson, "Neuromagnetic evidence of abnormal movement-related beta desynchronization in parkinson's disease," *NeuroImage: Clinical*, vol. 2, pp. 585–593, 2013. DOI: 10.1016/j.nicl.2013.04.008.

[296] A. Gulberti and colleagues, "Premotor cortical beta synchronization and the network mechanisms of motor impairment in parkinson's disease," *Neurobiology of Disease*, 2024. DOI: 10.1016/j.nbd.2024.106259.

[297] A. Miladinović and colleagues, "Eeg changes and motor deficits in parkinson's disease patients: Correlation of motor scales and eeg power bands," *arXiv preprint*, 2021. eprint: 2106.02387. [Online]. Available: https://arxiv.org/abs/2106.02387.

[298] A. Anjum and colleagues, "Resting-state eeg measures cognitive impairment in parkinson's disease," *npj Parkinson's Disease*, vol. 10(no. 1, pp. 1–10, 2024. DOI: 10.1038/s41531-023-00602-0.

[299] A. Singh and colleagues, "Evoked midfrontal activity predicts cognitive dysfunction in parkinson's disease," *Brain*, vol. 146(no. 2, pp. 552–567, 2023. DOI: 10.1093/brain/awac367.

[300] H.-C. Baggio et al., "Functional brain networks and cognitive deficits in parkinson's disease," *Human brain mapping*, vol. 35(no. 9, pp. 4620–4634, 2014.

[301] G. Vervoort et al., "Structural brain alterations in motor subtypes of parkinson's disease: Evidence from probabilistic tractography and shape analysis," *PloS one*, vol. 11(no. 6, e0157743, 2016.

[302] E. Fiorenzato et al., "Dynamic functional connectivity changes associated with dementia in parkinson's disease," *Brain*, vol. 142(no. 9, pp. 2860–2872, 2019.

[303] A. Singh, S. P. Richardson, N. Narayanan, and J. F. Cavanagh, "Midfrontal theta activity is diminished during cognitive control in parkinson's disease," *Neuropsychologia*, vol. 117, pp. 113–122, 2018.

[304] G. Yogev-Seligmann, J. M. Hausdorff, and N. Giladi, "The role of executive function and attention in gait," *Movement disorders: official journal of the Movement Disorder Society*, vol. 23(no. 3, pp. 329–342, 2008.

[305] S.-H. Yu, R.-M. Wu, and C.-Y. Huang, "Attentional resource associated with visual feedback on a postural dual task in parkinson's disease," *Neurorehabilitation and Neural Repair*, vol. 34(no. 10, pp. 891–903, 2020.

[306] P. Tait et al., "Neuroimaging and cognitive correlates of postural control in parkinson's disease: A systematic review," *Journal of NeuroEngineering and Rehabilitation*, vol. 22(no. 1, p. 24, 2025.

[307] L. I. Boon et al., "A systematic review of meg-based studies in parkinson's disease: The motor system and beyond," *Human brain mapping*, vol. 40(no. 9, pp. 2827–2848, 2019.